

**APPENDIX F Acoustic Televiewer (ATV) and Borehole Suspension
Logging Report**



**LAST CHANCE GRADE
BOREHOLE GEOPHYSICS
CRESCENT CITY, CALIFORNIA**

Prepared for

Kleinfelder

2882 Prospect Park Drive, Suite 200
Rancho Cordova, California 95670
(916) 366 - 1701

Prepared by

GEOVision Geophysical Services

1124 Olympic Drive
Corona, California 92881
(951) 549 - 1234

April 6, 2022

Report 20020-02 Rev 1

Report 20020-02 REVISION HISTORY

DATE	REVISION NUMBER	REASON FOR CHANGE
3/15/2021	0	Draft Issue
4/6/2022	1	Final Issue

TABLE OF CONTENTS

REPORT 20020-02 REVISION HISTORY	2
TABLE OF CONTENTS.....	3
TABLE OF FIGURES	5
TABLE OF TABLES	7
INTRODUCTION.....	8
SCOPE OF WORK	8
INSTRUMENTATION.....	10
SUSPENSION VELOCITY	10
ACOUSTIC TELEVIEWER / BOREHOLE DEVIATION	12
OPTICAL TELEVIEWER / BORING DEVIATION	14
DUAL INDUCTION / NATURAL GAMMA	16
CALIPER / NATURAL GAMMA	17
MEASUREMENT PROCEDURES	19
SUSPENSION VELOCITY	19
ACOUSTIC TELEVIEWER / BORING DEVIATION	19
OPTICAL TELEVIEWER	20
DUAL INDUCTION / NATURAL GAMMA	21
CALIPER / NATURAL GAMMA	22
DATA ANALYSIS	24
SUSPENSION VELOCITY	24
ACOUSTIC TELEVIEWER.....	26
OPTICAL TELEVIEWER.....	26
DUAL INDUCTION / NATURAL GAMMA	27
CALIPER / NATURAL GAMMA	27
RESULTS	28

SUSPENSION VELOCITY	28
ACOUSTIC TELEVIEWER / OPTICAL TELEVIEWER / BORING DEVIATION	28
DUAL INDUCTION / CALIPER/ NATURAL GAMMA.....	29
DISCUSSION OF RESULTS	30
SUSPENSION VELOCITY	30
TELEVIEWER / BORING DEVIATION.....	31
DUAL INDUCTION / CALIPER/ NATURAL GAMMA.....	31
QUALITY ASSURANCE.....	33
TELEVIEWER DATA RELIABILITY	33
SUSPENSION VELOCITY DATA RELIABILITY	33
CERTIFICATION.....	34
FIGURES	35
TABLES.....	84
APPENDIX A SUSPENSION VELOCITY MEASUREMENT SOURCE TO RECEIVER ANALYSIS RESULTS	131
APPENDIX B PROCESSED TELEVIEWER IMAGES WITH TADPOLES	142
APPENDIX C DUAL INDUCTION, CALIPER, AND NATURAL GAMMA LOGS	143
APPENDIX D BORING GEOPHYSICAL LOGGING SYSTEMS - NIST TRACEABLE CALIBRATION RECORDS.....	144

Table of Figures

Figure 1. Concept illustration of P-S logging system.....	36
Figure 2. Concept illustration of televiewer probe	37
Figure 3. Example of filtered (1400 Hz lowpass) suspension record.....	38
Figure 4. Example of unfiltered suspension record	39
Figure 5. Borehole RC-20-017 (B-18), Acoustic Stereonet Diagram	40
Figure 6. Borehole RC-20-017 (B-18), Acoustic Rose Diagram	41
Figure 7. Borehole RC-20-017 (B-18), Deviation Cylindrical Projection	42
Figure 8. Borehole RC-20-017 (B-18), Deviation Bullseye Projection	43
Figure 9. Borehole RC-20-005 (B-28), Optical Stereonet Diagram	44
Figure 10. Borehole RC-20-005 (B-28), Optical Rose Diagram	45
Figure 11. Borehole RC-20-005 (B-28), Deviation Cylindrical Projection	46
Figure 12. Borehole RC-20-005 (B-28), Deviation Bullseye Projection	47
Figure 13: Borehole RC-20-014 (B-29), Suspension R1-R2 P- and SH-wave velocities..	48
Figure 14. Borehole RC-20-014 (B-29), Acoustic Stereonet Diagram	49
Figure 15. Borehole RC-20-014 (B-29), Acoustic Rose Diagram	50
Figure 16. Borehole RC-20-014 (B-29), Deviation Cylindrical Projection	51
Figure 17. Borehole RC-20-014 (B-29), Deviation Bullseye Projection	52
Figure 18. Borehole RC-20-014 (B-29), Induction, Caliper, and Natural Gamma Log	53
Figure 19: Borehole RC-20-011 (B-32), Suspension R1-R2 P- and SH-wave velocities..	54
Figure 20. Borehole RC-20-011 (B-32), Acoustic Stereonet Diagram	55
Figure 21. Borehole RC-20-011 (B-32), Acoustic Rose Diagram	56
Figure 22. Borehole RC-20-011 (B-32), Acoustic Deviation Cylindrical Projection.....	57
Figure 23. Borehole RC-20-011 (B-32), Acoustic Deviation Bullseye Projection.....	58
Figure 24. Borehole RC-20-011 (B-32), Optical Stereonet Diagram	59
Figure 25. Borehole RC-20-011 (B-32), Optical Rose Diagram	60
Figure 26. Borehole RC-20-011 (B-32), Optical Deviation Cylindrical Projection	61
Figure 27. Borehole RC-20-011 (B-32), Optical Deviation Bullseye Projection	62
Figure 28. Borehole RC-20-011 (B-32), Induction, Caliper, and Natural Gamma Log	63
Figure 29. Borehole RC-20-020 (B-46), Caliper and Natural Gamma Log	64
Figure 30. Borehole RC-21-001 (B-47), Acoustic Stereonet Diagram	65

Figure 31. Borehole RC-21-001 (B-47), Acoustic Rose Diagram	66
Figure 32. Borehole RC-21-001 (B-47), Acoustic Deviation Cylindrical Projection.....	67
Figure 33. Borehole RC-21-001 (B-47), Acoustic Deviation Bullseye Projection.....	68
Figure 34. Borehole RC-21-001 (B-47), Optical Stereonet Diagram	69
Figure 35. Borehole RC-21-001 (B-47), Optical Rose Diagram	70
Figure 36. Borehole RC-21-001 (B-47), Optical Deviation Cylindrical Projection	71
Figure 37. Borehole RC-21-001 (B-47), Optical Deviation Bullseye Projection.....	72
Figure 38: Borehole RC-20-019 (B-50), Suspension R1-R2 P- and SH-wave velocities..	73
Figure 39. Borehole RC-20-019 (B-50), Acoustic Stereonet Diagram	74
Figure 40. Borehole RC-20-019 (B-50), Acoustic Rose Diagram	75
Figure 41. Borehole RC-20-019 (B-50), Acoustic Deviation Cylindrical Projection.....	76
Figure 42. Borehole RC-20-019 (B-50), Acoustic Deviation Bullseye Projection.....	77
Figure 43. Borehole RC-20-019 (B-50), Induction, Caliper, and Natural Gamma Log	78
Figure 44. Borehole RC-20-016 (WP-3), Optical Stereonet Diagram.....	79
Figure 45. Borehole RC-20-016 (WP-3), Optical Rose Diagram	80
Figure 46. Borehole RC-20-016 (WP-3), Optical Deviation Cylindrical Projection.....	81
Figure 47. Borehole RC-20-016 (WP-3), Optical Deviation Bullseye Projection.....	82
Figure 48. Interpreting Conductivity and Resistivity	83

Table of Tables

Table 1. Borehole Logging Dates and Locations.....	85
Table 2. Logging Tools, Depth Ranges and Sample Intervals	85
Table 3. Televiwer Deviation Data Summary	86
Table 4. Borehole RC-20-017 (B-18), Acoustic Televiwer Feature depth, dip azimuth, dip, aperture, and type	87
Table 5. Borehole RC-20-005 (B-28), Optical Televiwer Feature depth, dip azimuth, dip, aperture, and type	96
Table 6. Borehole RC-20-014 (B-29), Suspension R1-R2 depths and P- and SH-wave velocities	101
Table 7. Borehole RC-20-014 (B-29), Acoustic Televiwer Feature depth, dip azimuth, dip, aperture, and type	104
Table 8. Borehole RC-20-011 (B-32), Suspension R1-R2 depths and P- and SH-wave velocities	110
Table 9. Borehole RC-20-011 (B-32), Acoustic Televiwer Feature depth, dip azimuth, dip, aperture, and type	112
Table 10. Borehole RC-20-011 (B-32), Optical Televiwer Feature depth, dip azimuth, dip, aperture, and type	116
Table 11. Borehole RC-21-001 (B-47), Acoustic Televiwer Feature depth, dip azimuth, dip, aperture, and type	119
Table 12. Borehole RC-21-001 (B-47), Optical Televiwer Feature depth, dip azimuth, dip, aperture, and type	120
Table 13. Borehole RC-20-019 (B-50), Suspension R1-R2 depths and P- and SH-wave velocities	121
Table 14. Borehole RC-20-019 (B-50), Acoustic Televiwer Feature depth, dip azimuth, dip, aperture, and type	123
Table 15. Borehole RC-20-016 (WP-3), Optical Televiwer Feature depth, dip azimuth, dip, aperture, and type	126
Table 16. Summary of PS Suspension Data Quality Evaluation Using Five Criteria.....	130

INTRODUCTION

Borehole geophysical measurements were collected in eight boreholes for the Last Chance Grade Project near Crescent City, California as part of an investigation conducted by Kleinfelder. **GEOVision** performed data acquisition between October 26 and December 17, 2020. Additional televiewer data acquired by Crux Subsurface, Inc. was processed by **GEOVision**. Data analysis and report preparation were reviewed by a **GEOVision** Professional Geophysicist or Engineer.

SCOPE OF WORK

This report presents the results of borehole geophysical measurements collected in eight boreholes as detailed in Table 1. PS Suspension velocity (PS), acoustic televiewer (ATV), optical televiewer (OTV), dual induction (DUIN), mechanical caliper (CAL), and natural gamma (NG) data were acquired. The purpose of these measurements was to supplement borehole data obtained during the drilling investigation, to obtain information about fracture location, dip, orientation, and aperture, and to acquire shear wave velocities and compressional wave velocities as a function of depth.

The OYO Suspension PS Logging System (Suspension System) was used to obtain in-situ horizontal shear (S_H) and compressional (P) wave velocity measurements in three boreholes at 1.6-foot intervals. Measurements followed **GEOVision** Procedure for PS Suspension Seismic Velocity Logging, revision 1.5. Acquired data were analyzed and a profile of velocity versus depth was produced for both S_H and P waves.

A detailed reference for the suspension PS velocity measurement techniques used in this study is:

Guidelines for Determining Design Basis Ground Motions, Report TR-102293,
Electric Power Research Institute, Palo Alto, California, November 1993, Sections 7
and 8.

Either a Robertson Geo high resolution acoustic televiewer or ALT ABI-40 acoustic televiewer (ATV) was used to collect acoustic televiewer images and/or borehole deviation data in five boreholes and optical images in four boreholes. Acquired data were analyzed and a profile of

borehole deviation versus depth was produced for each borehole. Borehole images were analyzed and features such as bedding planes and fractures were identified with calculated feature dip and azimuth.

A Robertson Geo (RG) Dual Induction probe (DUIN) was used to collect long and short conductivity and natural gamma data at 0.05-foot intervals in the three boreholes.

A Robertson Geo 3ACS mechanical caliper probe (CAL) was used to collect boring diameter and natural gamma data at 0.05-foot intervals in four boreholes.

Measurement procedures followed these ASTM standards:

- ASTM D5753-18, “Planning and Conducting Boring Geophysical Logging”

INSTRUMENTATION

Suspension Velocity

Suspension velocity measurements were performed using the suspension PS logging system, manufactured by OYO Corporation, and their subsidiary, Robertson Geo (RG). This system directly determines the average velocity of a 3.3-foot-high segment of the soil column surrounding the boring of interest by measuring the elapsed time between arrivals of a wave propagating upward through the soil column. The receivers that detect the wave, and the source that generates the wave, are moved as a unit in the boring producing relatively constant amplitude signals at all depths.

The suspension system probe consists of a combined reversible polarity solenoid horizontal shear-wave source (S_H) and compressional-wave source (P), joined to two biaxial receivers by a flexible isolation cylinder, as shown in Figure 1. The separation of the two receivers is 3.3 feet, allowing average wave velocity in the region between the receivers to be determined by inversion of the wave travel time between the two receivers. The total length of the probe as used in these surveys is approximately 22 feet, with the center point of the receiver pair 12.5 feet above the bottom end of the probe.

The probe receives control signals from, and sends the digitized receiver signals to, instrumentation on the surface via an armored conductor cable. The cable is wound onto the drum of a winch and is used to support the probe. Cable travel is measured to provide probe depth data using a sheave of known circumference fitted with a digital rotary encoder.

The entire probe is suspended in the borehole by the cable; therefore, source motion is not coupled directly to the boring walls; rather, the source motion creates a horizontally propagating impulsive pressure wave in the fluid filling the boring and surrounding the source. This pressure wave is converted to P- and S_H -waves in the surrounding soil and rock as it passes through the casing and grout annulus (if present) and impinges upon the wall of the boring. These waves propagate through the soil and rock surrounding the boring, in turn causing a pressure wave to be generated in the fluid surrounding the receivers as the soil waves pass their location. Separation of the P- and S_H -waves at the receivers is performed using the following steps:

1. Orientation of the horizontal receivers is maintained parallel to the axis of the source, maximizing the amplitude of the recorded S_H -wave signals.
2. At each depth, S_H -wave signals are recorded with the source actuated in opposite directions, producing S_H -wave signals of opposite polarity, providing a characteristic S_H -wave signature distinct from the P-wave signal.
3. The 6.3-foot separation of source and receiver 1 permits the P-wave signal to pass and damp significantly before the slower S_H -wave signal arrives at the receiver.
4. In saturated soils, the received P-wave signal is typically of much higher frequency than the received S_H -wave signal, permitting additional separation of the two signals by low pass filtering.
5. Direct arrival of the original pressure pulse in the fluid is not detected at the receivers because the wavelength of the pressure pulse in fluid is significantly greater than the dimension of the fluid annulus surrounding the probe (feet versus inches scale), preventing significant energy transmission through the fluid medium.

In operation, a distinct, repeatable pattern of impulses is generated at each depth as follows:

1. The source is fired in one direction producing dominantly horizontal shear with some vertical compression, and the signals from the horizontal receivers situated parallel to the axis of motion of the source are recorded.
2. The source is fired again in the opposite direction and the horizontal receiver signals are recorded.
3. The source is fired again, and the vertical receiver signals are recorded. The repeated source pattern facilitates the picking of the P- and S_H -wave arrivals; reversal of the source changes the polarity of the S_H -wave pattern but not the P-wave pattern.

The data from each receiver during each source activation is recorded as a different channel on the recording system. The Suspension PS system has six channels (two simultaneous recording channels), each with a 1024 sample record. The recorded data are displayed as six channels with a common time scale. Data are stored on disk for further processing.

Review of the displayed data on the recorder or computer screen allows the operator to set the gains, filters, delay time, pulse length (energy), and sample rate to optimize the quality of the data before recording.

Verification of the calibration of the Suspension P-S digital recorder is performed at least every twelve months using a NIST traceable frequency source and counter and **GEOVision** Suspension P-S Seismic Logger/Recorder Calibration Procedure Revision 2.1. Calibration records are reproduced in Appendix D.

Acoustic Televiewer / Borehole Deviation

Acoustic televiewer data were collected in five boreholes by Crux using an ALT ABI40 acoustic borehole imager probe. A simple diagram of the tool is presented in Figure 2.

The acoustic borehole imager generates a 3D image from the borehole wall. The tool emits ultrasound pulses towards the formation and records the amplitude and the travel time of the reflected signal. A built-in high precision orientation package incorporating a 3-axis magnetometer and 3-axis accelerometer allows orientation of the images to a global reference and determination of the borehole's azimuth and inclination. The amplitude of the reflection from the borehole wall is representative of the acoustic properties of the formation. The travel time is used to determine exceptionally accurate borehole diameter data, which makes the tool ideal for borehole deformation description and casing inspection.

The tool generates an image of the borehole wall by transmitting ultrasound pulses and recording the amplitude and the travel time of the reflected signal and is capable of detecting multiple reflections. This multi-echo system is achieved by digital recording of the reflected acoustic wave train. Online analysis of the acoustic data is made by a DSP (Digital Signal Processor). Sophisticated algorithms allow the system to detect the reflection from the acoustic window and to separate all subsequent echoes. This probe features automatic optimization of the measurement window under

all borehole conditions with very high travel time resolution and the caliper resolution is better than 0.1 mm.

The probe contains an APS 544 3-axis magnetometer to monitor magnetic north, and all raw televiewer data are referenced to magnetic north. Processed data are referenced to true north, using site and logging date-specific declination (14.25 degrees east) obtained from NOAA (<https://www.ngdc.noaa.gov/geomag/calculators/magcalc.shtml#declination>). Also, a three-axis accelerometer is enclosed in the probe to record boring deviation data while logging; this permits correction of structure dip angle from apparent dip, referenced to boring axis, to true dip (referenced to a vertical axis) in non-vertical borings. The probe is centered in the borehole by two sets of flat spring centralizers.

Optical Televiewer / Boring Deviation

Optical televiewer data were collected in one borehole using an RG Optical Televiewer (OTV) slimhole probe controlled by RG's OPTV program.

The probe receives control signals from, and sends the digitized measurement values to, a Micrologger II (MLII) unit on the surface via an armored multi-conductor cable. The cable is wound onto the drum of a winch and is used to support the probe. Cable travel is measured to provide depth using a sheave of known circumference fitted with a digital rotary encoder. The probe and depth data are transmitted by USB link from the MLII unit to a laptop computer where it is displayed and stored.

The high-resolution optical televiewer system uses a unique optical system based on a fisheye lens allowing the probe to survey 360 degrees simultaneously. The probe provides a continuous very high-resolution image of the borehole wall using a white LED light source. The image is referenced to magnetic north, allowing the cylinder to be “unwrapped” with north as the edge of the unwrapped image. Circular resolutions of 360 to 1440 pixels are available. In order to generate the highest resolution image, a circular resolution of 1440 pixels is used in these surveys.

The probe contains a fluxgate magnetometer to monitor magnetic north, and all raw televiewer data are referenced to magnetic north. Also, a three-axis accelerometer is enclosed in the probe to record boring deviation data while logging, this permits correction of structure dip angle from apparent dip, referenced to boring axis, to true dip (referenced to a vertical axis) in non-vertical borings. The probe is centered in the borehole by two sets of flat spring centralizers. Processed images and deviation data remain referenced to magnetic north while processed data are referenced to true north, using site and logging date-specific declination (14.25 degrees east) obtained from NOAA:

(<https://www.ngdc.noaa.gov/geomag/calculators/magcalc.shtml#declination>).

Optical televiewer data were collected by Crux in three boreholes using an ALT OBI40 optical borehole imager.

The optical borehole imager generates a continuous true color image of the borehole wall via an optical imaging system using a downhole CCD camera that records the image of the borehole wall in a prism. A built-in high precision orientation package incorporating a 3-axis magnetometer and 3-axis accelerometer allows orientation of the images to a global reference and determination of the borehole's azimuth and inclination. Resolutions up to 0.5 mm vertical and 720 pixels azimuthal can be achieved. The tool is fully downhole digital and runs on standard wirelines.

The tool incorporates a high resolution, high sensitivity CCD digital camera with matching Pentax optics. The CCD camera, located above a conical mirror, captures the reflection of the borehole wall. The light source is provided by a light ring assembly located in the optical head. The camera CCD sensor consists of an array of light sensors, each representing one pixel of the complete image. Due to manufacturing limitations individual sensors have a slightly different response and calibration factor. To produce a coherent image the camera processing system checks all the pixels and compensates for variations (white balance). The displayed log image is derived from a single annulus extracted from the total pixel array. Azimuthal resolutions available are 720, 360, 180 and 90 points per recorded circle. By using processed camera data in combination with deviation sensor data, the tool can generate an unwrapped 360° oriented image.

The probe contains an APS 544 3-axis magnetometer to monitor magnetic north, and all raw televiewer data are referenced to magnetic north. Processed data were referenced to true north, using site and logging date-specific declination (14.25 degrees east) obtained from NOAA (<https://www.ngdc.noaa.gov/geomag/calculators/magcalc.shtml#declination>). Also, a three-axis accelerometer is enclosed in the probe to record boring deviation data while logging, this permits correction of structure dip angle from apparent dip, referenced to boring axis, to true dip (referenced to a vertical axis) in non-vertical borings. The probe is centered in the boring by two sets of flat spring centralizers.

Dual Induction / Natural Gamma

Formation conductivity and natural gamma data were collected in three boreholes using a dual induction probe (DUIN), manufactured by RG. This tool can operate in fluid- or air-filled boreholes and works best in relatively conductive media such as sedimentary formations consisting of sands, silts and clays.

The probe receives control signals from, and sends the digitized measurement values to, an RG MLII on the surface via an armored 4 conductor cable. The cable is wound onto the drum of a winch and is used to support the probe. Cable travel is measured to provide probe depth data, using a sheave of known circumference fitted with a digital rotary encoder. The probe and depth data are transmitted by USB link from the MLII unit to a laptop computer where it is displayed and stored on hard disk.

An electromagnetic (EM) induction probe consists of transmitter and receiver coils. An alternating current is applied to the transmitter coil, causing the coil to radiate a primary EM field. This primary EM field generates eddy currents in subsurface materials, which give rise to a secondary EM field. The secondary EM field is measured as an alternating current in the receiver coils, which is proportional to formation conductivity. The probe coil spacing is optimized to achieve high vertical resolution, minimal borehole influence and large radius of investigation. The RG focused dual induction probe has effective coil spacings of 1.6 and 2.6 feet, operates at a frequency of 39 kHz, has 1 millisiemens/meter resolution, and operates over a 5 to 3000 millisiemens/meter conductivity range.

Natural gamma measurements rely upon small quantities of radioactive material contained in soil and rocks to emit gamma radiation as they decay. Trace amounts of uranium and thorium are present in a few minerals, where potassium-bearing minerals such as feldspar, mica and clays will include traces of a radioactive isotope of potassium. These isotopes have an extremely long half-life and emit gamma radiation as they decay. This radiation is detected by scintillation - the production of a tiny flash of light when gamma rays strike a crystal of sodium iodide. The light is converted into an electrical pulse by a photomultiplier tube. Pulses above a threshold value of 60 KeV are counted by the probe's microprocessor. The measurement is useful because the radioactive elements are

concentrated in certain soil and rock types, e.g., clay or shale, and depleted in others, e.g., sandstone or coal.

Caliper / Natural Gamma

Caliper and natural gamma data were collected using a Model 3ACS three-leg caliper probe, manufactured by RG. With the short arm configuration used in the survey, the probe permitted measurement of boring diameters between 1.6 and 8 inches. With this tool, caliper measurements were collected concurrent with measurement of natural gamma emission from the boring walls. The length of the probe as used in this survey is 6.82 feet.

The probe receives control signals from, and sends the digitized measurement values to, an RG MLII unit on the surface via an armored multi-conductor cable. The cable is wound onto the drum of a winch and is used to support the probe. Cable travel is measured to provide probe depth data, using a sheave of known circumference fitted with a digital rotary encoder. The probe and depth data are transmitted by USB link from the MLII unit to a laptop computer where it is displayed and stored on hard disk.

The caliper consists of three arms, each with a toothed quadrant at their base, pivoted in the lower probe body. A toothed rack engages with each quadrant, thus constraining the arms to move together. Linear movement of the rack is coupled to opening and closing of the arms. Springs hold the arms open in the operating position. A motor drive is provided to retract the arms, allowing the probe to be lowered into the boring. The rack is coupled to a potentiometer which converts movement into a voltage sensed by the probe's microprocessor.

Natural gamma measurements rely upon small quantities of radioactive material in soil/rock to emit gamma radiation during decay. Trace amounts of uranium and thorium are present in a few minerals, where potassium-bearing minerals such as feldspar, mica and clays will include traces of a radioactive isotope of potassium. These emit gamma radiation during decay with an extremely long half-life. This radiation is detected by scintillation - the production of a tiny flash of light when gamma rays strike a crystal of sodium iodide. The light is converted into an electrical pulse by a

photomultiplier tube. Pulses above a threshold value of 60 KeV are counted by the probe's microprocessor. The measurement is useful because the radioactive elements are concentrated in certain soil/rock types e.g., clay or shale and depleted in others e.g., sandstone or coal.

MEASUREMENT PROCEDURES

Suspension Velocity

Five boreholes were logged with the PS Suspension tool. Measurements followed the **GEOVision** Procedure for PS Suspension Seismic Velocity Logging, revision 1.5. Prior to logging, the probe was positioned with the top of the probe even with a stationary reference point. The electronic depth counter was set to the distance between the mid-point of the receiver and the top of the probe, minus the height of the stationary reference point, if any, verified with a tape measure, and recorded on the field logs. The probe was lowered to the bottom of the boring, stopping at 1.6-foot intervals to collect data, as summarized in Table 2.

At each measurement depth the measurement sequence of two opposite horizontal records and one vertical record was performed, and the gains were adjusted as required. The data from each depth were viewed on the computer display, checked, and recorded to disk before moving to the next depth.

Upon completion of the measurements, the probe zero depth indication at the depth reference point was verified prior to removal from the boring.

Acoustic Televiwer / Boring Deviation

All boreholes were logged from total depth to bottom of casing or fluid level. The ATV probe requires a fluid filled boring for proper operation. Acoustic televiwer was collected by Crux Subsurface, Inc.

Prior to logging, the ATV probe was positioned with the top of the probe even with a stationary reference point and the electronic depth counter was set to the specified length of the probe, minus the height of the reference point. Once verified with a tape measure, these calculations were recorded on a field log. The probe was lowered to the bottom of the borehole while collecting a low vertical

resolution image. At the bottom of the borehole, this image was closed, and a high vertical resolution image was acquired on ascent. The probe was raised at a rate of approximately 3 feet per minute to the surface, or bottom of casing, with an acquisition rate of 250 samples/foot, giving an equivalent vertical pixel size of 0.004 feet (0.048 inches). The rotational scan resolution was set to the maximum, 360 samples per revolution, giving a horizontal pixel size of 0.035 inches.

Upon completion of the measurements, the probe zero depth indication at the depth reference point was verified prior to removal from the boring.

Optical Televiewer

The OTV probe does not require a fluid filled boring for proper operation. Borings were logged with the optical televiewer from total depth to ground surface. Data in three of four boreholes logged with optical televiewer were acquired by Crux Subsurface, Inc. Measurements in one borehole collected by **GEOVision** followed the following procedure.

The OTV probe was positioned with the top of the probe even with a stationary reference point, and the electronic depth counter was set to the specified length of the probe minus the height of the reference point. These calculations were recorded on a field log. The probe was lowered to the bottom of the uncased stable borehole. Once at the bottom of the borehole, the probe was raised at approximately 3 feet/minute to the surface, with an acquisition rate of 820 samples/foot, giving an equivalent vertical pixel size of 0.0012 feet (approximately 0.0144 inches). Horizontal image resolution was set to the maximum 1,440 pixels, giving a horizontal pixel size of approximately 0.009 inches

Upon completion of the measurements, the probe zero depth indication at the depth reference point was verified prior to removal from the boring.

Dual Induction / Natural Gamma

DUIN NG data were acquired in three boreholes. Measurement procedures followed these ASTM standards:

- ASTM D5753-18 (Re-approved 2018), “Planning and Conducting Boring Geophysical Logging”
- ASTM D6274-18 (Re-approved 2018), “Conducting Boring Geophysical Logging – Gamma”
- ASTM D6726-15 (Re-approved 2015), “Conducting Boring Geophysical Logging – Electromagnetic Induction”

Prior to logging, the probe was positioned with the top of the probe even with a stationary reference point and the electronic depth counter was set to the specified length of the probe, minus the height of the reference point. Once verified with a tape measure, these calculations were recorded on a field log. Offset distances between probe tip and measurement points are adjusted by the acquisition software. The probe was lowered to the bottom of the borehole and data were acquired on ascent. The probe was returned to the surface at approximately 10 - 15 feet/minute, collecting data continuously at 0.05-foot spacing, as summarized in Table 2.

This probe was not calibrated in the field, as it is used to provide qualitative measurements, not quantitative values, and is used only to assist in picking transitions between stratigraphic units, as described in ASTM D5753-05 (Reapproved 2018), “Planning and Conducting Borehole Geophysical Logging”. A functional test was performed prior to logging by placing a coil with an effective conductivity value over the probe and recording the output. Results were noted on field logs.

Natural gamma was not calibrated in the field, as it is a qualitative measurement, not a quantitative value, and is used only to assist in picking transitions between stratigraphic units, as described in ASTM D6274-10, “Conducting Borehole Geophysical Logging – Gamma”.

Upon completion of the measurements, the probe zero depth indication at the depth reference point was verified prior to removal from the boring.

Caliper / Natural Gamma

Caliper NG data were acquired in four boreholes. Measurement procedures followed these ASTM standards:

- ASTM D5753-18, “Planning and Conducting Geotechnical Borehole Geophysical Logging”
- ASTM D6167-11, “Conducting Borehole Geophysical Logging, Mechanical Caliper”
- ASTM D6274-18, “Conducting Borehole Geophysical Logging, Gamma”

The probe was not calibrated in the field, as it is used to provide qualitative measurements, not quantitative values, and is used only to assist in picking transitions between stratigraphic units, as described in ASTM D5753-18, “Planning and Conducting Geotechnical Borehole Geophysical Logging”.

Prior to and following the logging run(s) in the borehole, the caliper tool was verified using an approved **GEO***Vision* verification plate. The verification plate is a circular aluminum plate with a series of four machined annular slots in the top surface into which the tips of the caliper arms fit. The slots have outside diameters from 2.1 to 8.0 inches. The verification plate is placed on the probe with its nose section passing through the plates’ central hole. The caliper probe arms are opened under program control, and a log is recorded as the tips of the arms are placed in the slots on the plate. The measured dimensions, as displayed on the recording computer screen, were recorded on the field log sheet, as well as in the digital files, and compared with the verification plate known dimensions. These functional verification checks are recorded on the field logs.

If the verification records did not fall within +/- 0.05 inches of the verification jig values, the caliper tool is re-adjusted using the four-point verification plate, then the verification log is repeated. As with the initial verification, the tips of the caliper arms are placed in the holes marked with the required diameter. During re-adjustment, the value of the current point, as stamped on the verification plate, is entered via the control computer. The system counts for 15 seconds to make an

average of the response. The procedure is repeated for the remaining openings. The computation and generation of the adjustment file is entirely automatic. The adjustment file is simply the set of coefficients of a quadratic curve which fits the three data points.

Natural gamma was not calibrated in the field, as it is a qualitative measurement, not a quantitative value, and is used only to assist in picking transitions between stratigraphic units, as described in ASTM D6274-18, “Conducting Borehole Geophysical Logging, Gamma”.

Prior to each logging run, the sensor positions were referenced to ground level. This was done by placing the top of the probe at grade, and the electronic depth counter was set to the probe length. These calculations are recorded on the field logs. Offset distances between probe tip, the caliper arms and natural gamma sensors are corrected for in the data acquisition software. The probe was lowered into the borehole and data acquisition performed as the probe was returned to the surface at approximately 10 to 15 feet/minute, collecting data continuously at 0.05-foot intervals, as summarized in Table 2.

Upon completion of the measurements, the probe zero depth indication at the depth reference point was verified prior to removal from the boring. Field data were backed up daily to USB drive.

DATA ANALYSIS

Suspension Velocity

Using the proprietary OYO program PSLOG.EXE version 1.0, the recorded digital waveforms were analyzed to locate the most prominent first minima, first maxima, or first break on the vertical axis records, indicating the arrival of P-wave energy. The difference in travel time between receiver 1 and receiver 2 (R1-R2) arrivals was used to calculate the P-wave velocity for that 1.0-meter segment of the soil column. When observable, P-wave arrivals on the horizontal axis records were used to verify the velocities determined from the vertical axis data. The time picks were then transferred into a Microsoft Excel® template to complete the velocity calculations based on the arrival time picks made in PSLOG. The Microsoft Excel® analysis files were previously delivered. Due to the longevity of this project, results were delivered at intervals as requested.

The P-wave velocity over the 6.3-foot interval from source to receiver 1 (S-R1) was also picked using PSLOG, and calculated and plotted in Microsoft Excel®, for a check of the reasonableness of the velocity derived from the travel time between receivers. In this analysis, the depth values as recorded were increased by 4.8 feet to correspond to the mid-point of the 6.3-foot S-R1 interval. Travel times were obtained by picking the first break of the P-wave signal at receiver 1 and subtracting 0.35 milliseconds, the calculated and experimentally verified delay from source trigger pulse (beginning of record) to source impact. This delay corresponds to the duration of acceleration of the solenoid before impact.

As with the P-wave records, the recorded digital waveforms were analyzed to locate clear S_H -wave pulses, as indicated by the presence of opposite polarity pulses on each pair of horizontal records. Ideally, the S_H -wave signals from the 'normal' and 'reverse' source pulses are very nearly inverted images of each other. Digital Fast Fourier Transform – Inverse Fast Fourier Transform (FFT – IFFT) lowpass filtering was used to remove the higher frequency P-wave signal from the S_H -wave signal. Different filter cutoffs were used to separate P- and S_H -waves at different depths, ranging from 600 Hz in the slowest zones to 4000 Hz in the regions of highest velocity. At each depth, the filter frequency was selected to be at least twice the fundamental frequency of the S_H -wave signal being filtered.

Generally, the first maxima were picked for the 'normal' signals and the first minima for the 'reverse' signals, although other points on the waveform were used if the first pulse was distorted. The absolute arrival time of the 'normal' and 'reverse' signals may vary by ± 0.2 milliseconds, due to differences in the actuation time of the solenoid source caused by constant mechanical bias in the source or by boring inclination. This variation does not affect the R1-R2 velocity determinations, as the differential time is measured between arrivals of waves created by the same source actuation. The final velocity value is the average of the values obtained from the 'normal' and 'reverse' source actuations.

As with the P-wave data, S_H -wave velocity calculated from the travel time over the 6.3-foot interval from source to receiver 1 was plotted for verification of the velocity derived from the travel time between receivers. In this analysis, the depth values were increased by 4.8 feet to correspond to the mid-point of the 6.3-foot S-R1 interval. Travel times were obtained by picking the first break of the S_H -wave signal at the near receiver and subtracting 0.35 milliseconds, the calculated and experimentally verified delay from the beginning of the record at the source trigger pulse to source impact.

Figure 3 shows an example of R1-R2 measurements on a sample filtered suspension record. In Figure 3, the time difference over the 3.3-foot interval of 1.88 milliseconds for the horizontal signals is equivalent to an S_H -wave velocity of 1745 feet/second. Whenever possible, time differences were determined from several phase points on the S_H -waveform records to verify the data obtained from the first arrival of the S_H -wave pulse. Figure 4 displays the same record before filtering of the S_H -waveform record with a 1400 Hz FFT - IFFT digital lowpass filter, illustrating the presence of higher frequency P-wave energy at the beginning of the record, and distortion of the lower frequency S_H -wave by residual P-wave signal.

Acoustic Televiewer

Acoustic televiewer feature classification followed **GEOVision** Televiewer Feature Notes and Picking Criteria (Appendix B). Acoustic televiewer data were processed using WellCAD Image & Structure Interpretation (ISI) Workspace. Sinusoidal projections of planar features on the borehole walls were interactively picked on the un-wrapped televiewer image and presented on the logs as colored sinusoids superimposed over the televiewer image. Sinusoidal projections were processed using the determined borehole gauge to calculate apparent dip angle. True dip was calculated, correcting for the plunge of the boreholes using recorded data from the accelerometers located in the probe, and presented in tadpole format, with true dip indicated by the tadpole position across the plot. The azimuth of dip (not strike) is indicated by the direction of the tadpole tail, with true north being “up.”

Televiewer data were also processed to extract deviation data and produce Excel data files and plots of borehole deviation.

Optical Televiewer

Optical televiewer feature classification followed **GEOVision** Televiewer Feature Notes and Picking Criteria (Appendix C). The optical televiewer data were processed using WellCAD Image & Structure Interpretation (ISI) Workspace. Sinusoidal projections of planar features on the boring walls were interactively picked on the un-wrapped televiewer image and presented on the logs as colored sinusoids superimposed over the televiewer image. Sinusoidal projections were processed using the determined boring gauge (from mechanical caliper log) to calculate apparent dip angle. True dip was calculated, correcting for the plunge of the borings using the recorded data from the accelerometers located in the probe, and presented in tadpole format, with true dip indicated by the arrow position across the plot. Azimuth of dip (not strike) is indicated by the direction of the tadpole tail, with true north being “up”.

Dual Induction / Natural Gamma

DUIN and NG data do not require analysis; however, depths to identifiable boring log features, such as distinct natural gamma transitions, were compared to verify consistent depth readings on all logs. Using WellCAD™ software, data were combined with caliper logs, where available. Where multiple data sets were collected over several depth intervals, each logging run is presented, as appropriate. Data were exported as LAS 2.0 and logs as PDF.

Caliper / Natural Gamma

No analysis is required with the caliper or natural gamma data; however, depths to identifiable boring log features, such as distinct natural gamma transitions, were compared to verify consistent depth readings. Using WellCAD™ software data, were combined with DUIN logs, where available. Where multiple data sets were collected over several depth intervals, each logging run is presented. Data were exported as LAS 2.0 and logs as PDF.

RESULTS

Borehole geophysical results are presented graphically in Figures 5 through 48, and in tabular format in Tables 4 through 16. Borehole geophysical results are grouped by borehole.

Suspension Velocity

Suspension R1-R2 P- and S_H -wave velocities for borings RC-20-014 (B-29), RC-20-011 (B-32), and RC-20-019 (B-50) are presented in Figures 13, 19 and 38, respectively. The suspension velocity data presented in these figures are also presented in Tables 6, 8 and 13, respectively. The Microsoft Excel® analysis files are provided in the data directory that accompanies this report.

P- and S_H -wave velocity data from R1-R2 analysis and S-R1 analysis are plotted together in Appendix A as Figures A-1 through A-3. It should be noted that R1-R2 data are an average velocity over a 3.3-foot segment of the soil column; S-R1 data are an average over 6.3 feet, creating a significant smoothing relative to the R1-R2 plots. The S-R1 velocity data displayed in these figures are also presented in Appendix A as Tables A-1 through A-3 and included in the Microsoft Excel® analysis files in the data directory. The Microsoft Excel® analysis files include Poisson's Ratio calculations, tabulated data, plots, and waveforms.

Acoustic Televiwer / Optical Televiwer / Boring Deviation

Acoustic televiwer and/or optical televiwer, and boring deviation data were collected and analyzed for seven boreholes. Acoustic televiwer was collected in boreholes RC-20-017 (B-18), RC-20-014 (B-29), RC-20-011 (B-32), RC-21-001 (B-47), and RC-20-019 (B-50), and optical televiwer was collected in boreholes RC-20-005 (B-28), RC-20-011 (B-32), RC-21-001 (B-47), and RC-20-016 (WP-3). Televiwer feature classification followed **GEOVision** Televiwer Feature Notes and Picking Criteria, presented in Appendix B. Sinusoidal features and corrected tadpoles are displayed on the televiwer feature log sheets in Appendix B. Corrected feature depth, dip, and azimuth of dip data are provided in the Tables section of this report. Depths on all figures and tables are referenced to ground surface.

The stereonet plots (Schmidt Plot, Upper Hemisphere) associated are contoured using a yellow to red gradient and are presented in the Figures section of this report, as well as the associated rose diagrams. Both were exported to PDF and are included in the boring specific sub-directories in the data submittal that accompanies this report.

Borehole deviation data extracted from the televiewer logs are presented graphically in the Figures section of this report and are summarized in Table 3. Deviation data plots in bitmap format and deviation data tabulated at 0.1-foot intervals in Excel[®] format are included in the boring specific sub-directories in the data submittal that accompanies this report.

Acoustic and optical televiewer deviation data were collected in each logged borehole. All borings were inclined at a dip of less than 1.1 degrees from vertical except for borehole RC-20-005 (B-28), inclined at 2.8 degrees. The greatest error between vertical depth and survey depth (borehole axis distance) due to this dip was 0.23 feet in about 236 vertical feet (0.09% of depth), in borehole RC-20-005 (B-28), as presented in Table 3. No adjustment of log depths is indicated.

Dual Induction / Caliper/ Natural Gamma

DUIN, Caliper, and NG data for the boreholes are presented in Appendix C as singlepage1:10 scaled log plots. Depths on all figures and tables are referenced to ground surface. Data exported as LAS 2.0 format also accompany this report.

DISCUSSION OF RESULTS

Suspension Velocity

Suspension PS velocity data are ideally collected in an uncased fluid filled boreholes, drilled with rotary mud (rotary wash) methods, as was the case for these boreholes.

Suspension PS velocity data quality is judged based upon 5 criteria.

- Consistent data between receiver to receiver (R1-R2) and source to receiver (S-R1) data.
- Consistency between data from adjacent depth intervals.
- Consistent relationship between P-wave and SH -wave (excluding transition to saturated soils)
- Clarity of P-wave and SH -wave onset, as well as damping of later oscillations.
- Consistency of profile between adjacent borings, if available.

Table 16 summarizes the evaluation of each borehole dataset with respect to these criteria.

These data indicate good consistency between R1-R2 and S-R1 velocities, and consistency between adjacent depths in the intervals tested.

P- and S_H-wave velocity measurement using the Suspension Method gives average velocities over a 3.3-foot interval of depth. This high resolution results in the scatter of values shown in the graphs. Individual measurements are very reliable with estimated accuracy of +/- 5%. Standardized field procedures and quality assurance checks contribute to the reliability of these data.

To improve reliability and minimize uncertainty, whenever possible, travel time differences were determined from several arrivals on the S_H-waveform records to verify the data obtained from the first arrival of the S_H-wave pulse. In addition, velocities from travel times from S-R1 were also determined and used to verify the velocities derived from the travel times between receivers R1-R2.

Televiewer / Boring Deviation

Acoustic and/or optical televiewer data were collected in seven boreholes. Imagery was fair in general. In several borings, low water level limited acoustic imaging to the lower portion of the boreholes.

Televiewer depth indications are very reliable with estimated accuracy of ± 0.2 feet. Estimated accuracy of dip is ± 5 degrees and azimuth of dip is ± 10 degrees. Standardized field procedures and quality assurance checks also add to the reliability of these data.

Dual Induction / Caliper/ Natural Gamma

Both gamma and conductivity are qualitative logs, not absolute; meaning relative changes in amplitude are more informative than the absolute values. With that in mind, the following presents some general interpretation guidelines.

Generally, conductivity is higher in materials in which electric and electromagnetic fields flow preferentially. For earth materials, typically hard rock, limestone, dry sands and similar exhibit relatively low conductivity (higher resistivity); whereas metallic ores and clays, and silts exhibit relatively high conductivity (low resistivity). For near surface materials, unconsolidated sediment is typically more conductive than consolidated sediment. Water content and salinity also contribute to increased conductivity, e.g., wet soil and sand is more conductive than dry. Figure 48 shows general conductivity ranges and corresponding soil types. Note there is overlap between soil types. (from <http://emgeo.sdsu.edu/emrockprop.html>, Palacky, G. J., 1988, Resistivity characteristics of geologic targets, in Investigations in Geophysics vol. 3: Electromagnetic methods in applied geophysics-theory, vol. 1, edited by M. N. Nabighian, Soc. Expl. Geophys., 53–129.)

Typical near surface soils and hard rock exhibits low conductivity, usually near the low, or left, axis close to (or less than) zero mS/m. In contrast, fat clays could be in the hundreds to low thousands mS/m.

NG is higher in materials that contain uranium, thorium, or potassium (or similar) bearing minerals, or soils / rocks in which these minerals are concentrated. For example, in near surface measurements NG is higher in clays or shales and lower in sandstones and coals. Typical sands or near surface unconsolidated materials are relatively low. Clay seams may spike very high, with higher values indicating more concentrated radioactive minerals.

Typical near surface soil often hovers around 100 API units or less, but this can vary by location. Fat clays can cause deflections to the right to several hundred API units.

Generally, there is an expected correlation between conductivity and natural gamma. For example, a clay seam would be expected to exhibit a NG high and a corresponding conductivity high, or resistivity low. A sand would be expected to have a relatively flat NG response and a corresponding low conductivity, or high resistivity. However, relative, abrupt changes in amplitude are more indicative of formational or lithologic changes, which may assist with observations in the borehole geologic logs.

The caliper logs for these borings shows the diameter of the uncased boreholes ranging between 4 and 6 inches, except for occasional voids or washouts. Caliper and natural gamma plots show transitions at the same depths and correspond well with changes in velocity. Natural gamma data collected with the caliper probe matches the natural gamma data collected with the induction probe very well, verifying the performance of the natural gamma measuring systems.

Dual Induction and caliper depth indications are very reliable with estimated accuracy of +/- 0.2 feet. Caliper diameter measurements have an estimated accuracy of +/- 0.2 inches. Standardized field procedures and quality assurance checks also add to the reliability of these data.

Quality Assurance

These borehole geophysical measurements were performed using industry-standard or better methods for measurements and analyses. All work was performed under **GEOVision** quality assurance procedures, which include:

- Use of NIST-traceable calibrations, where applicable, for field and laboratory instrumentation
- Use of standard field data logs
- Independent review of calculations and results by a registered professional engineer, geologist, or geophysicist.

Televiewer Data Reliability

Data were acquired in part by Crux Subsurface, Inc. using ALT acoustic and optical televiewers. Overall, from a processing standpoint, data were of good quality supported by consistent field notes provided with the data files.

Depth indications are very reliable, with an estimated accuracy of ± 0.2 feet. The estimated accuracy of dip is ± 5 degrees, and the azimuth of dip is ± 10 degrees. Standardized field procedures and quality assurance checks add to the reliability of these data.

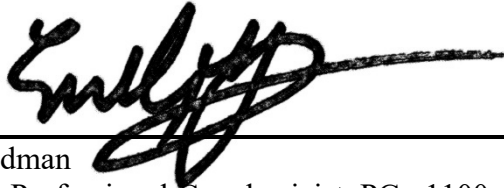
Suspension Velocity Data Reliability

P- and S_H-wave velocity measurement using the Suspension Method gives average velocities over a 3.3-foot interval of depth. This high resolution results in the scatter of values shown in the graphs. Individual measurements are very reliable, with an estimated accuracy of $\pm 5\%$. Depth indications are very reliable with an estimated accuracy of ± 0.2 feet. Standardized field procedures and quality assurance checks contribute to the reliability of these data.

CERTIFICATION

All geophysical data, analysis, interpretations, conclusions, and recommendations in this document have been prepared under the supervision of and reviewed by a **GEOVision** California Professional Geophysicist.

Prepared by



Emily Feldman
California Professional Geophysicist, PGp 1100
GEOVision Geophysical Services



4/6/2022

Date

Reviewed and approved by



Victor M Gonzalez
California Professional Geophysicist, PGp 1074
GEOVision Geophysical Services



4/6/2022

Date

- * This geophysical investigation was conducted under the supervision of a California Professional Geophysicist or Engineer using industry standard methods and equipment. A high degree of professionalism was maintained during all aspects of the project from the field investigation and data acquisition, through data processing, interpretation and reporting. All original field data files, field notes and observations, and other pertinent information are maintained in the project files and are available for the client to review for a period of at least one year.

A professional geophysicist's certification of interpreted geophysical conditions comprises a declaration of his/her professional judgment. It does not constitute a warranty or guarantee, expressed or implied, nor does it relieve any other party of its responsibility to abide by contract documents, applicable codes, standards, regulations or ordinances.

FIGURES

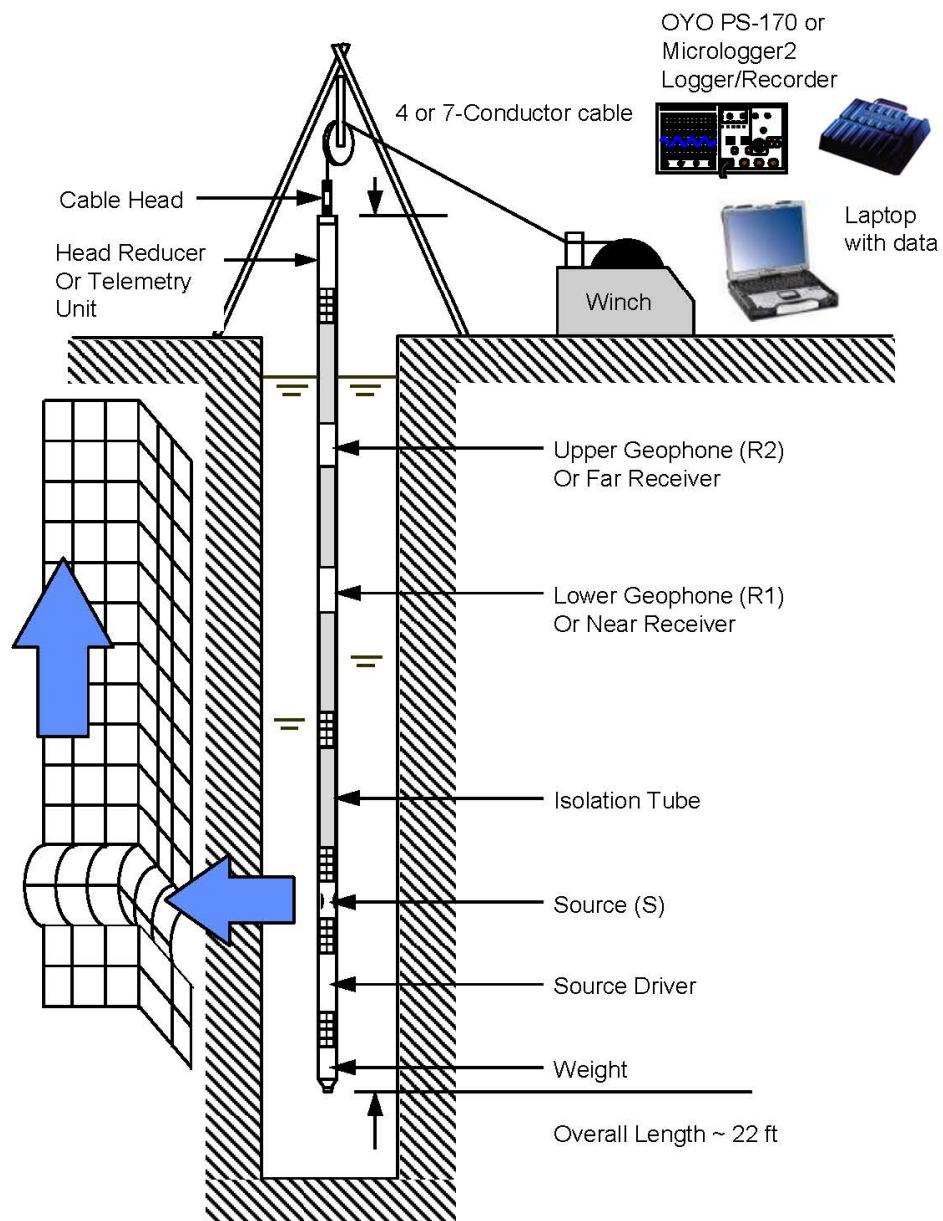


Figure 1. Concept illustration of P-S logging system

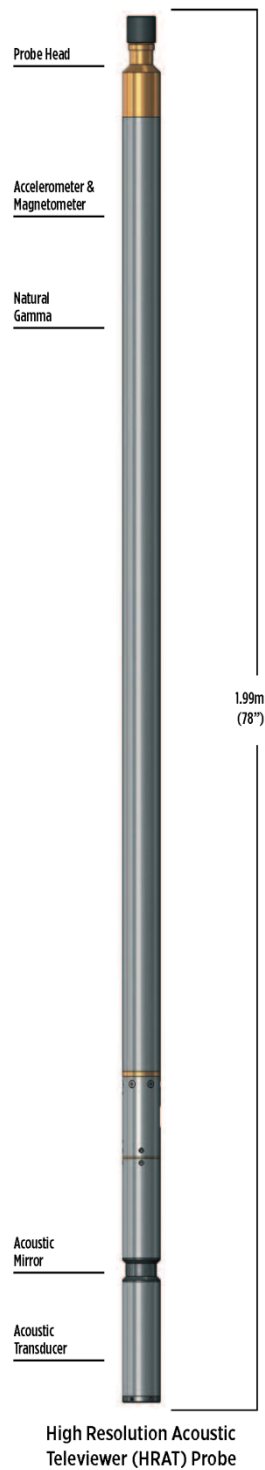


Figure 2. Concept illustration of televiewer probe

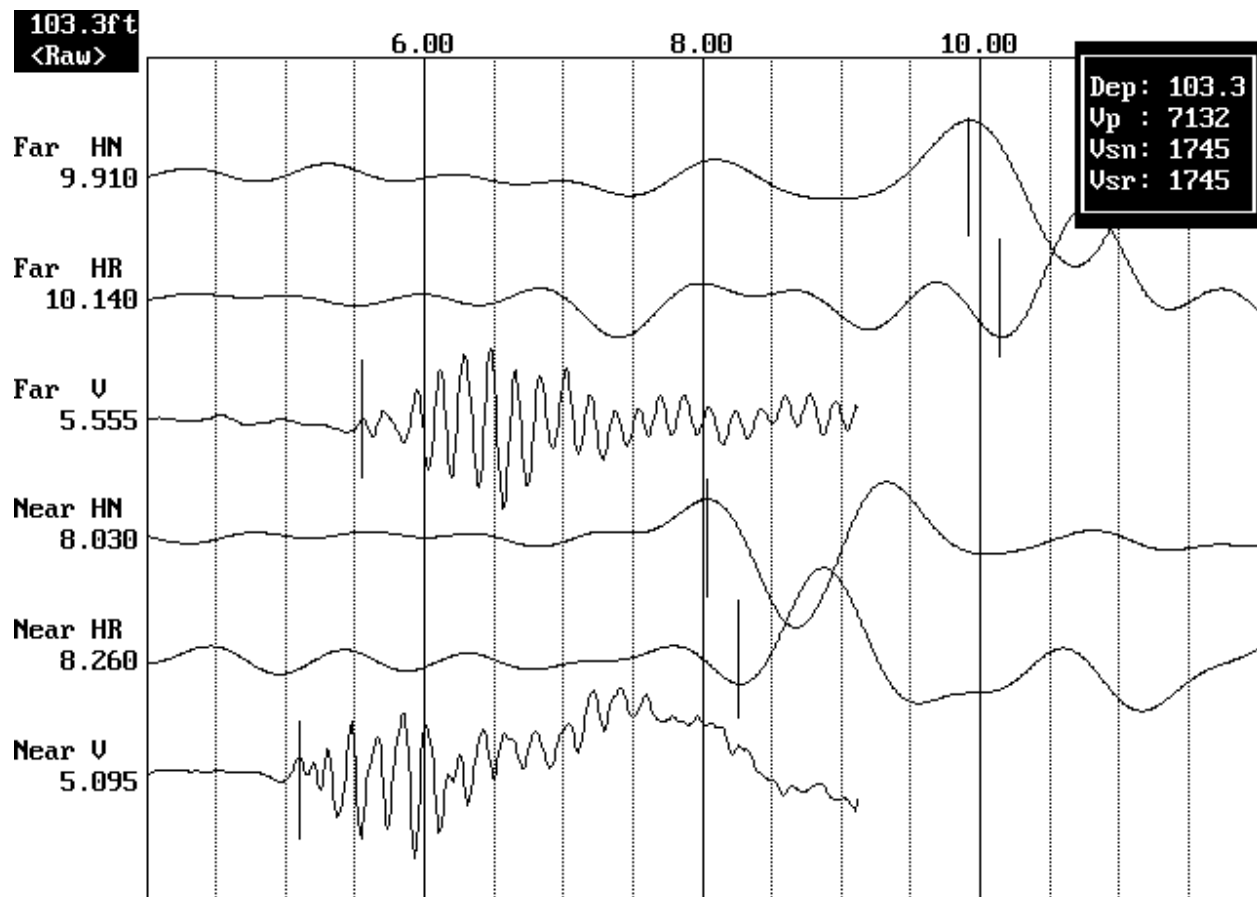


Figure 3. Example of filtered (1400 Hz lowpass) suspension record

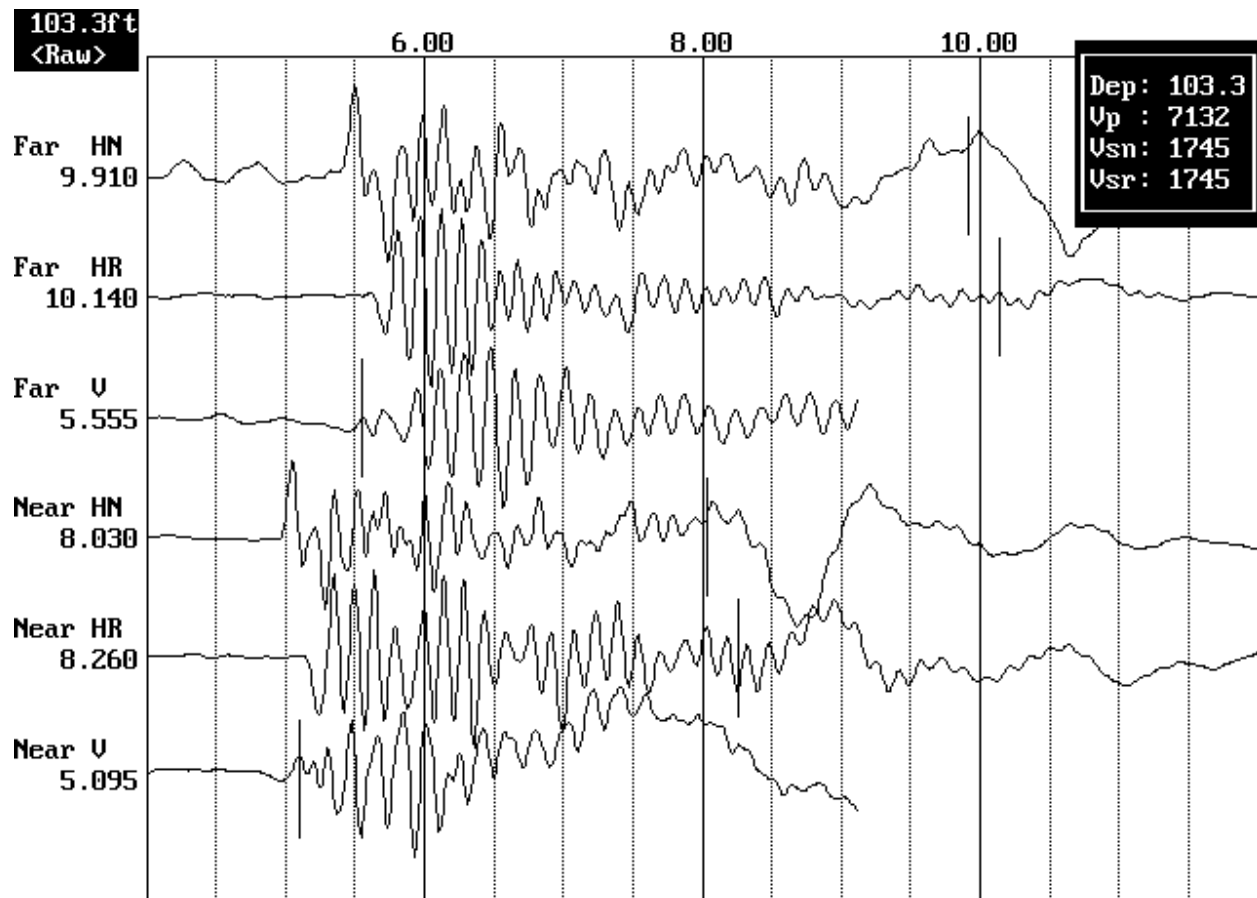


Figure 4. Example of unfiltered suspension record

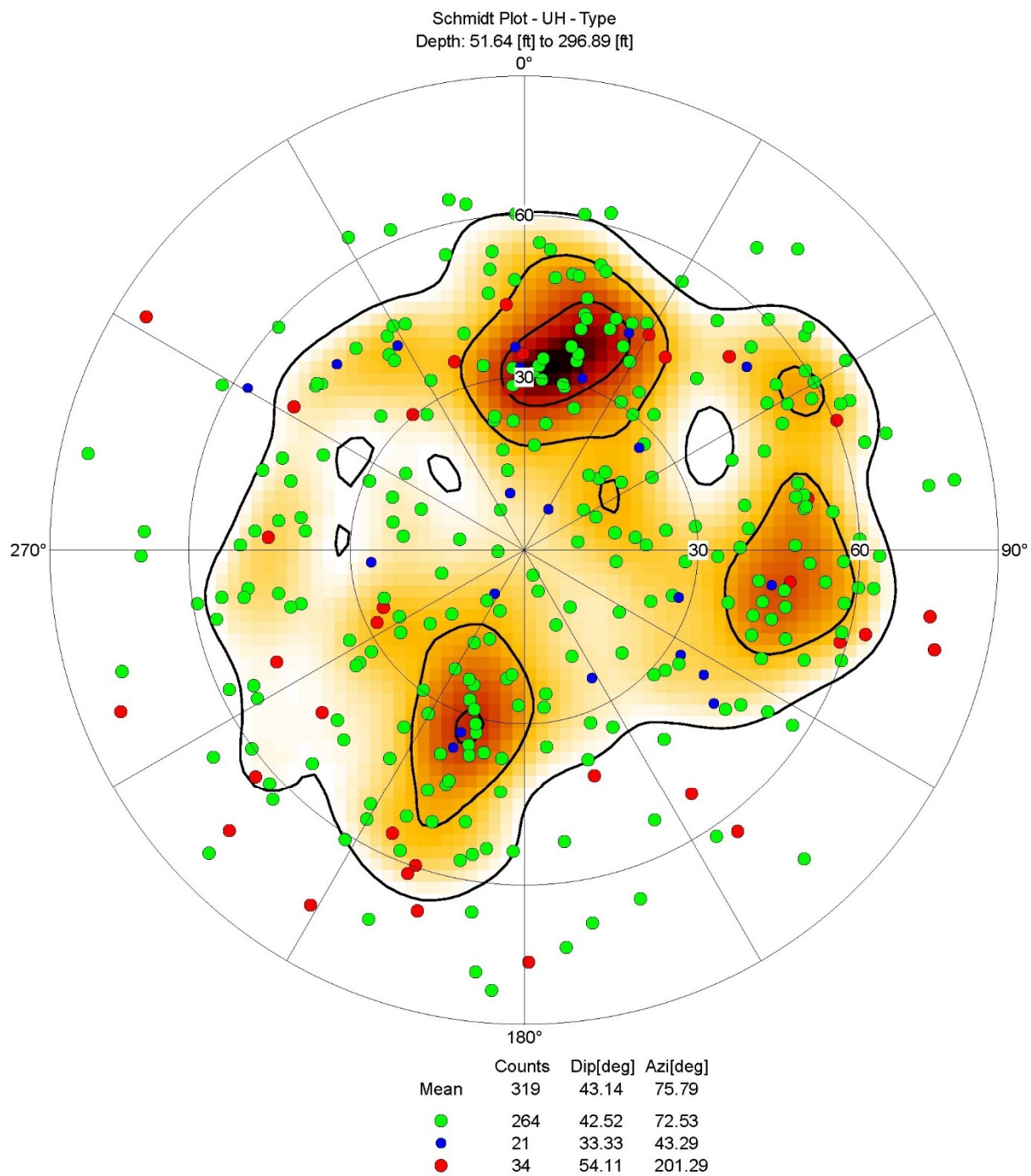


Figure 5. Borehole RC-20-017 (B-18), Acoustic Stereonet Diagram

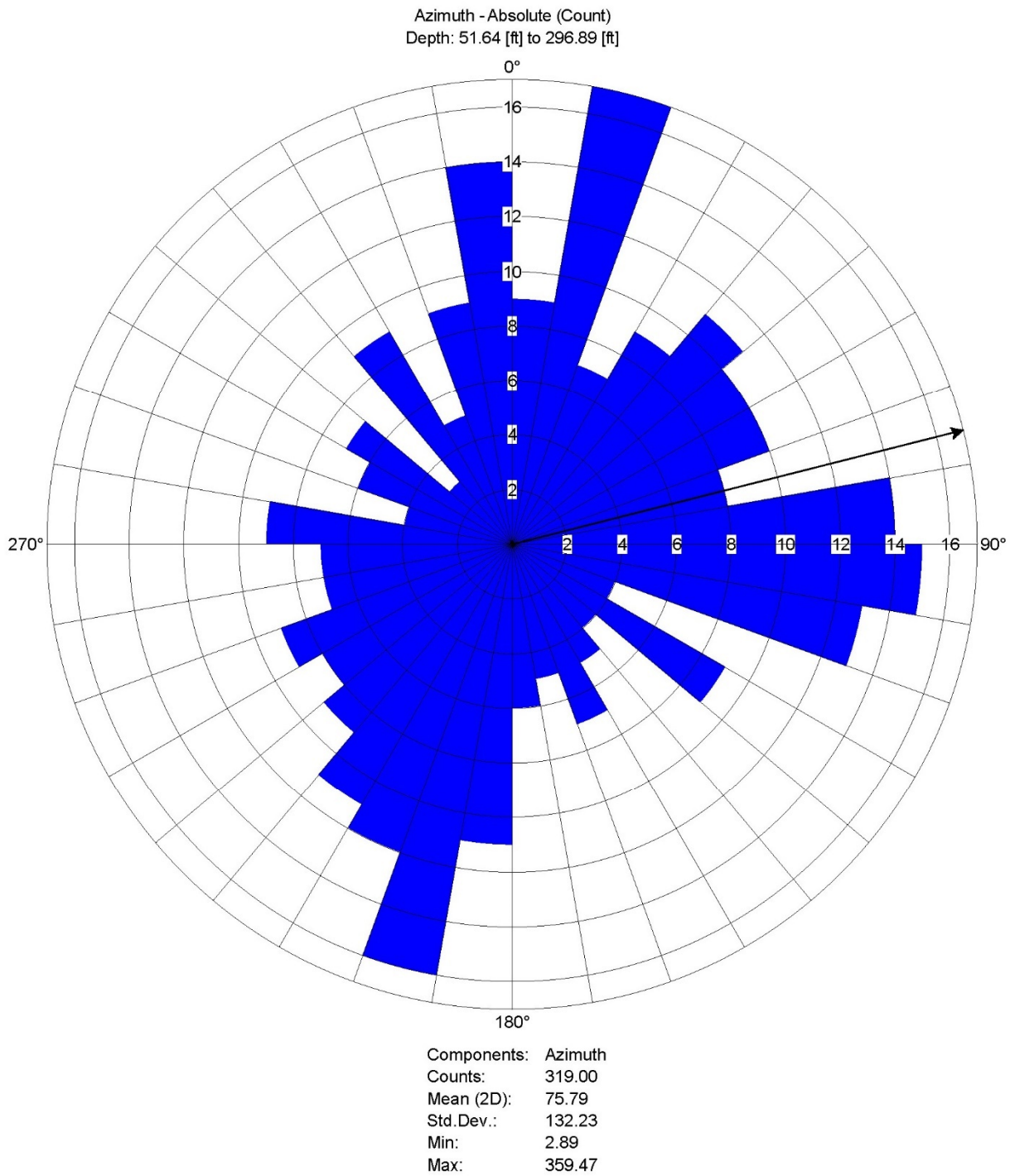


Figure 6. Borehole RC-20-017 (B-18), Acoustic Rose Diagram

Depth [m] 1:568
Horiz [m] 1:2

B-18

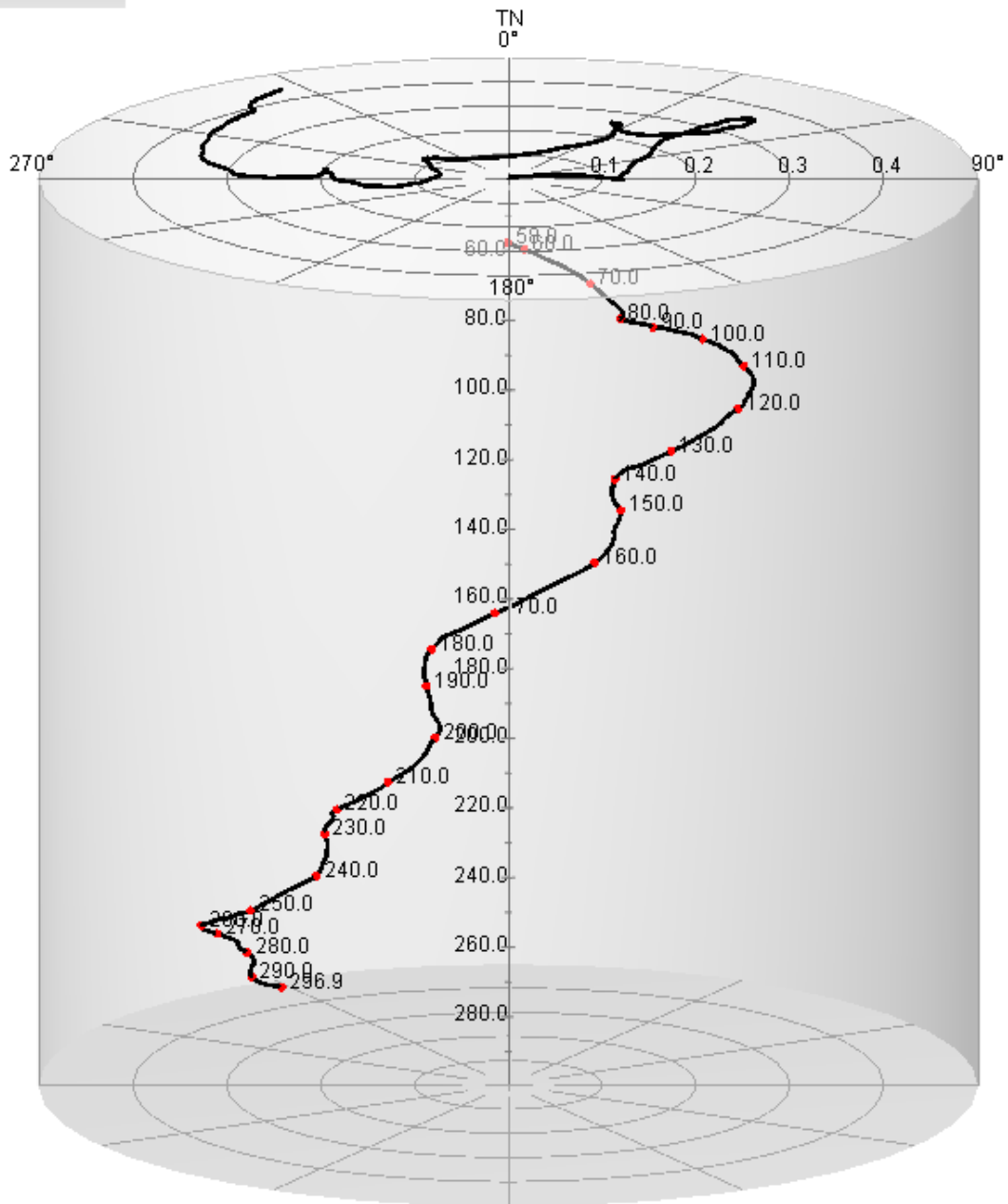


Figure 7. Borehole RC-20-017 (B-18), Deviation Cylindrical Projection

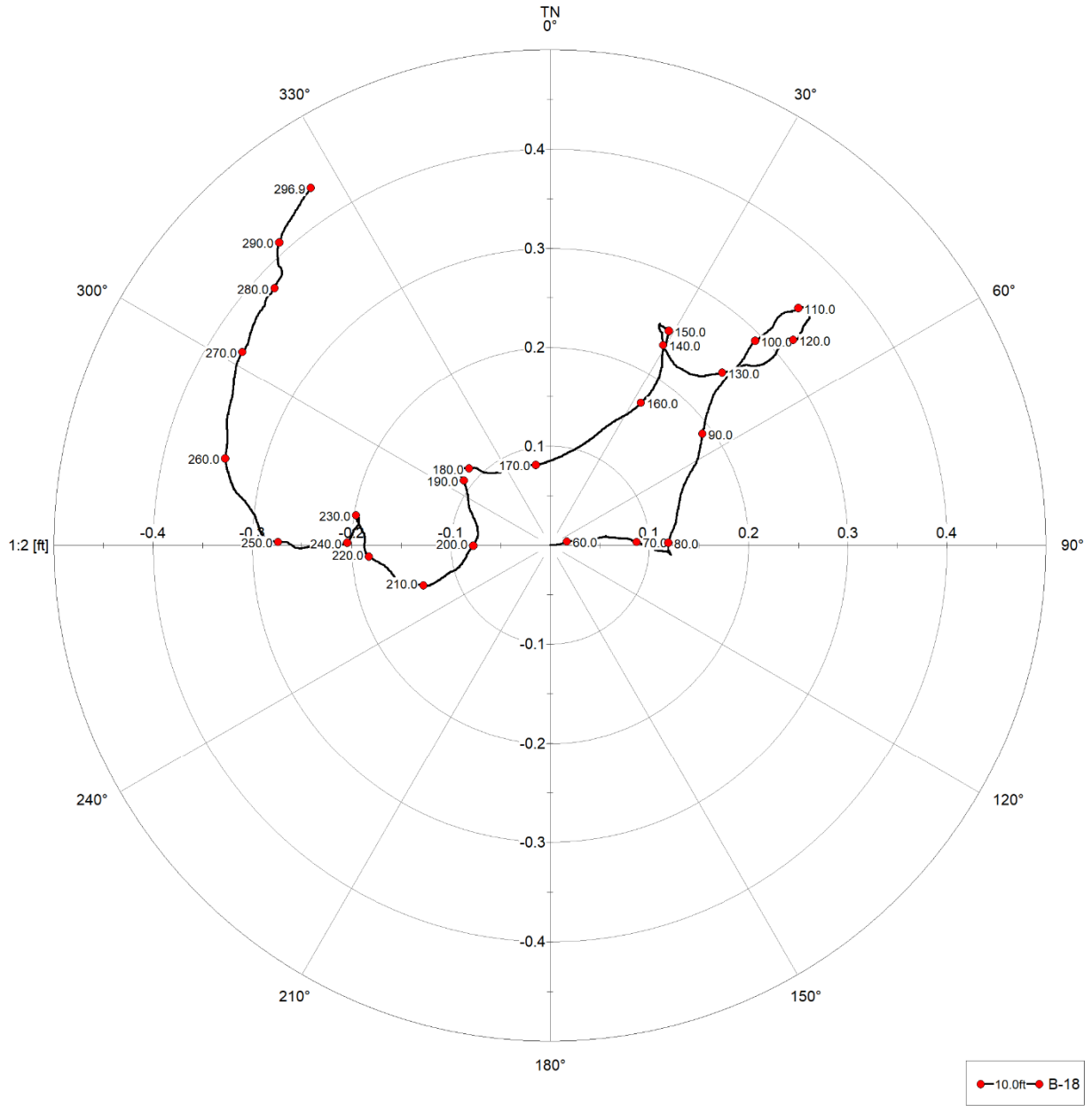


Figure 8. Borehole RC-20-017 (B-18), Deviation Bullseye Projection

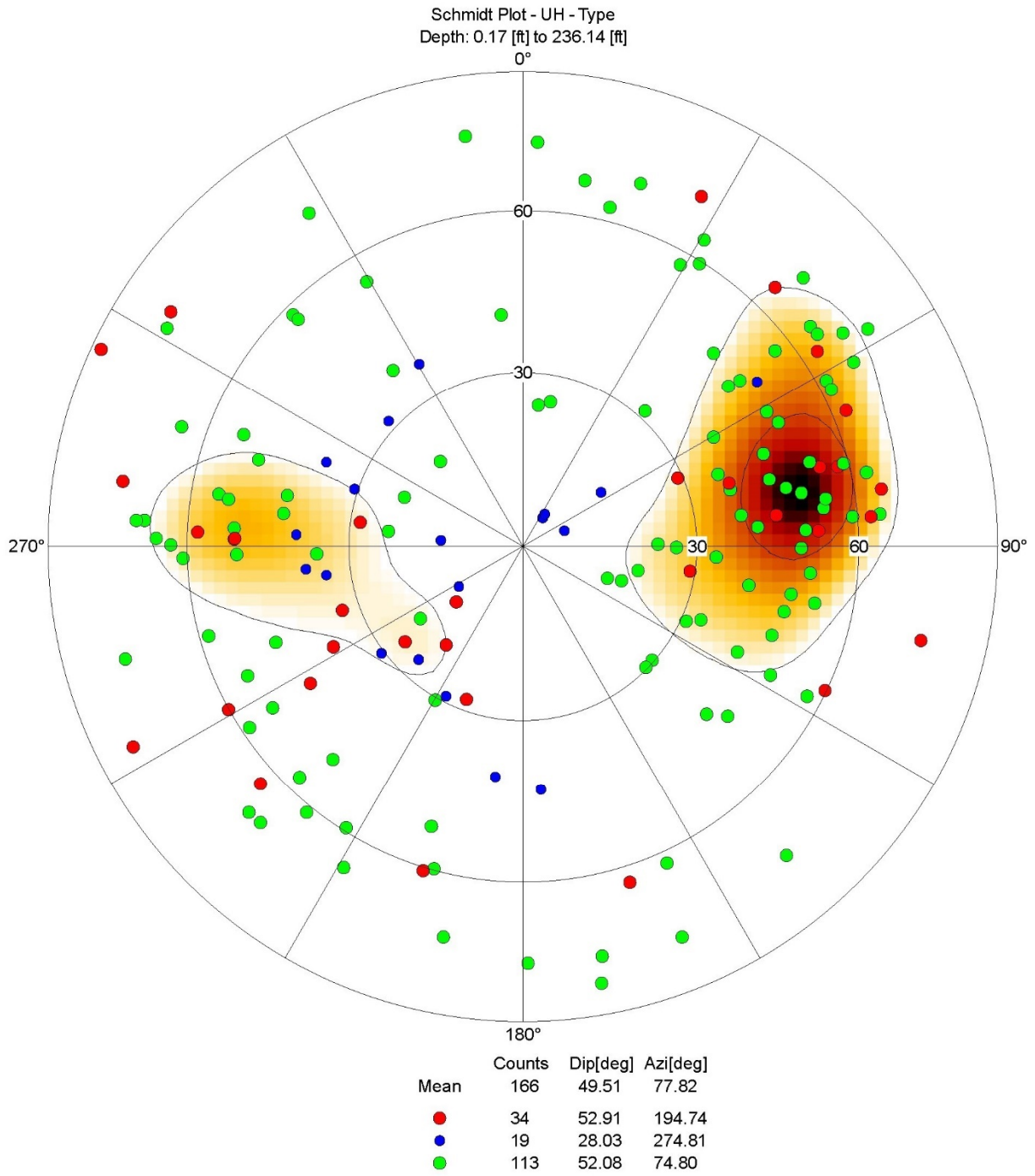


Figure 9. Borehole RC-20-005 (B-28), Optical Stereonet Diagram

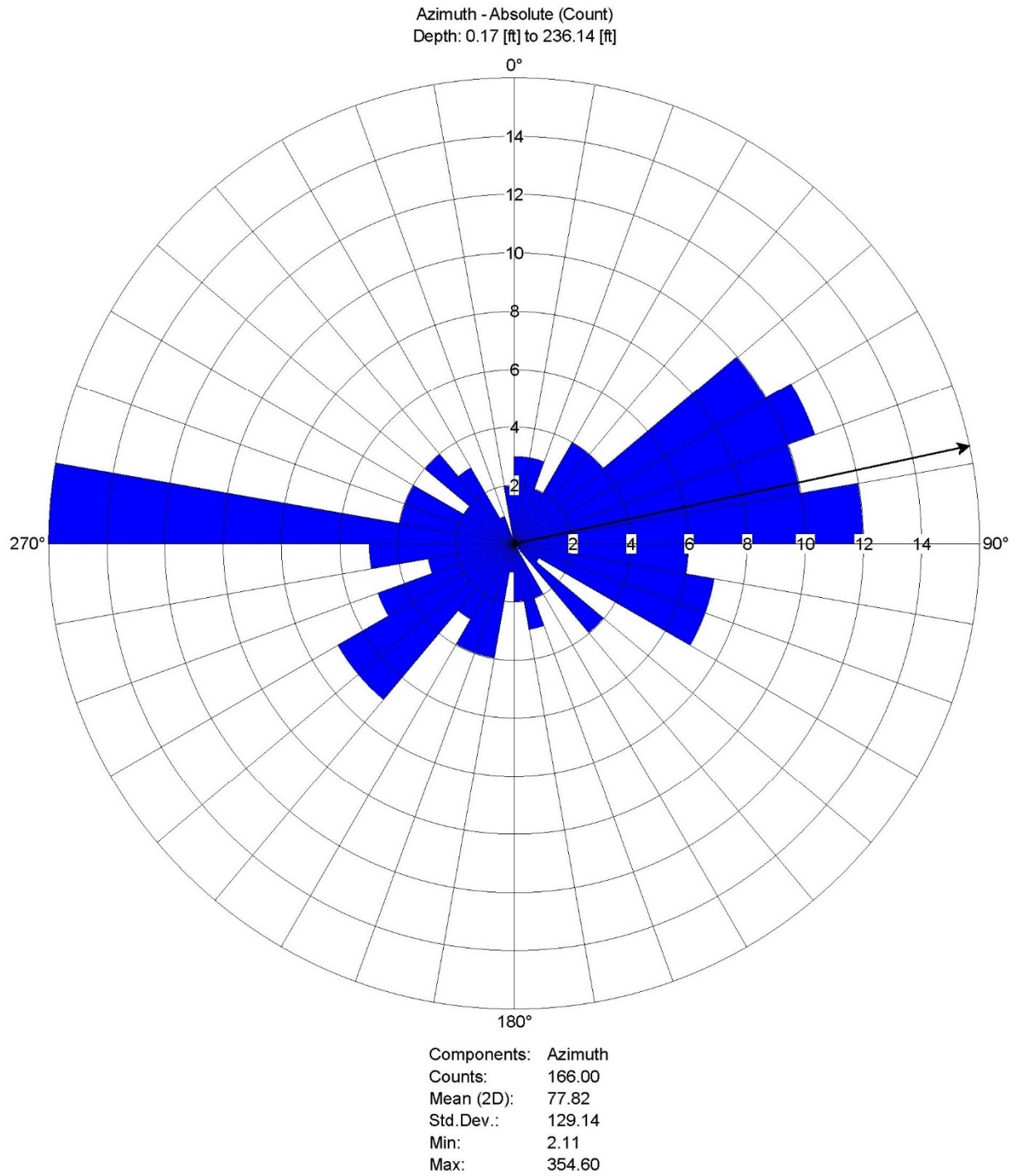


Figure 10. Borehole RC-20-005 (B-28), Optical Rose Diagram

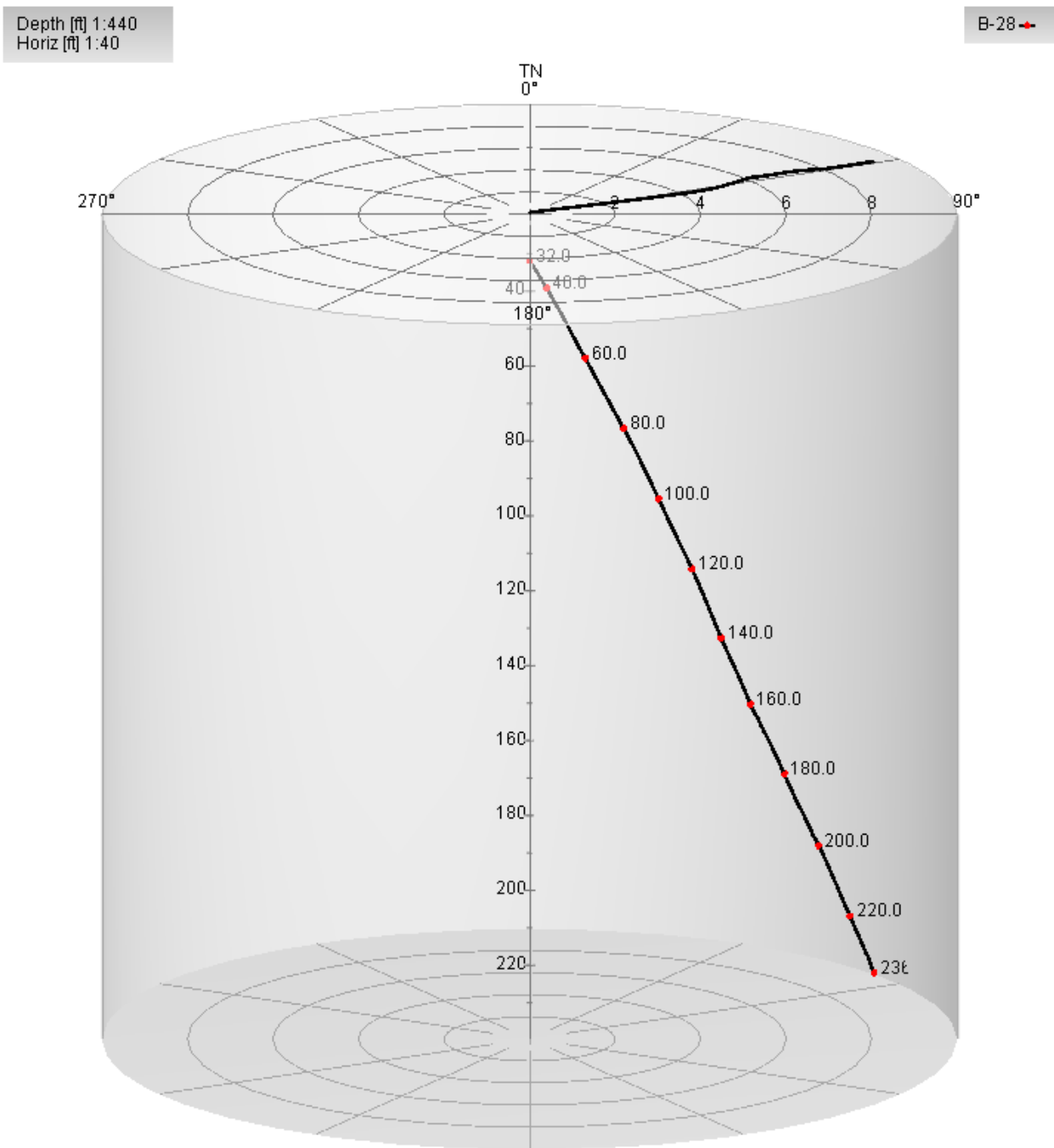


Figure 11. Borehole RC-20-005 (B-28), Deviation Cylindrical Projection

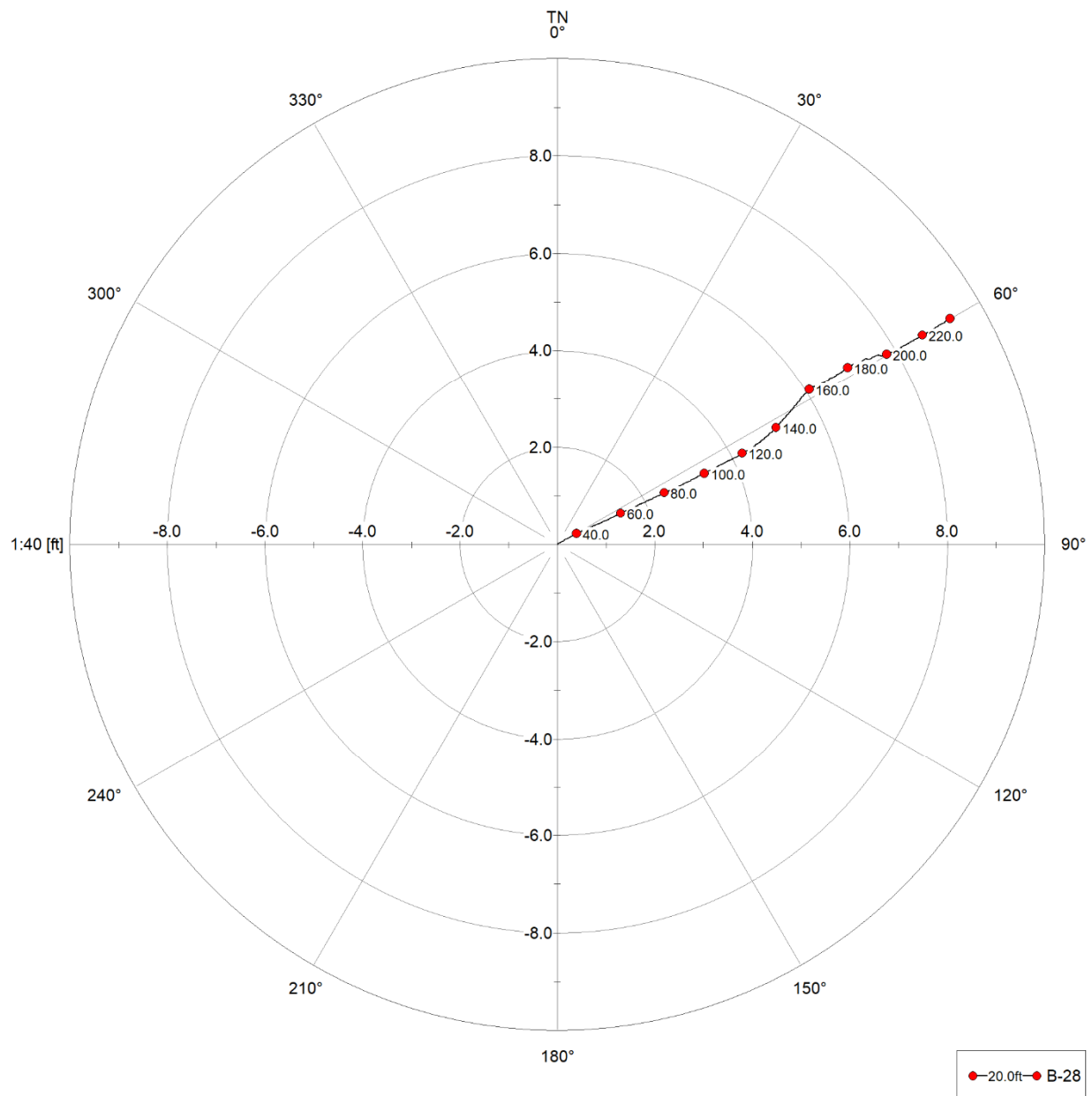


Figure 12. Borehole RC-20-005 (B-28), Deviation Bullseye Projection

LAST CHANCE GRADE BOREHOLE B-29
Receiver to Receiver V_s and V_p Analysis

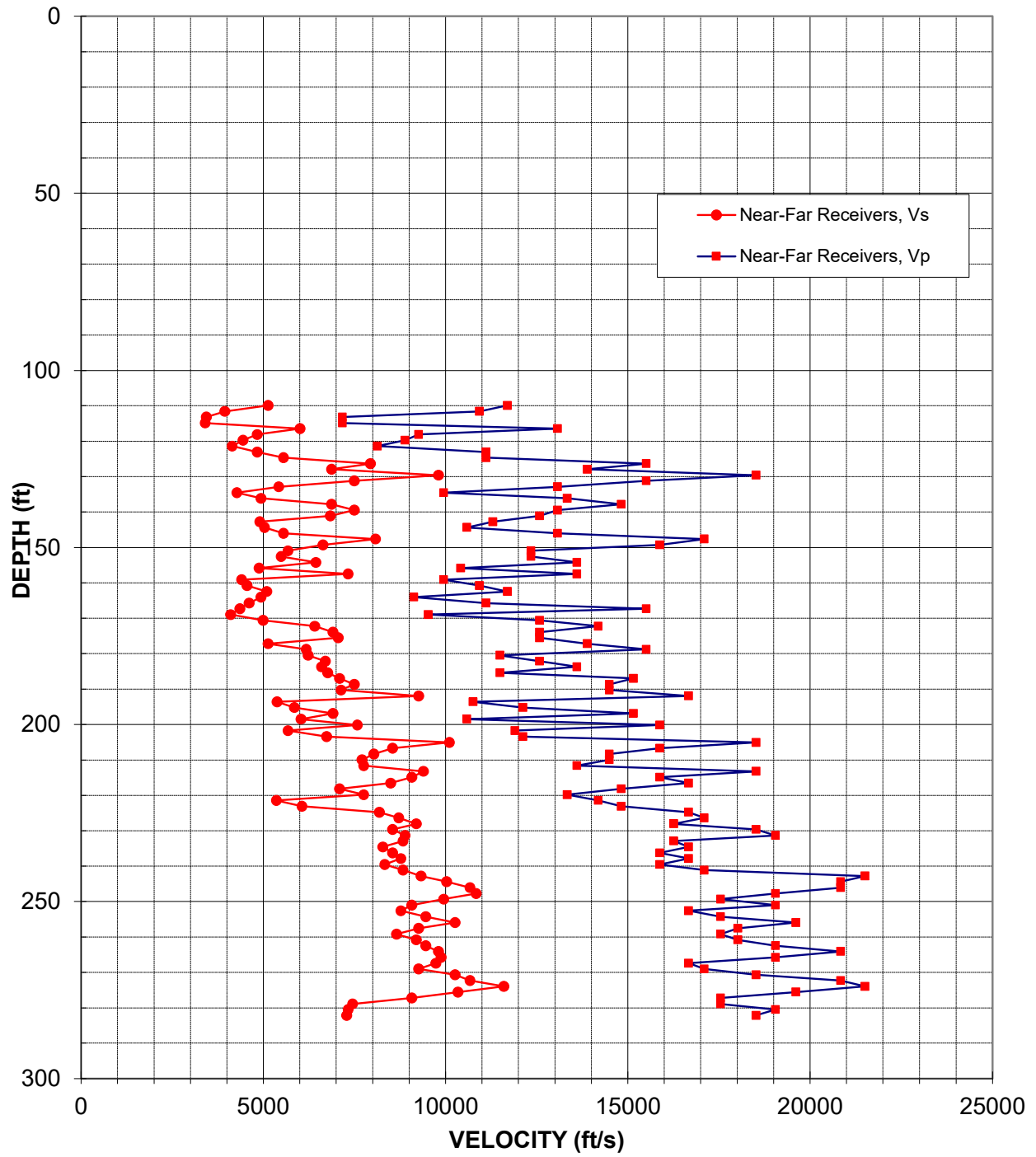


Figure 13: Borehole RC-20-014 (B-29), Suspension R1-R2 P- and SH-wave velocities

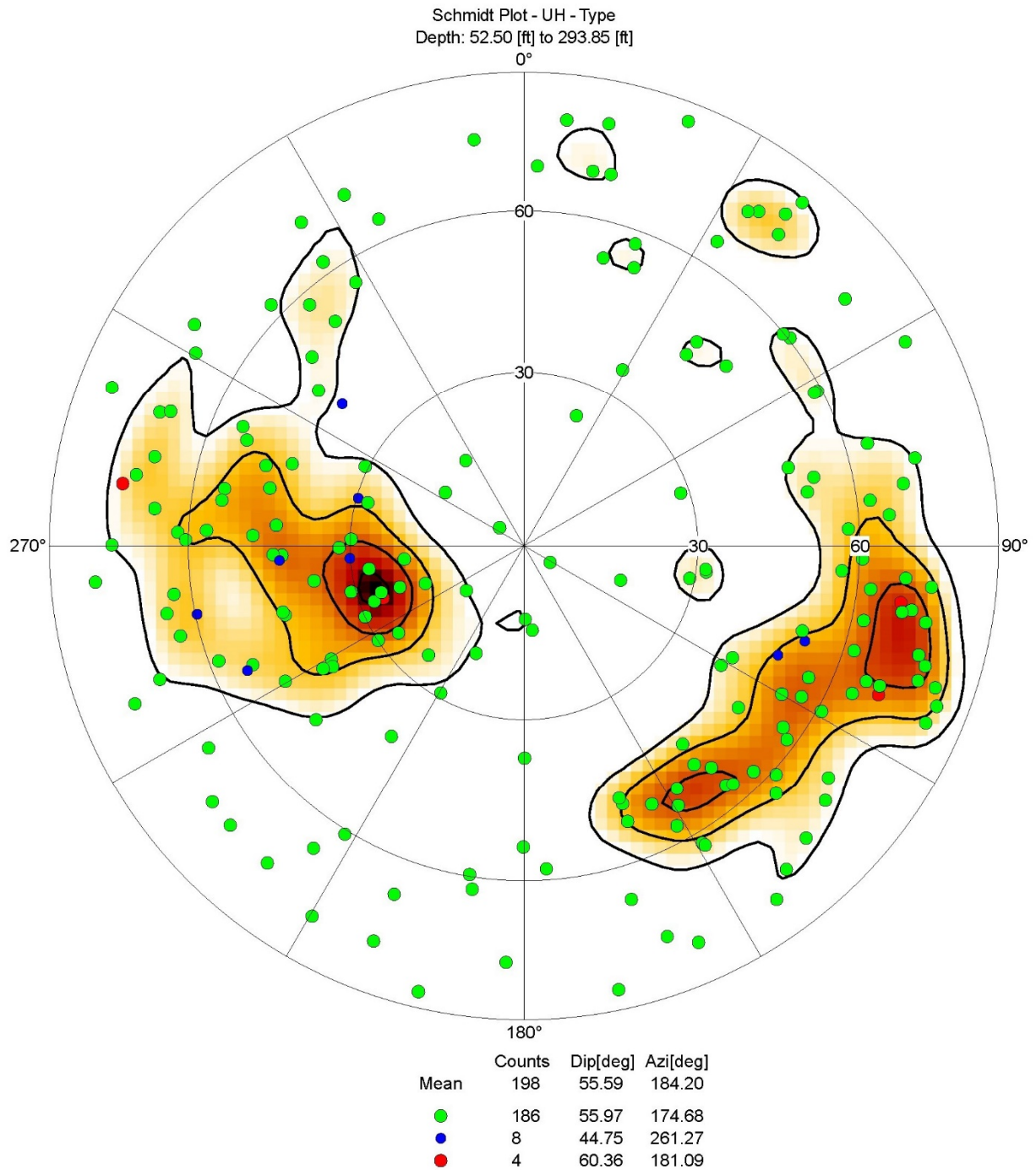


Figure 14. Borehole RC-20-014 (B-29), Acoustic Stereonet Diagram

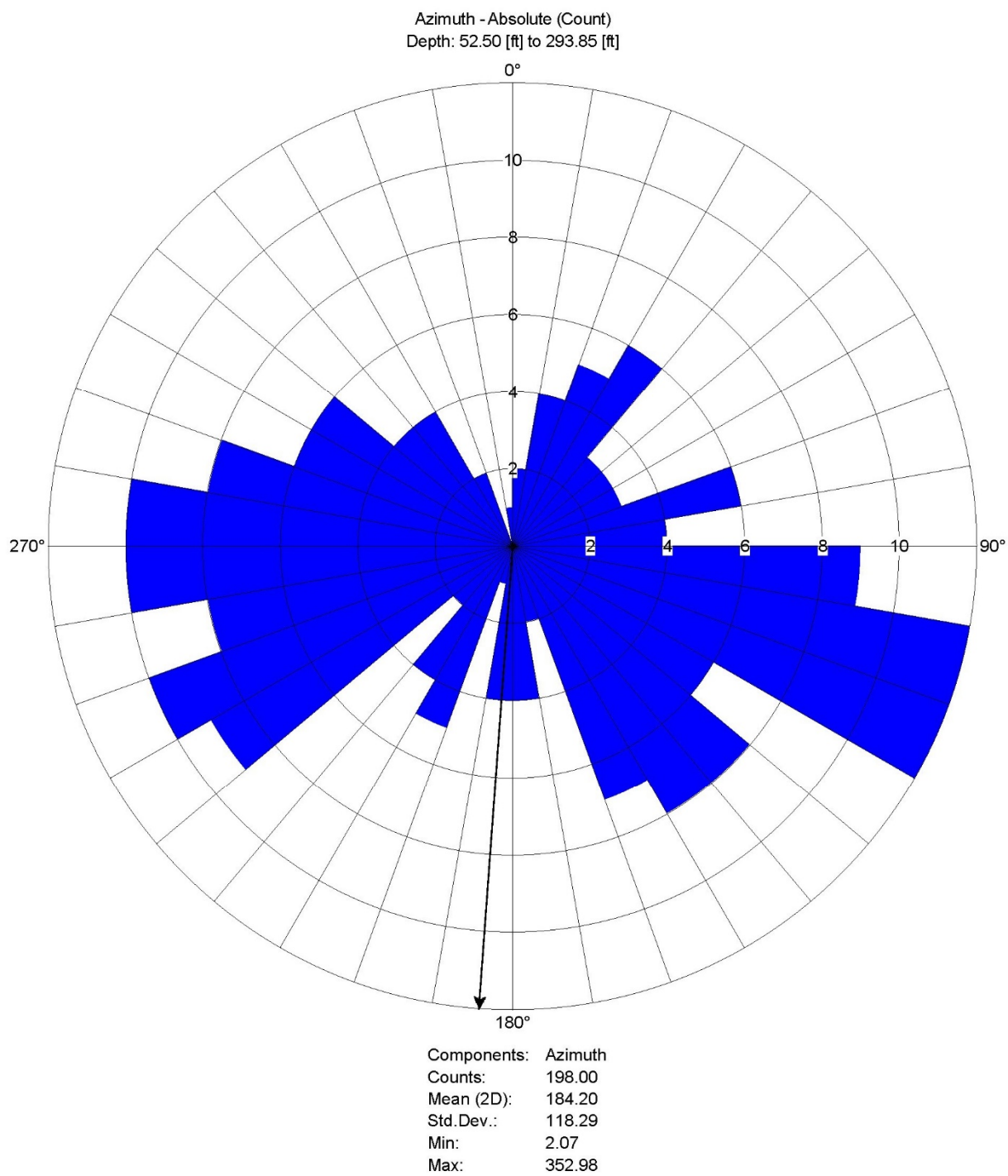


Figure 15. Borehole RC-20-014 (B-29), Acoustic Rose Diagram

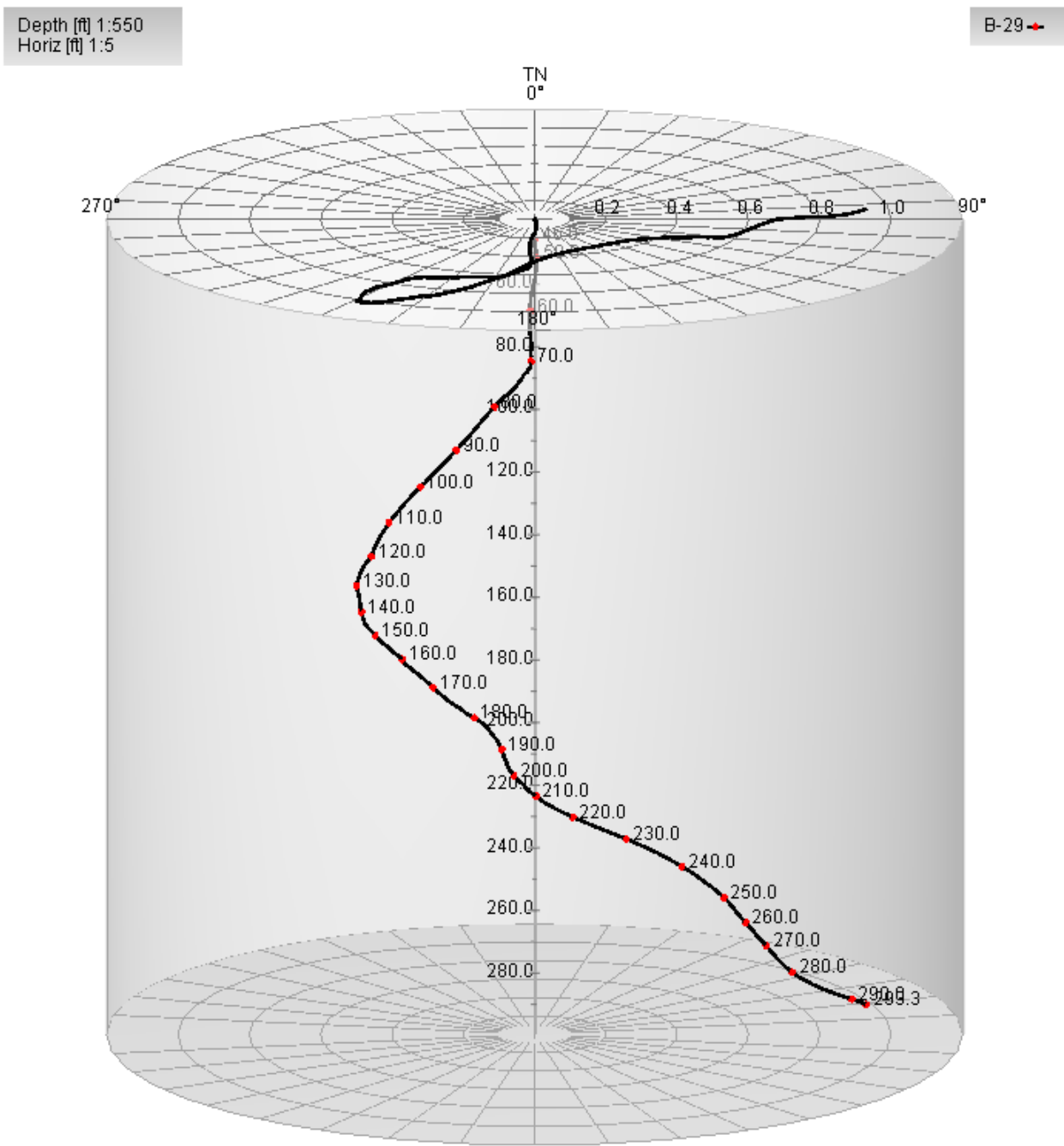


Figure 16. Borehole RC-20-014 (B-29), Deviation Cylindrical Projection

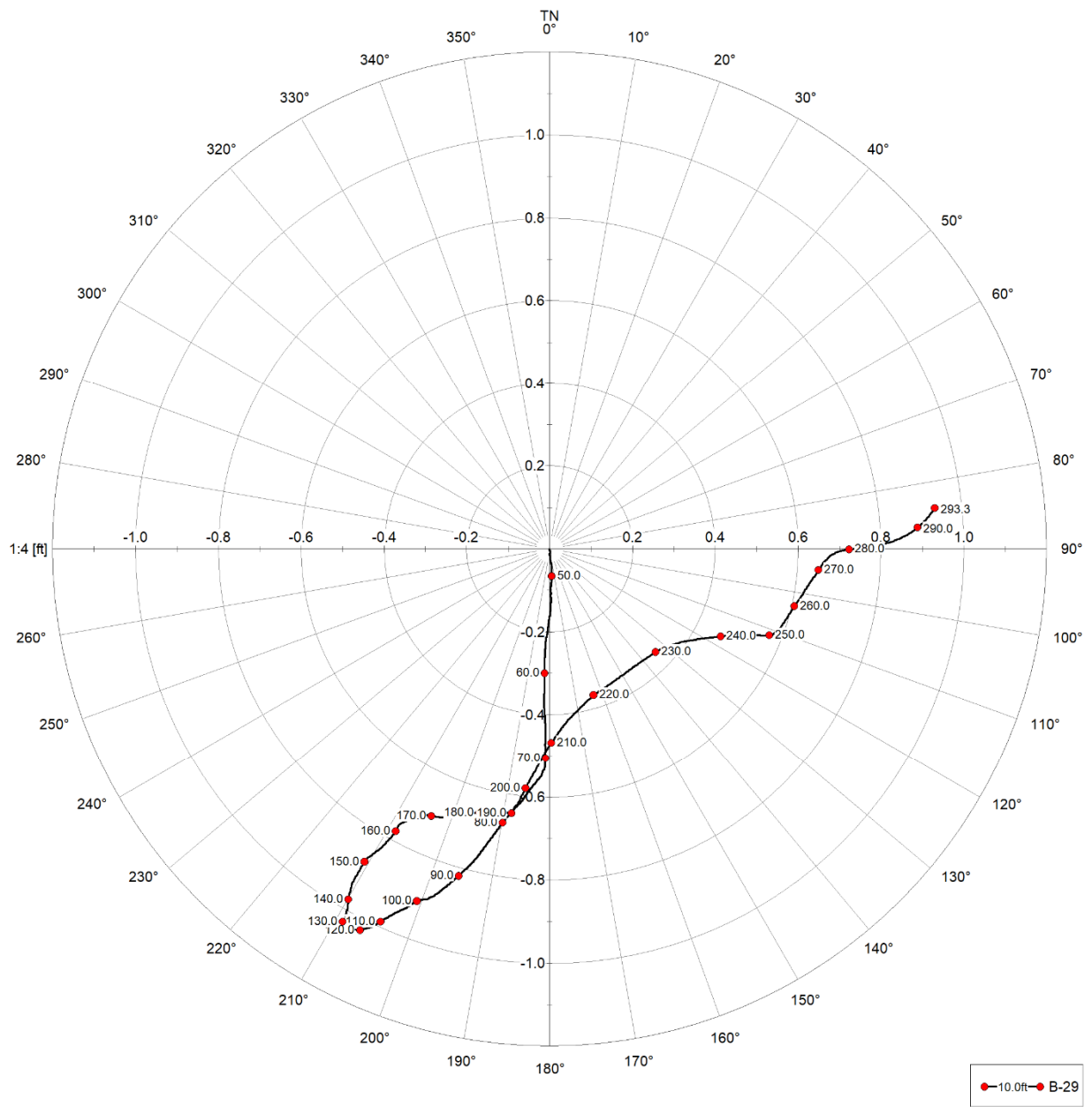


Figure 17. Borehole RC-20-014 (B-29), Deviation Bullseye Projection

	LOG TYPE	PROJECT	Last Chance Grade
	CAL	WELL	B-29
	NG	LOCATION	Last Chance Grade, HWY 101
	DUIN	LOGGER	ATM
CLIENT Kleinfelder		DATE	06 Nov 2020

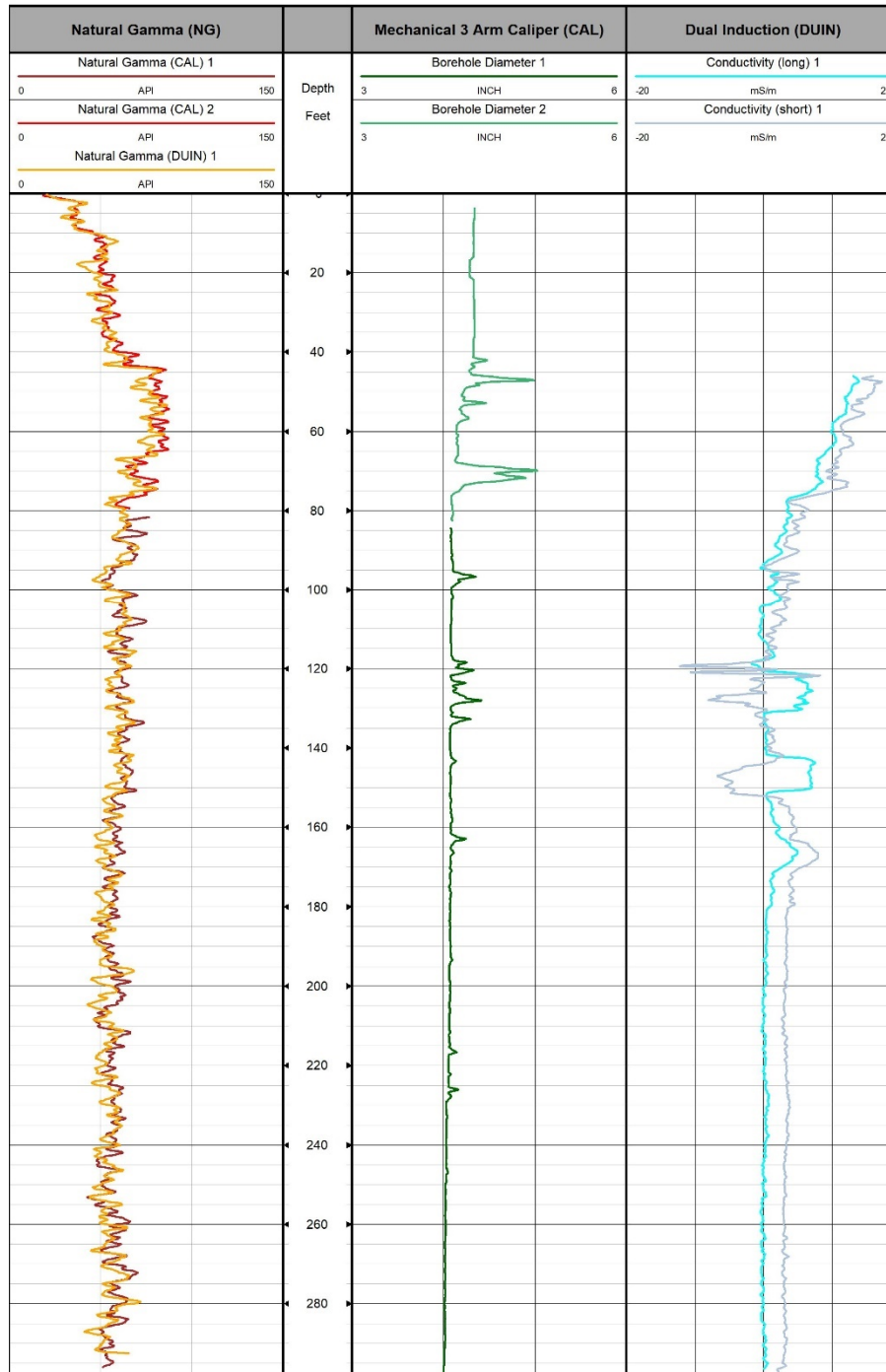


Figure 18. Borehole RC-20-014 (B-29), Induction, Caliper, and Natural Gamma Log

LAST CHANCE GRADE BOREHOLE B-32 **Receiver to Receiver V_s and V_p Analysis**

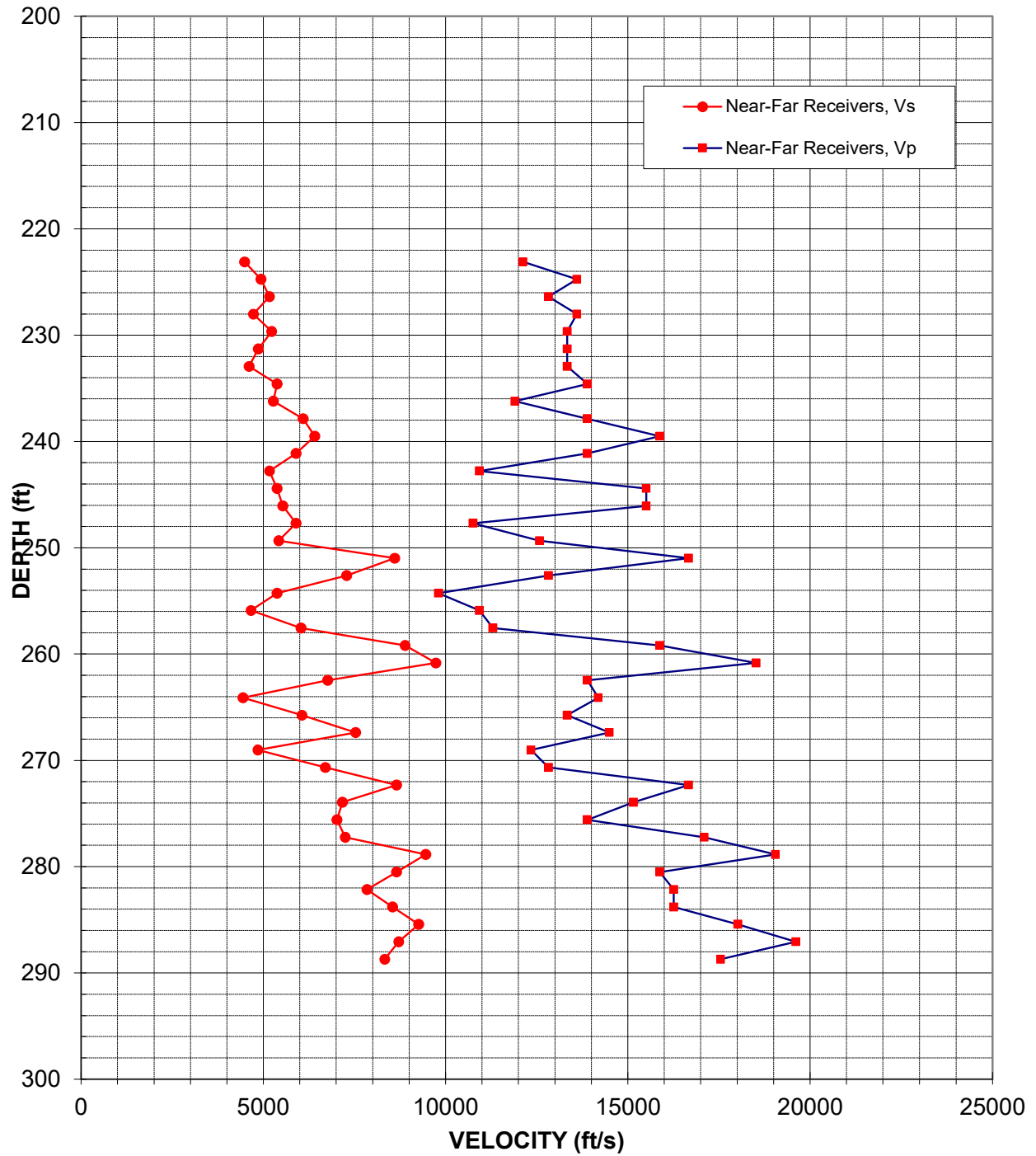


Figure 19: Borehole RC-20-011 (B-32), Suspension R1-R2 P- and SH-wave velocities

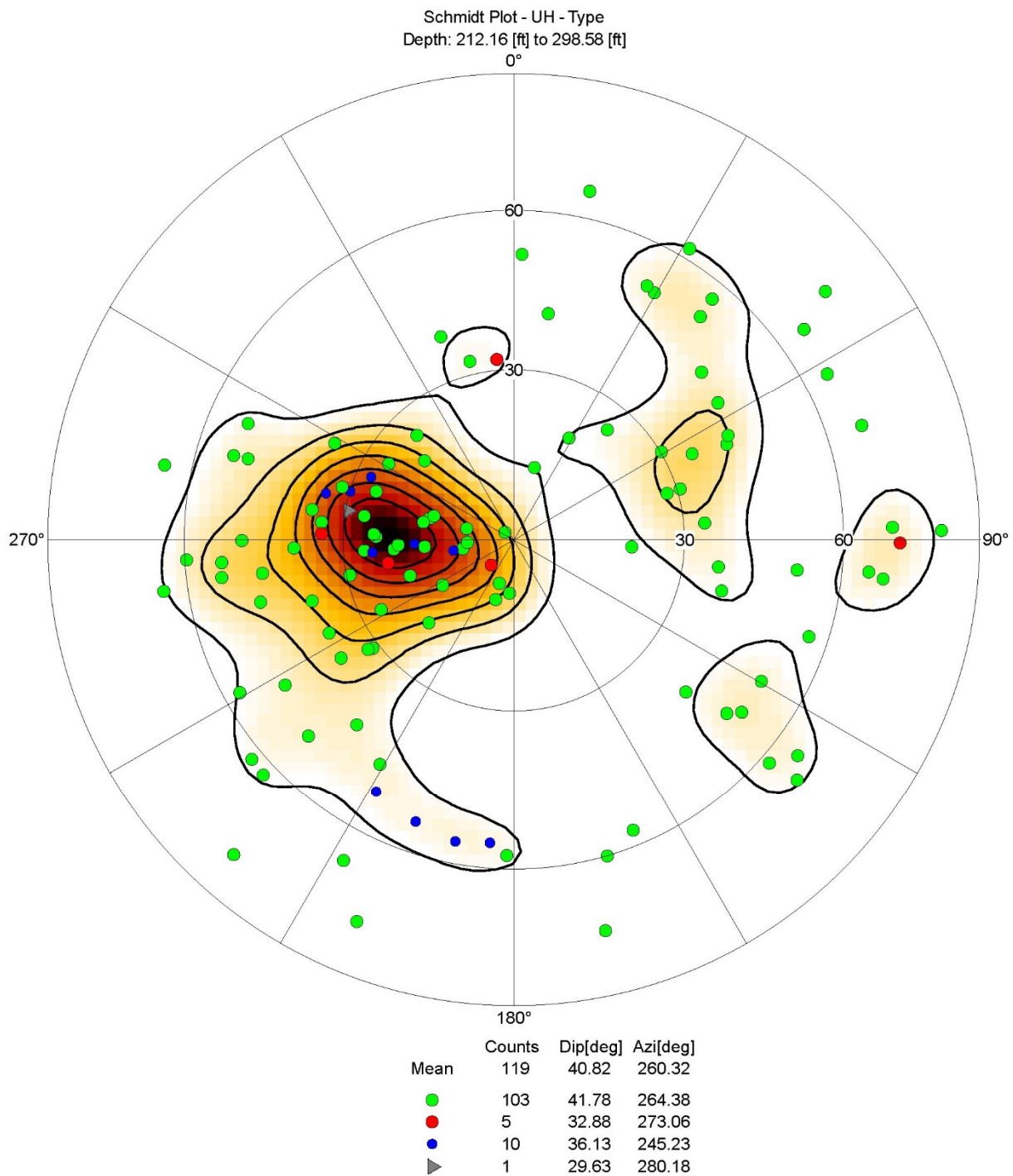


Figure 20. Borehole RC-20-011 (B-32), Acoustic Stereonet Diagram

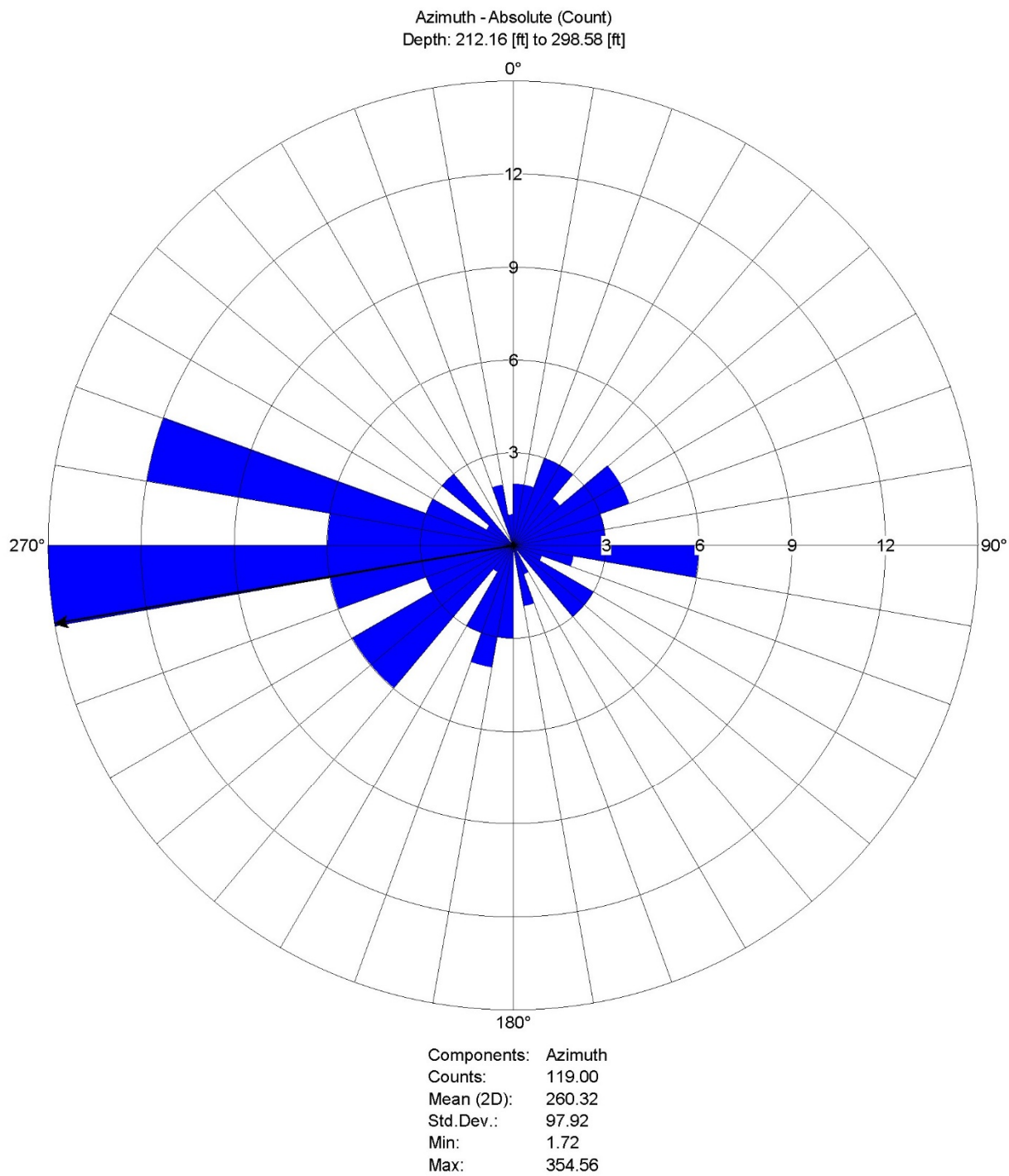


Figure 21. Borehole RC-20-011 (B-32), Acoustic Rose Diagram

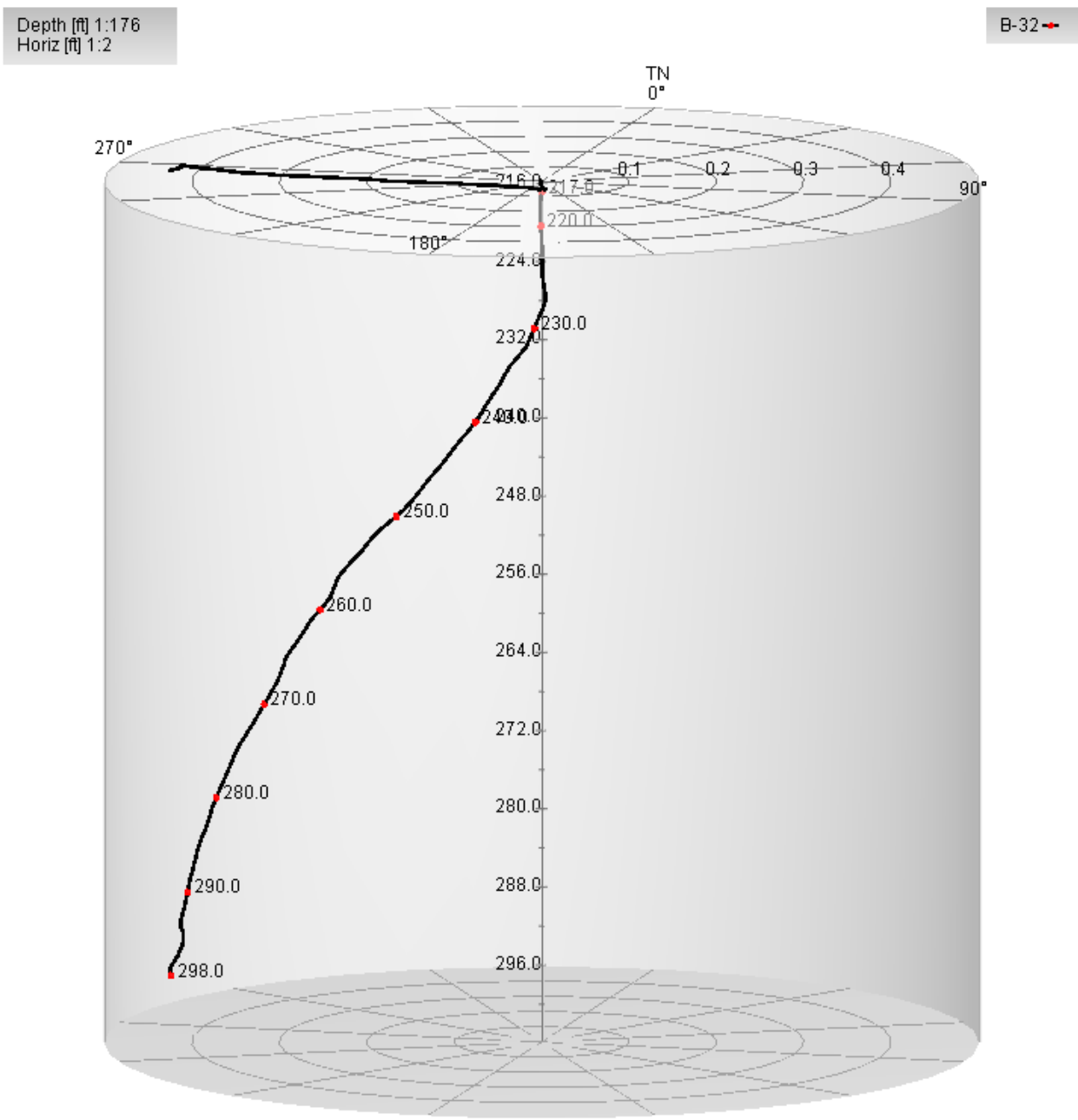


Figure 22. Borehole RC-20-011 (B-32), Acoustic Deviation Cylindrical Projection

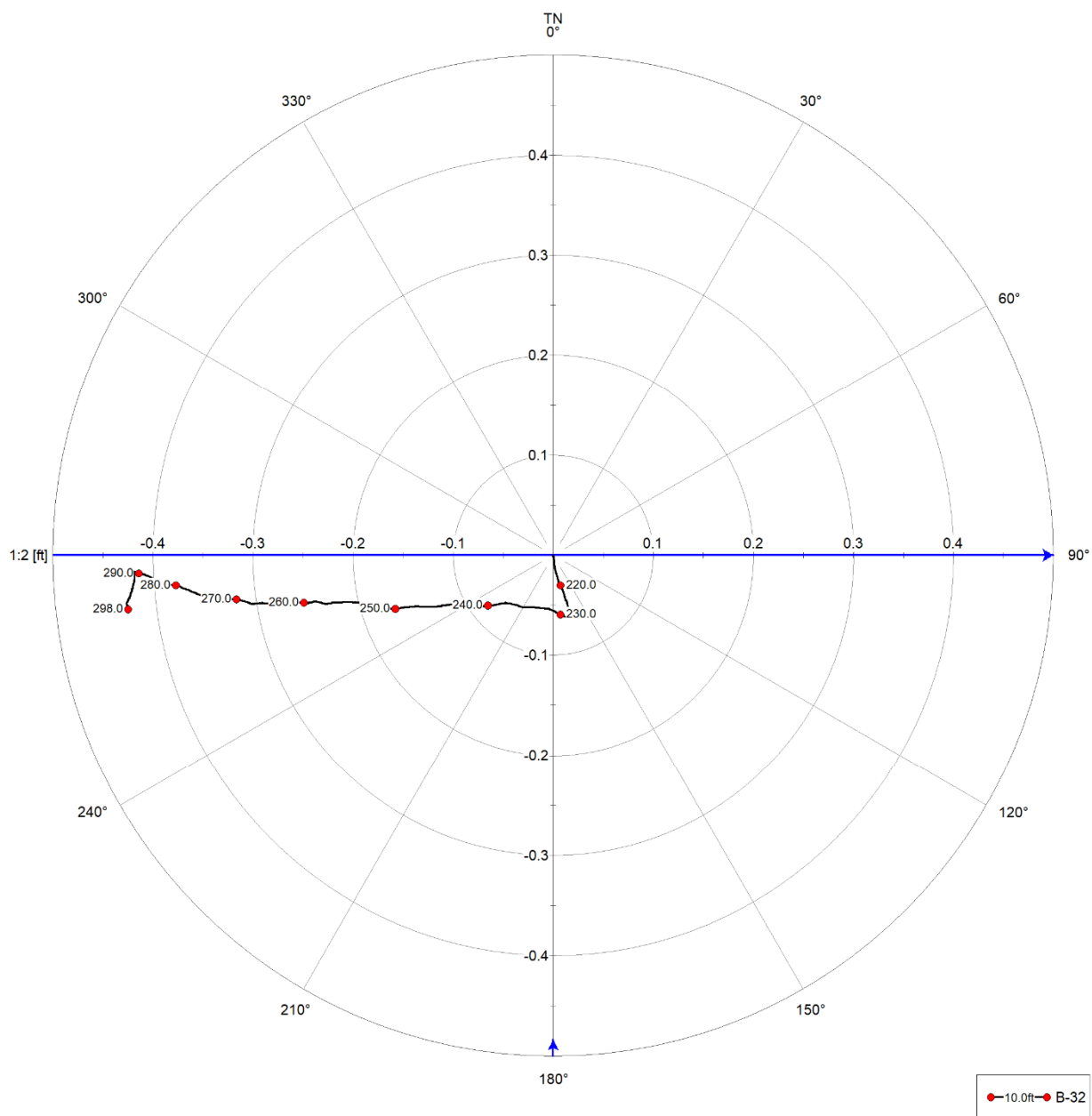


Figure 23. Borehole RC-20-011 (B-32), Acoustic Deviation Bullseye Projection

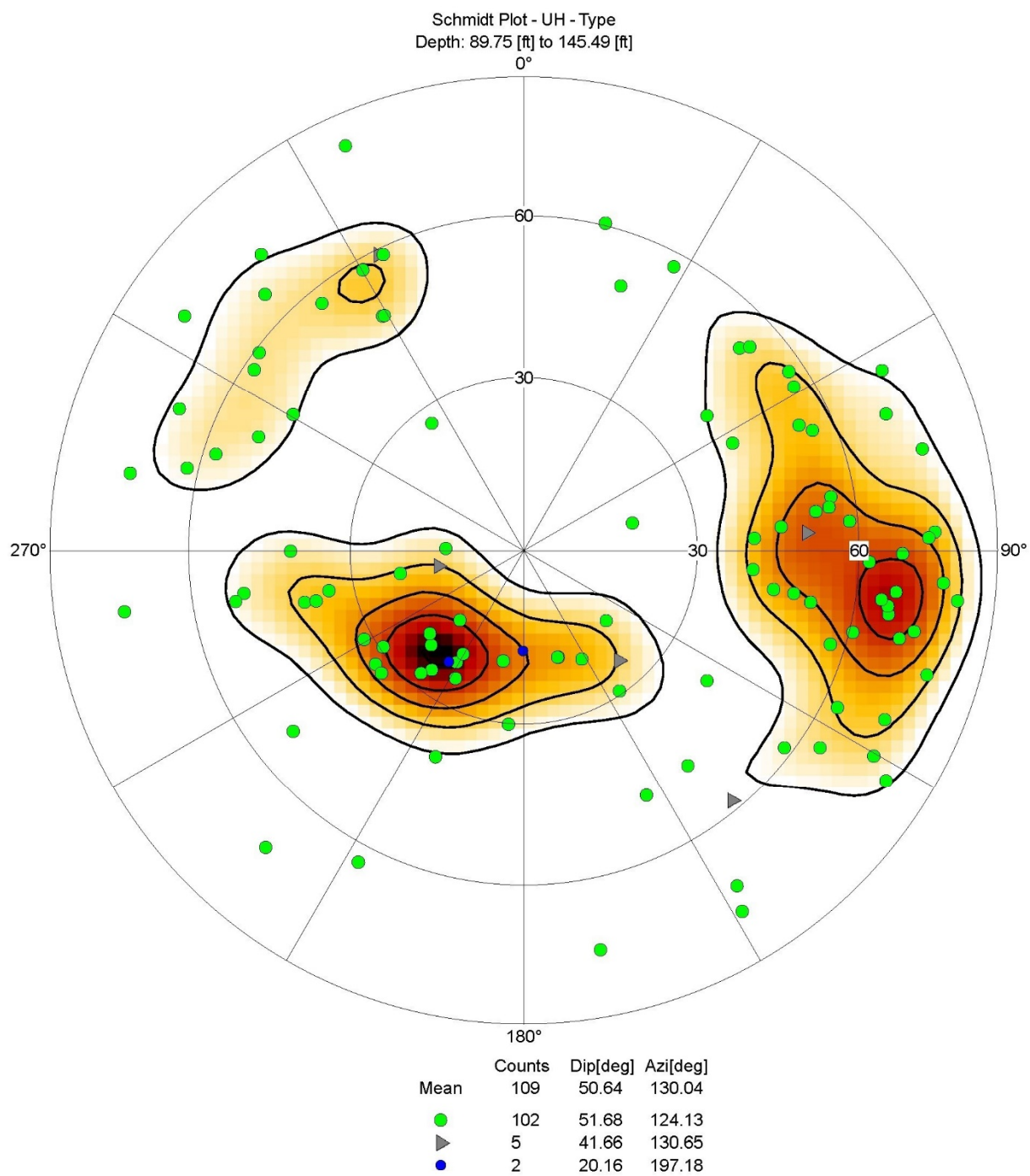


Figure 24. Borehole RC-20-011 (B-32), Optical Stereonet Diagram

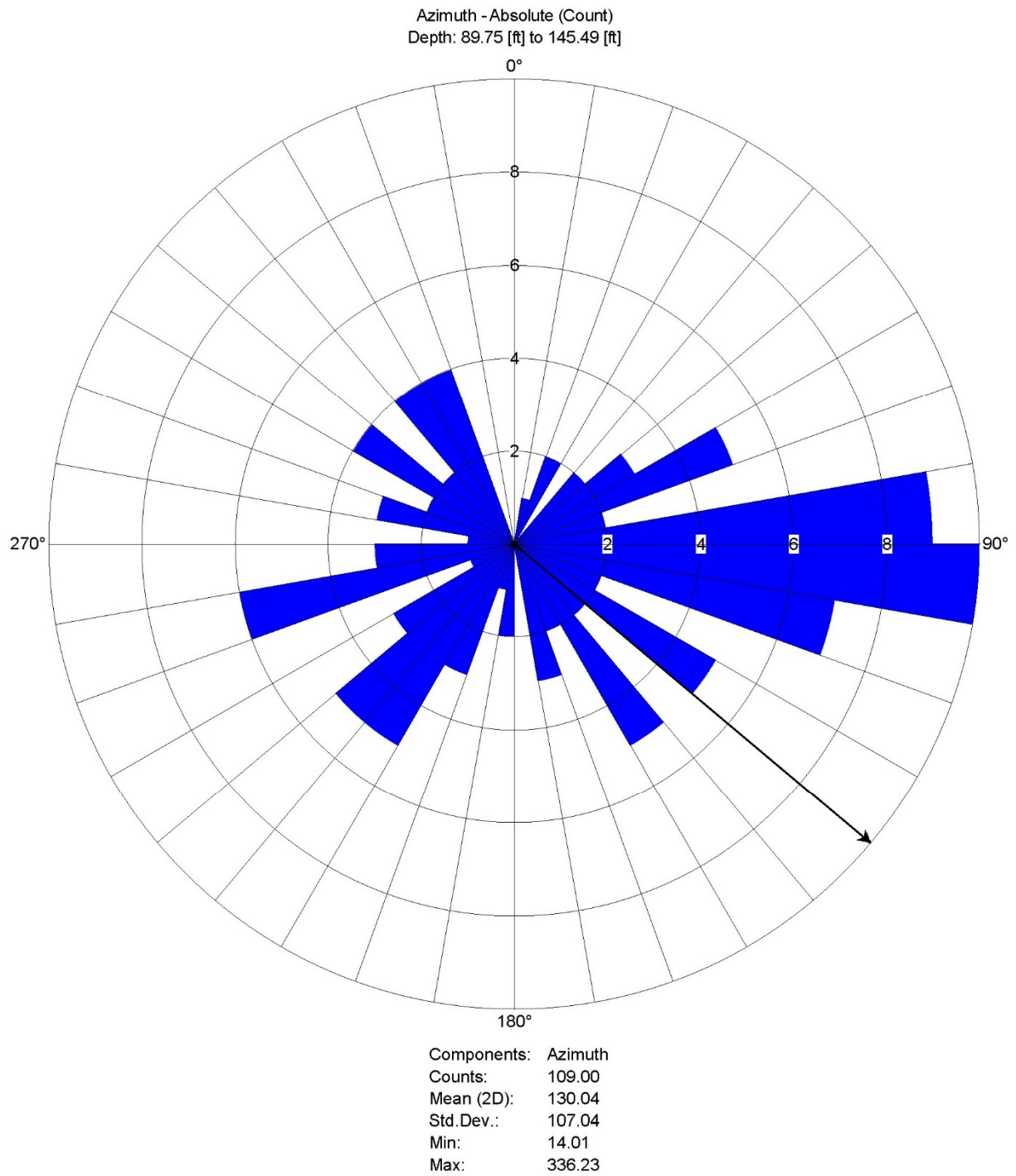


Figure 25. Borehole RC-20-011 (B-32), Optical Rose Diagram

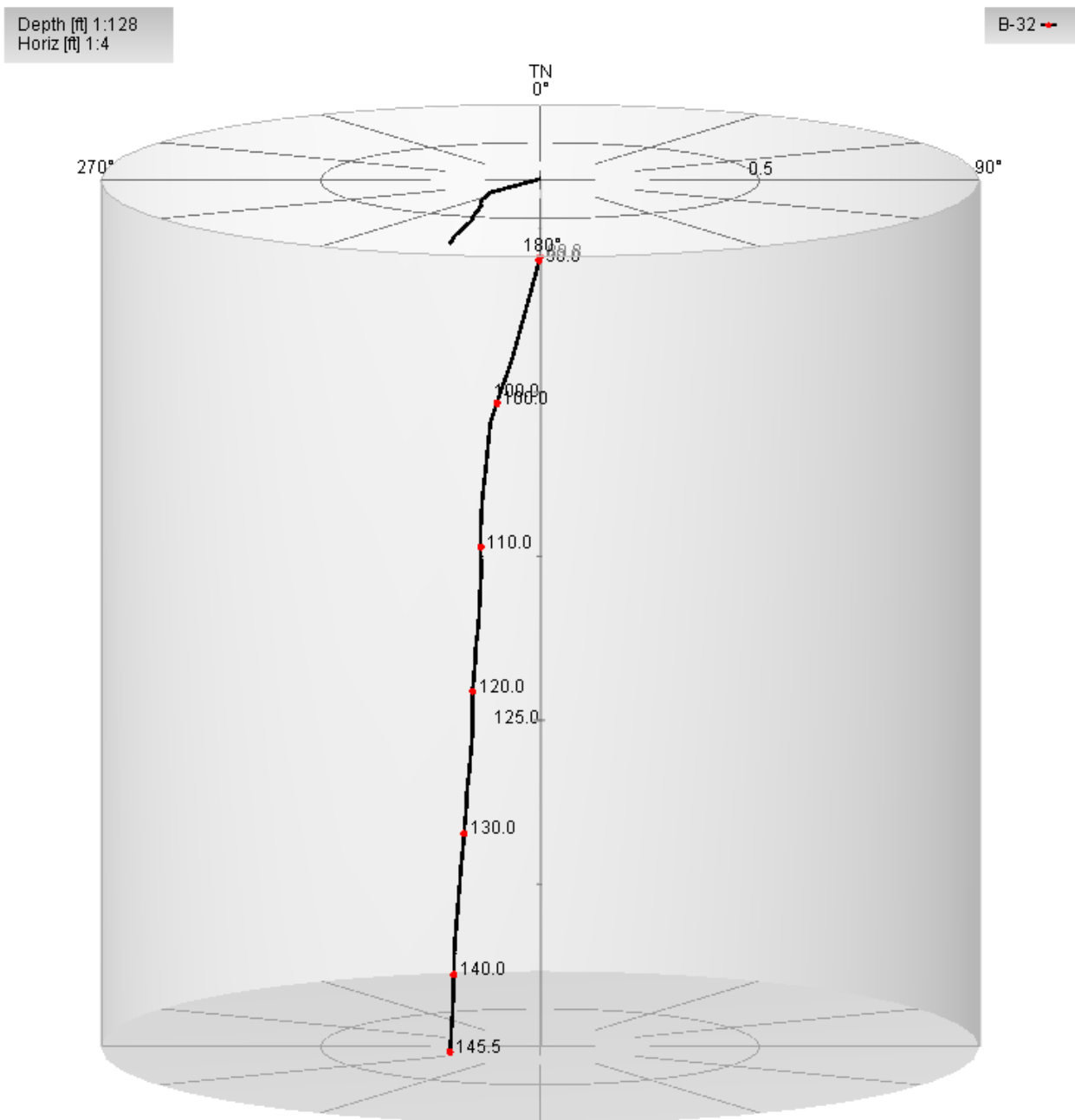


Figure 26. Borehole RC-20-011 (B-32), Optical Deviation Cylindrical Projection

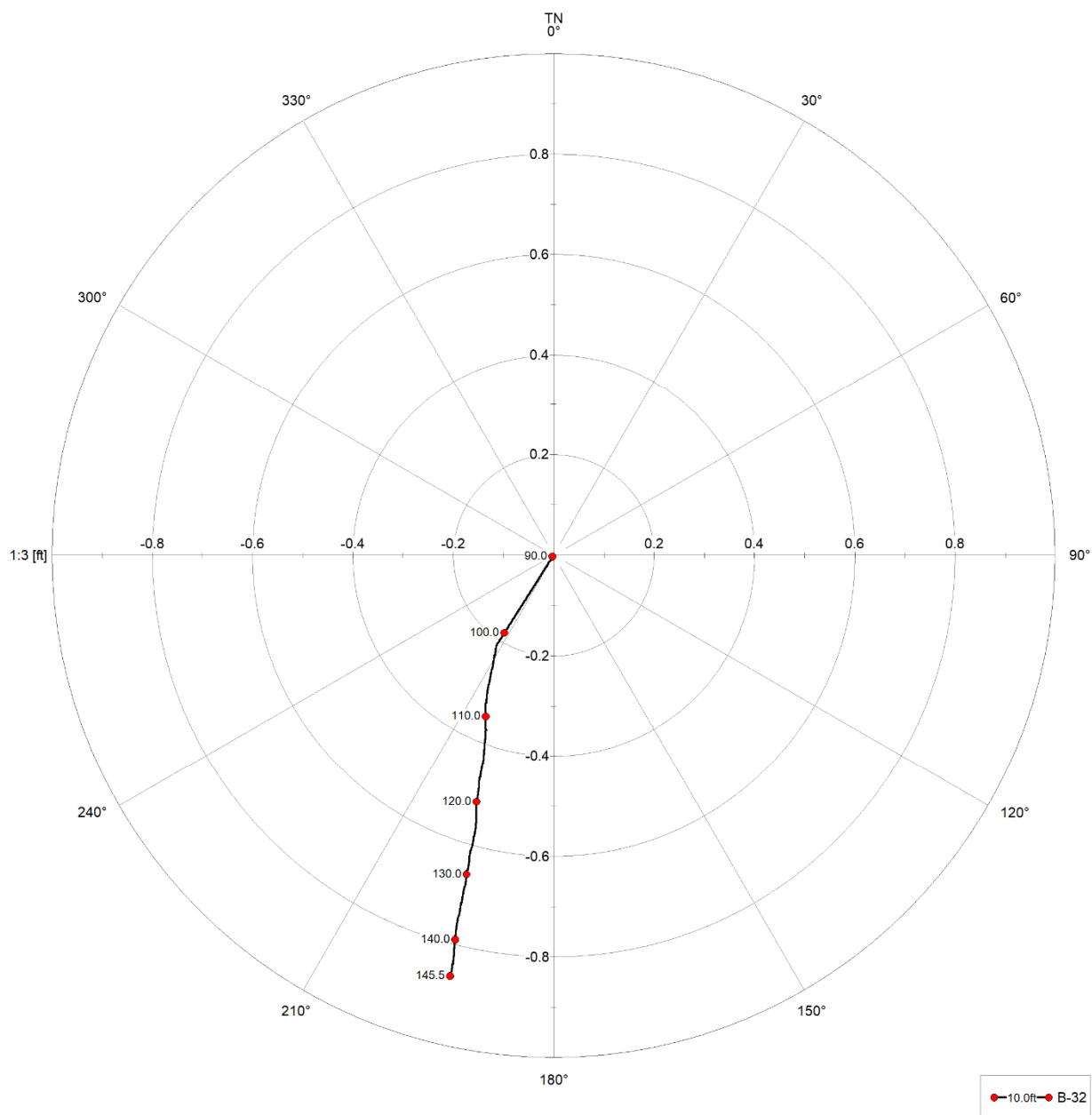


Figure 27. Borehole RC-20-011 (B-32), Optical Deviation Bullseye Projection

	LOG TYPE	PROJECT	Last Chance Grade
	CAL	WELL	B-32
CLIENT Kleinfielder	NG	LOCATION	Last Chance Grade, HWY 101
	DUIN	LOGGER	RAS, ATM
		DATE	26 Oct, 6 & 7 Nov 2020

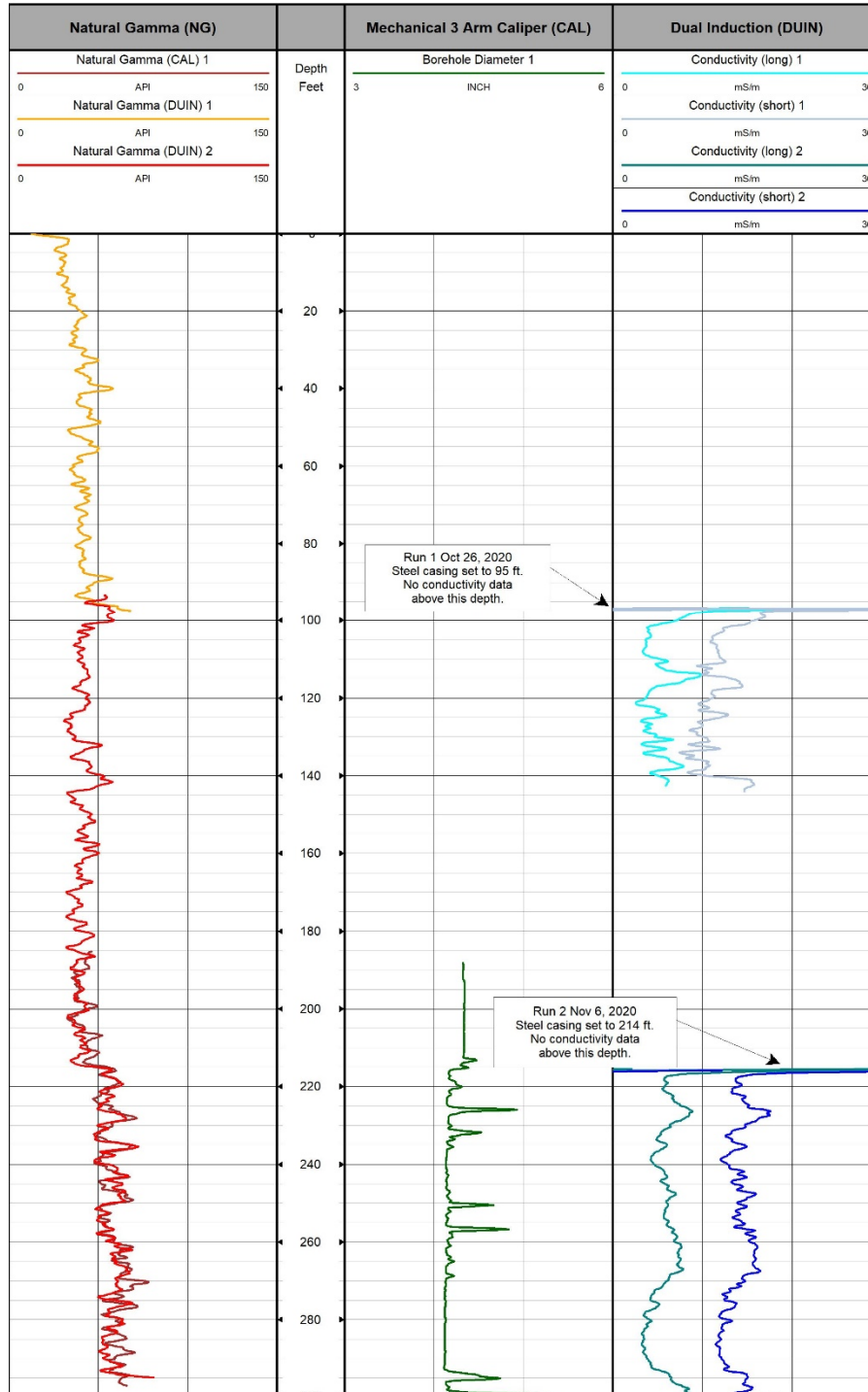


Figure 28. Borehole RC-20-011 (B-32), Induction, Caliper, and Natural Gamma Log

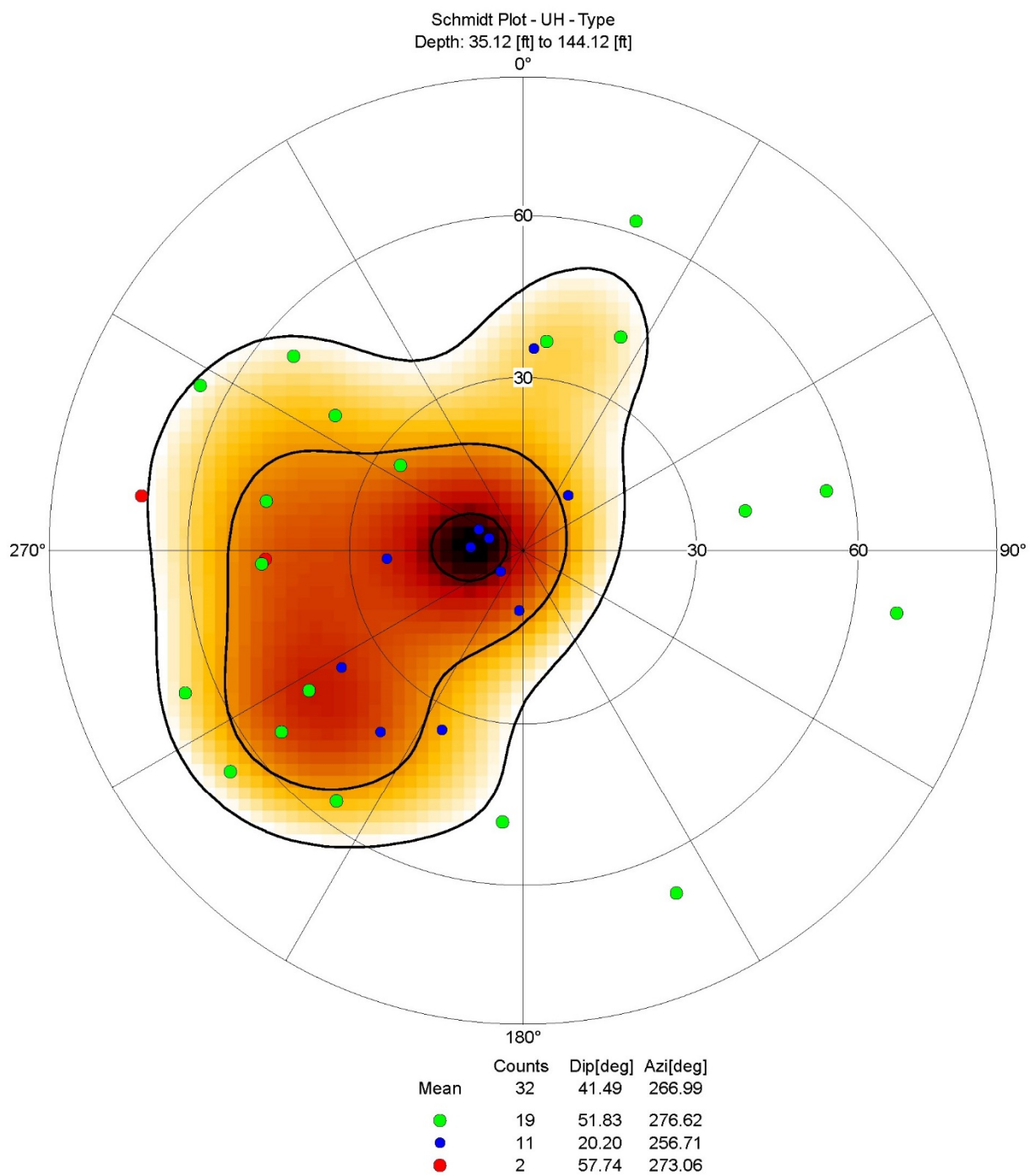


Figure 30. Borehole RC-21-001 (B-47), Acoustic Stereonet Diagram

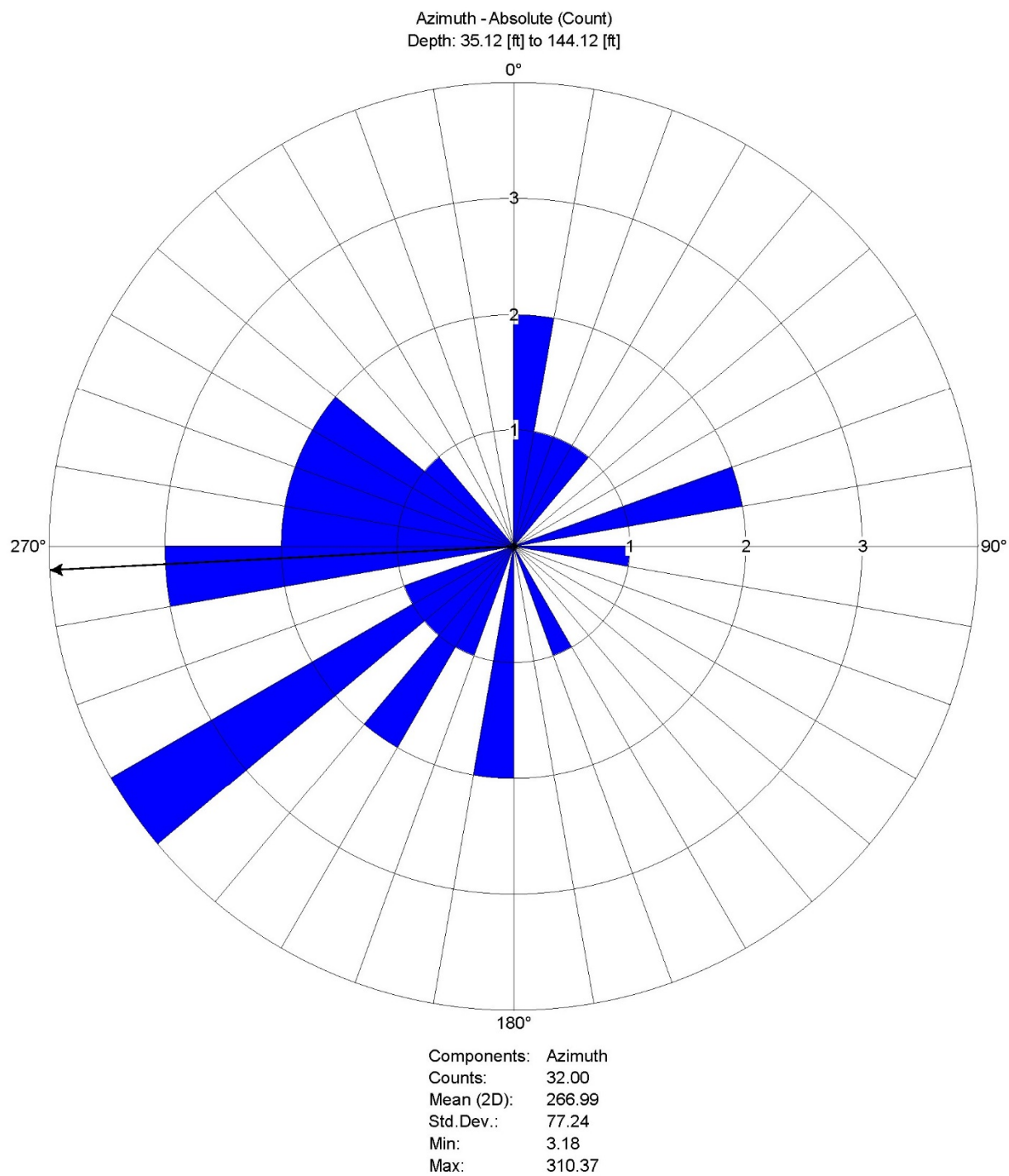


Figure 31. Borehole RC-21-001 (B-47), Acoustic Rose Diagram

Depth [ft] 1:279
Horiz [ft] 1:7

B-47 ATV

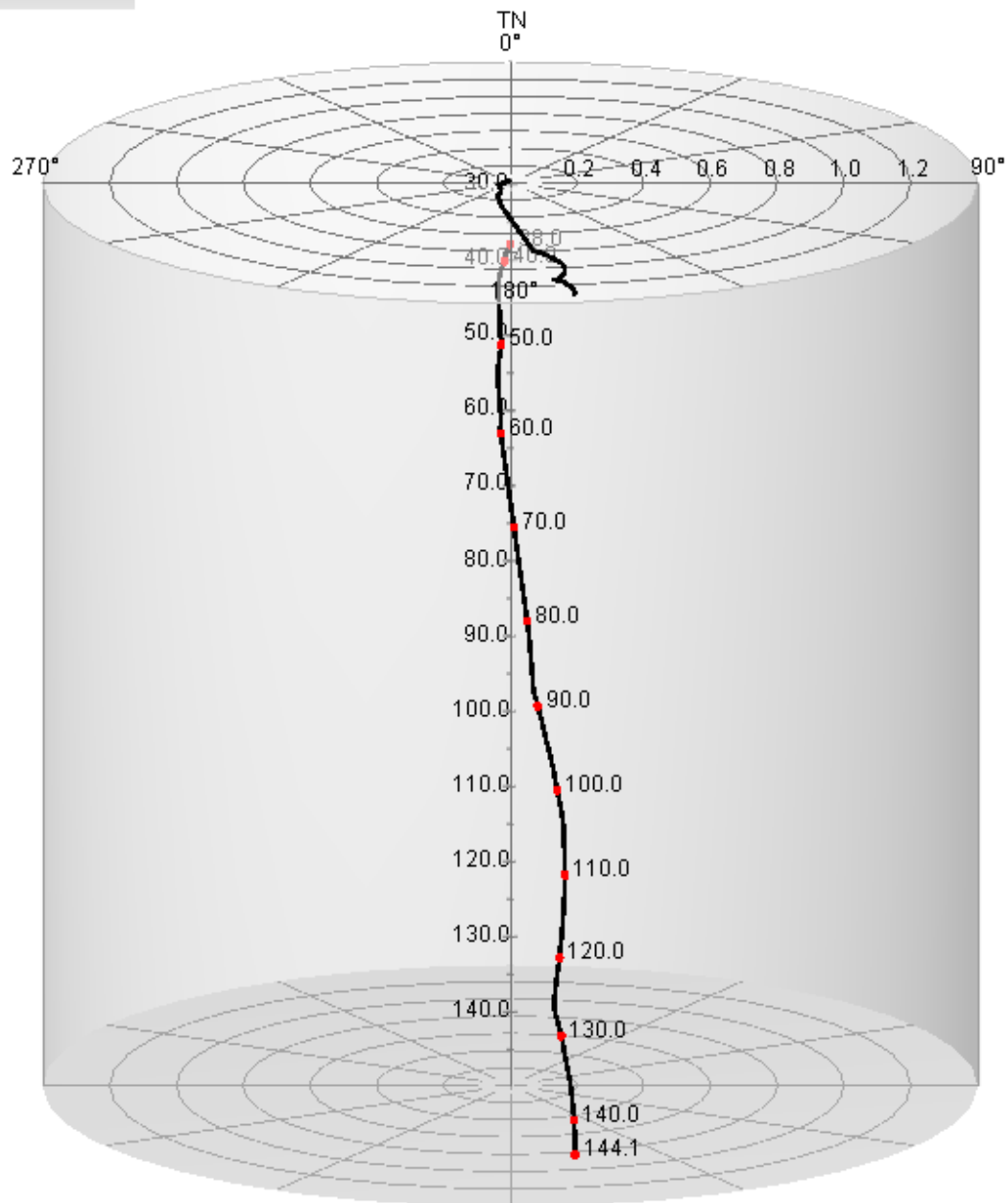


Figure 32. Borehole RC-21-001 (B-47), Acoustic Deviation Cylindrical Projection

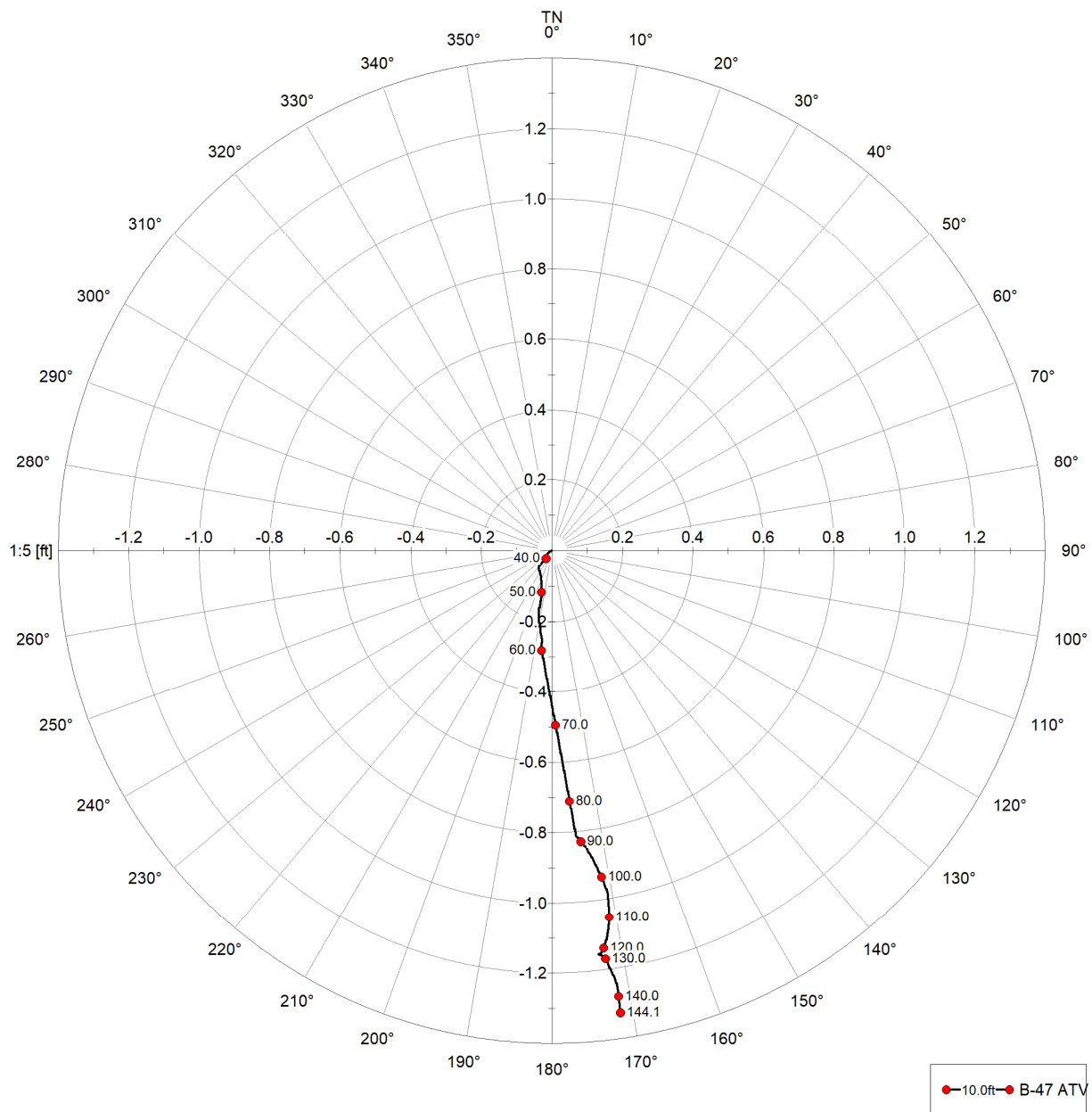


Figure 33. Borehole RC-21-001 (B-47), Acoustic Deviation Bullseye Projection

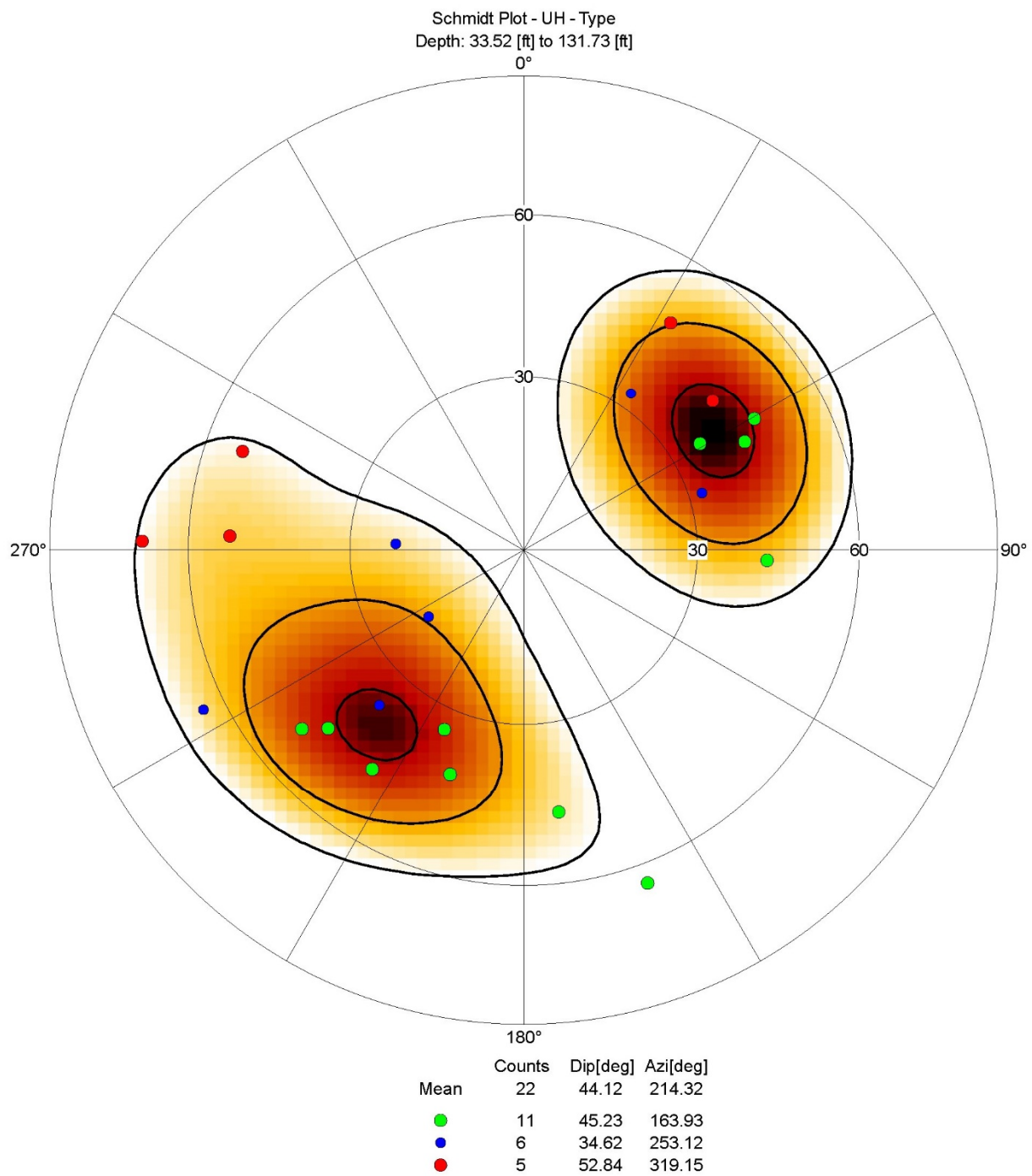


Figure 34. Borehole RC-21-001 (B-47), Optical Stereonet Diagram

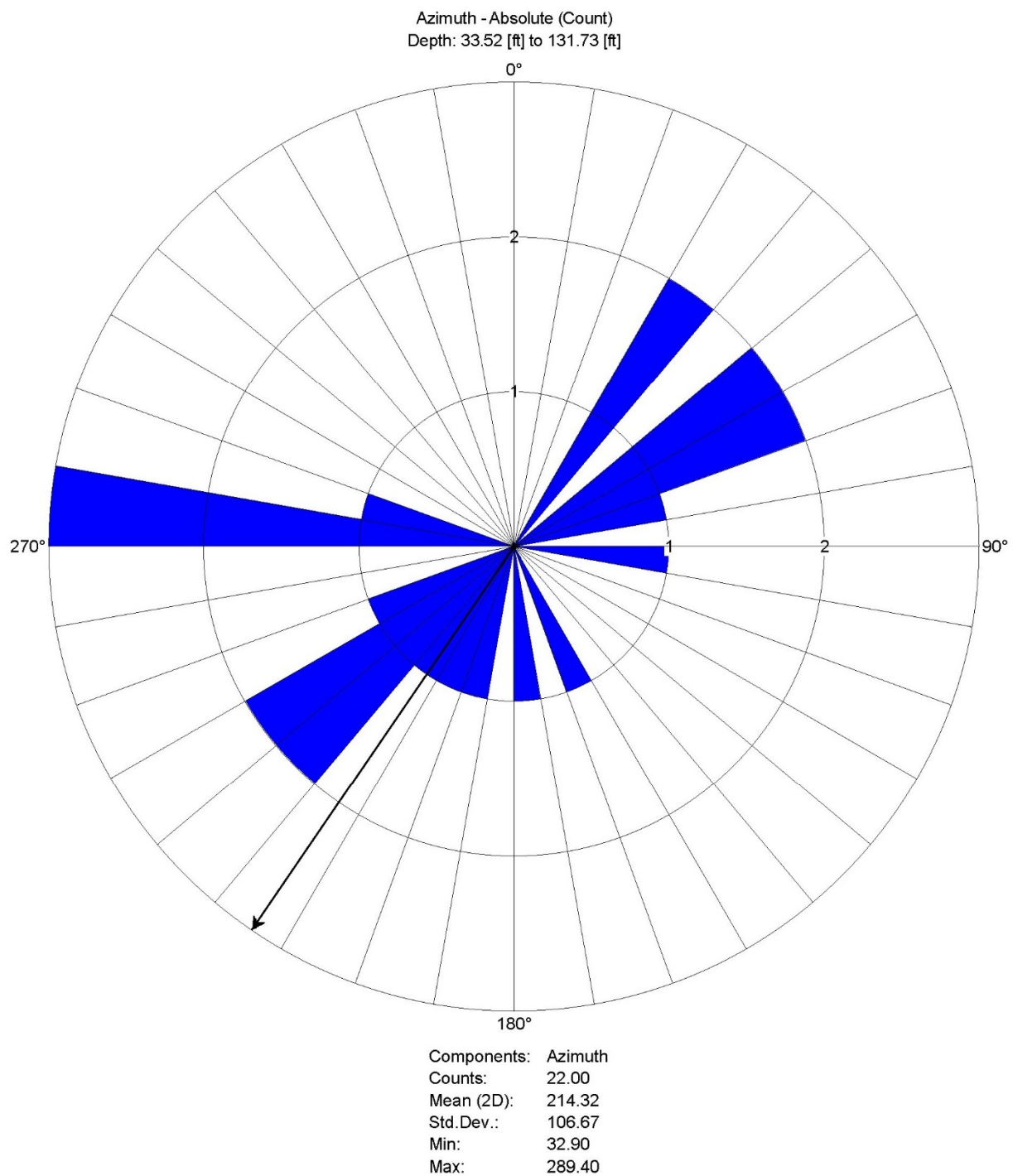


Figure 35. Borehole RC-21-001 (B-47), Optical Rose Diagram

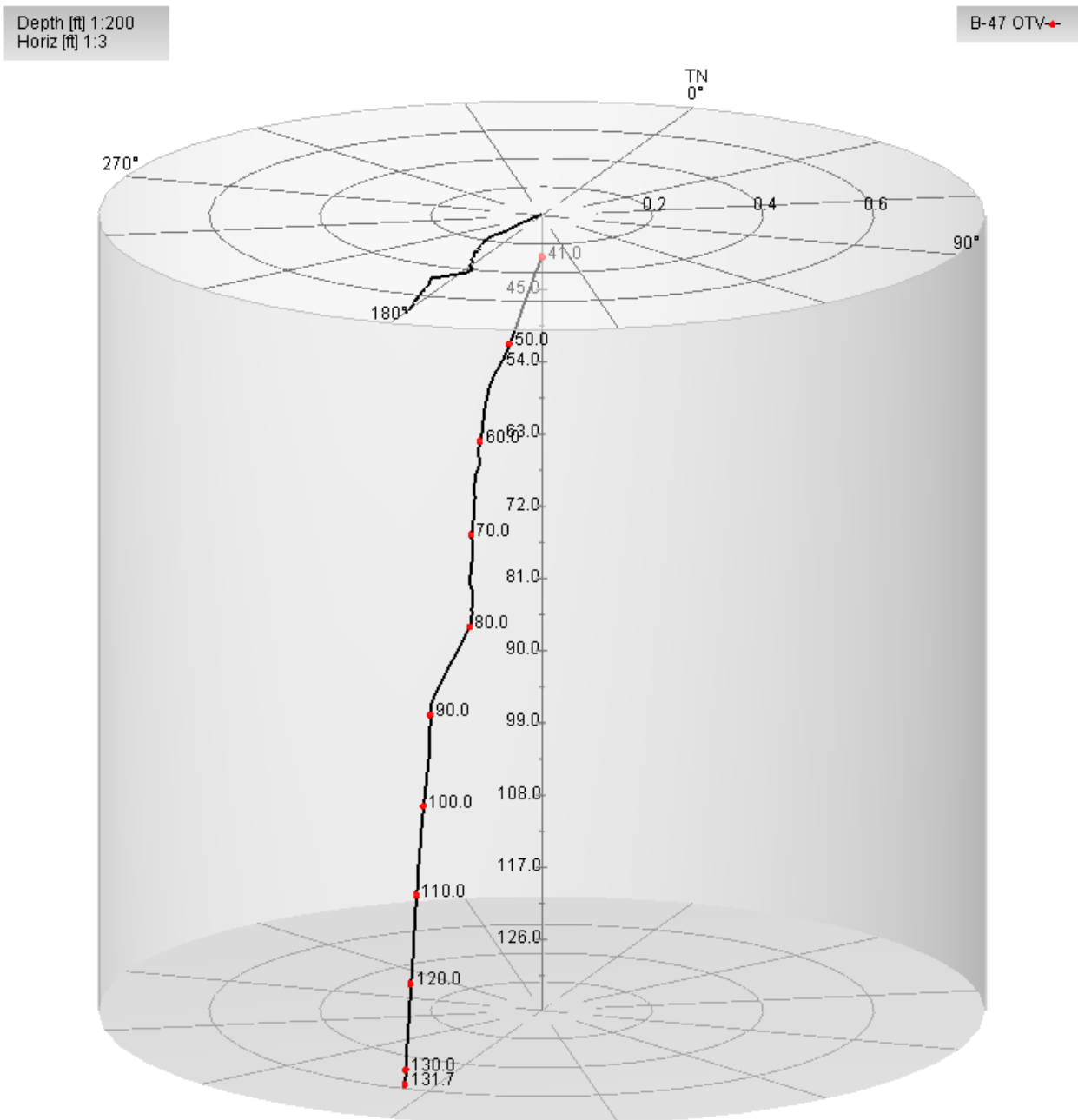


Figure 36. Borehole RC-21-001 (B-47), Optical Deviation Cylindrical Projection

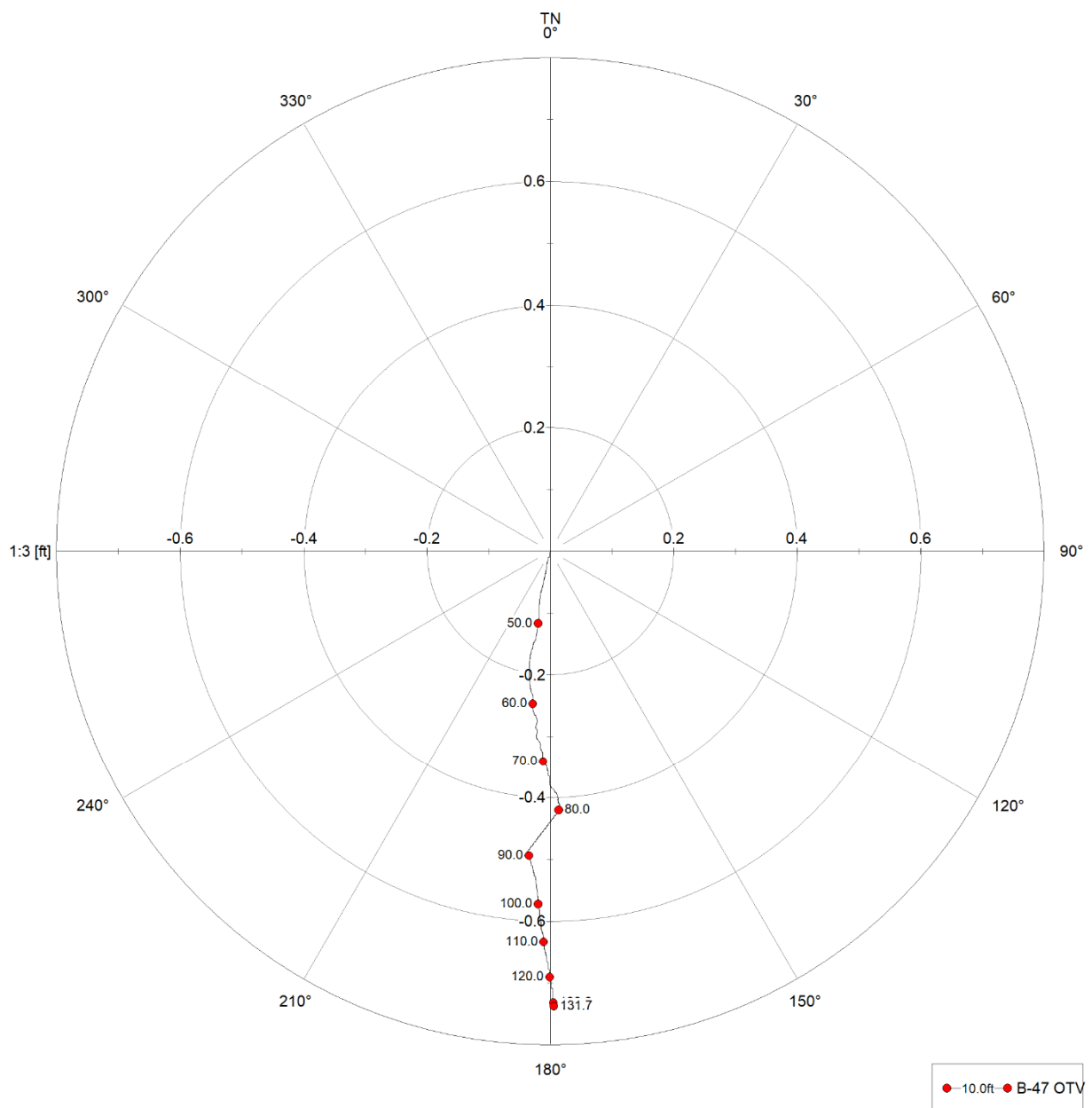


Figure 37. Borehole RC-21-001 (B-47), Optical Deviation Bullseye Projection

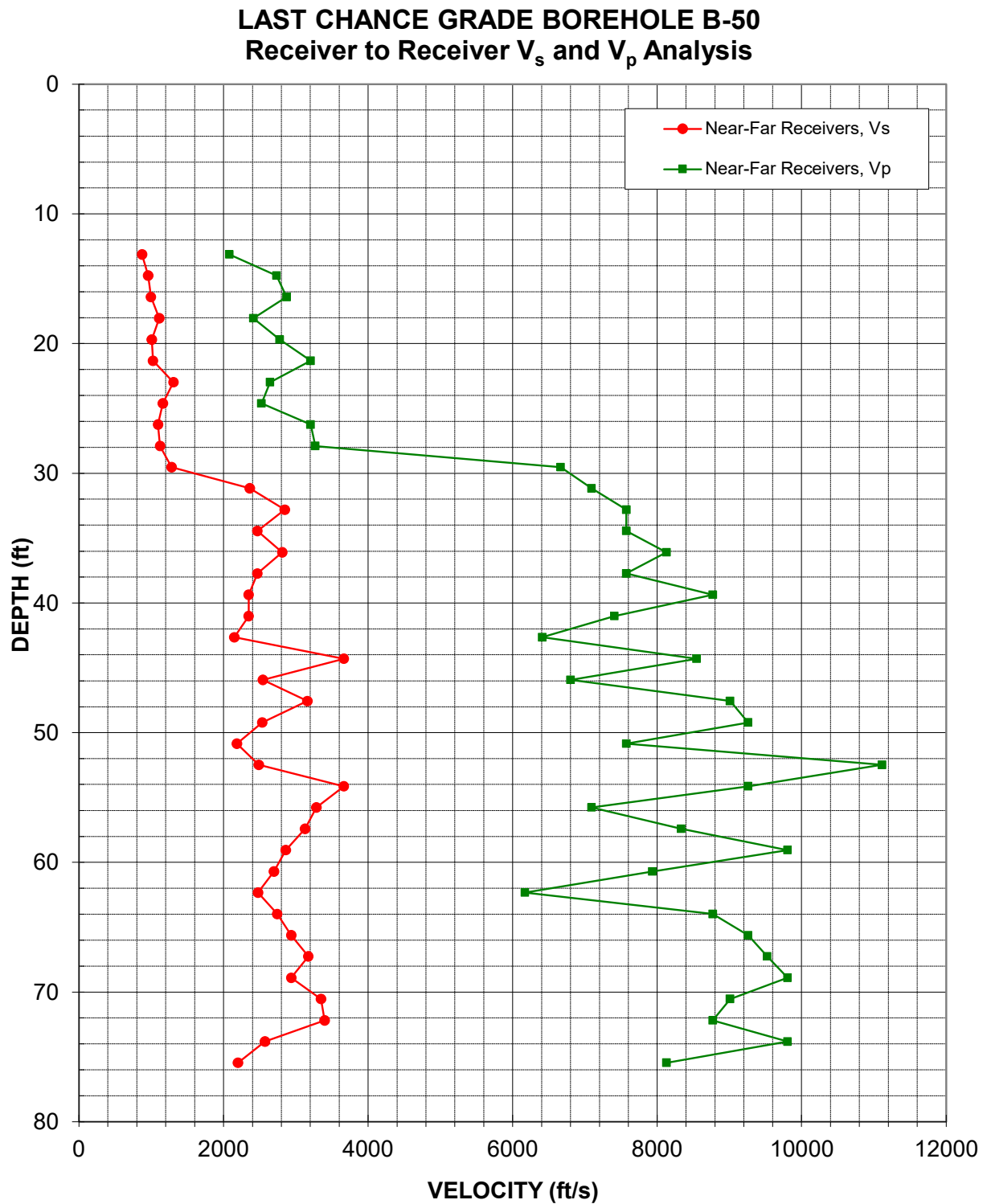


Figure 38: Borehole RC-20-019 (B-50), Suspension R1-R2 P- and SH-wave velocities

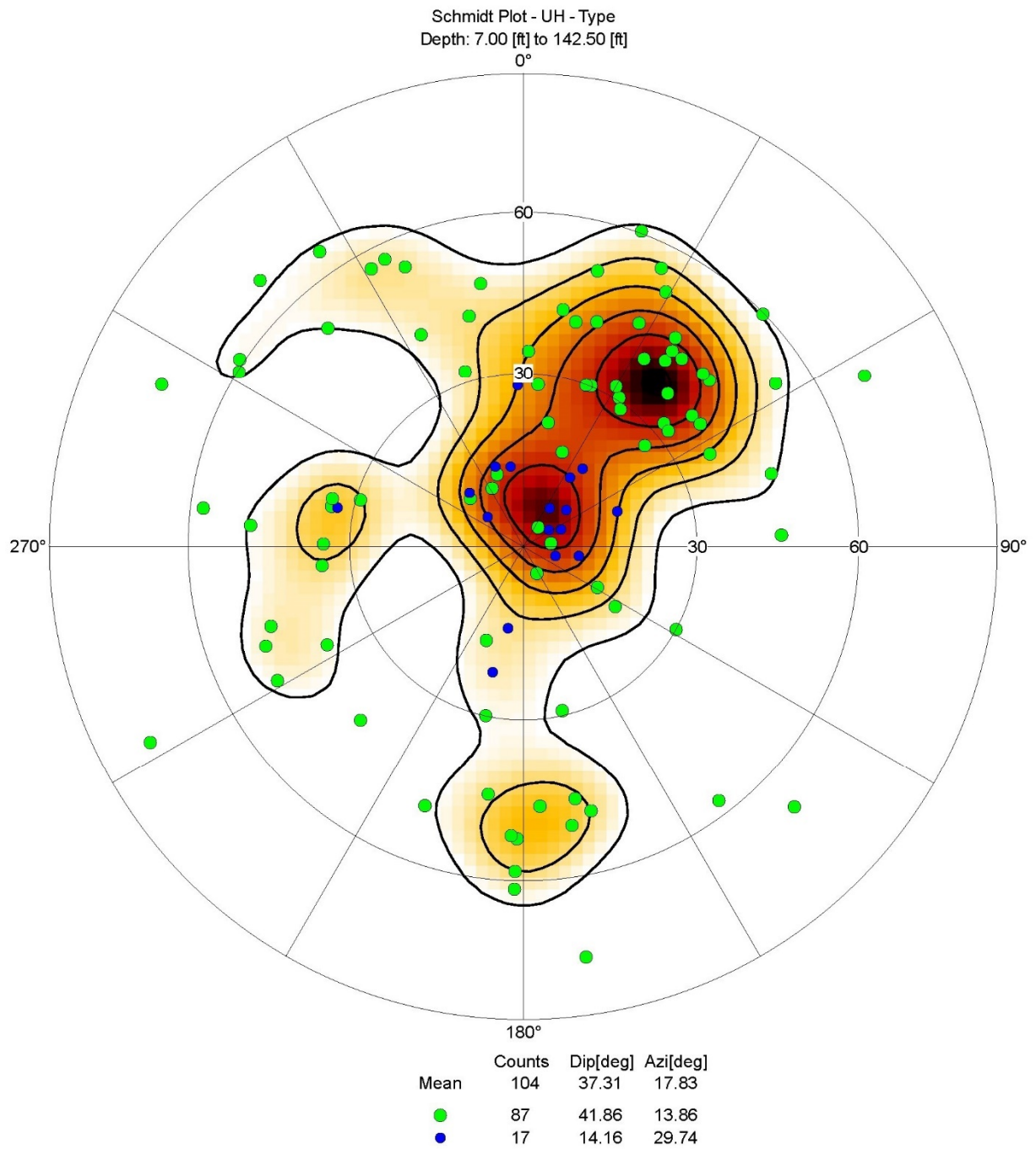


Figure 39. Borehole RC-20-019 (B-50), Acoustic Stereonet Diagram

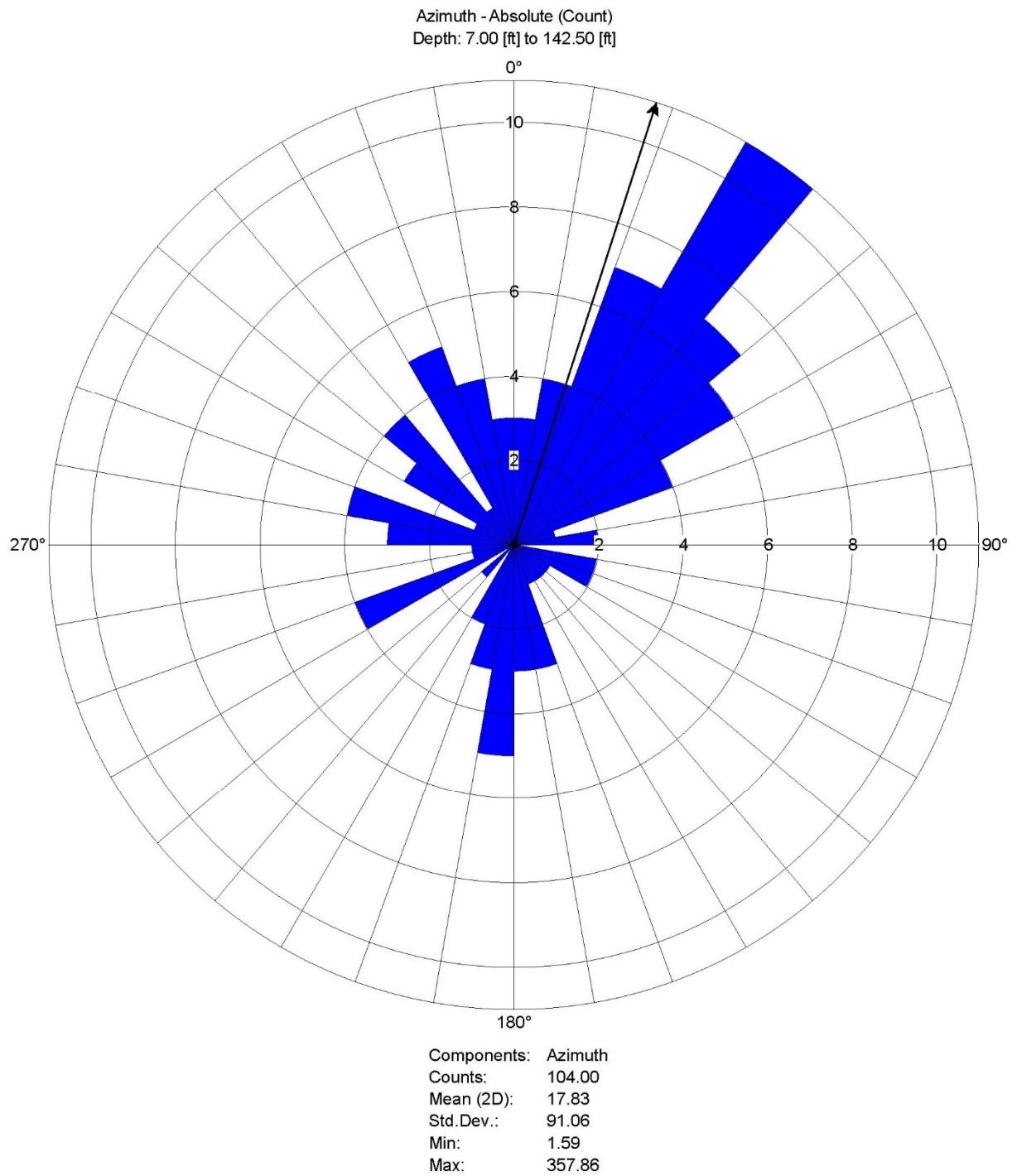


Figure 40. Borehole RC-20-019 (B-50), Acoustic Rose Diagram

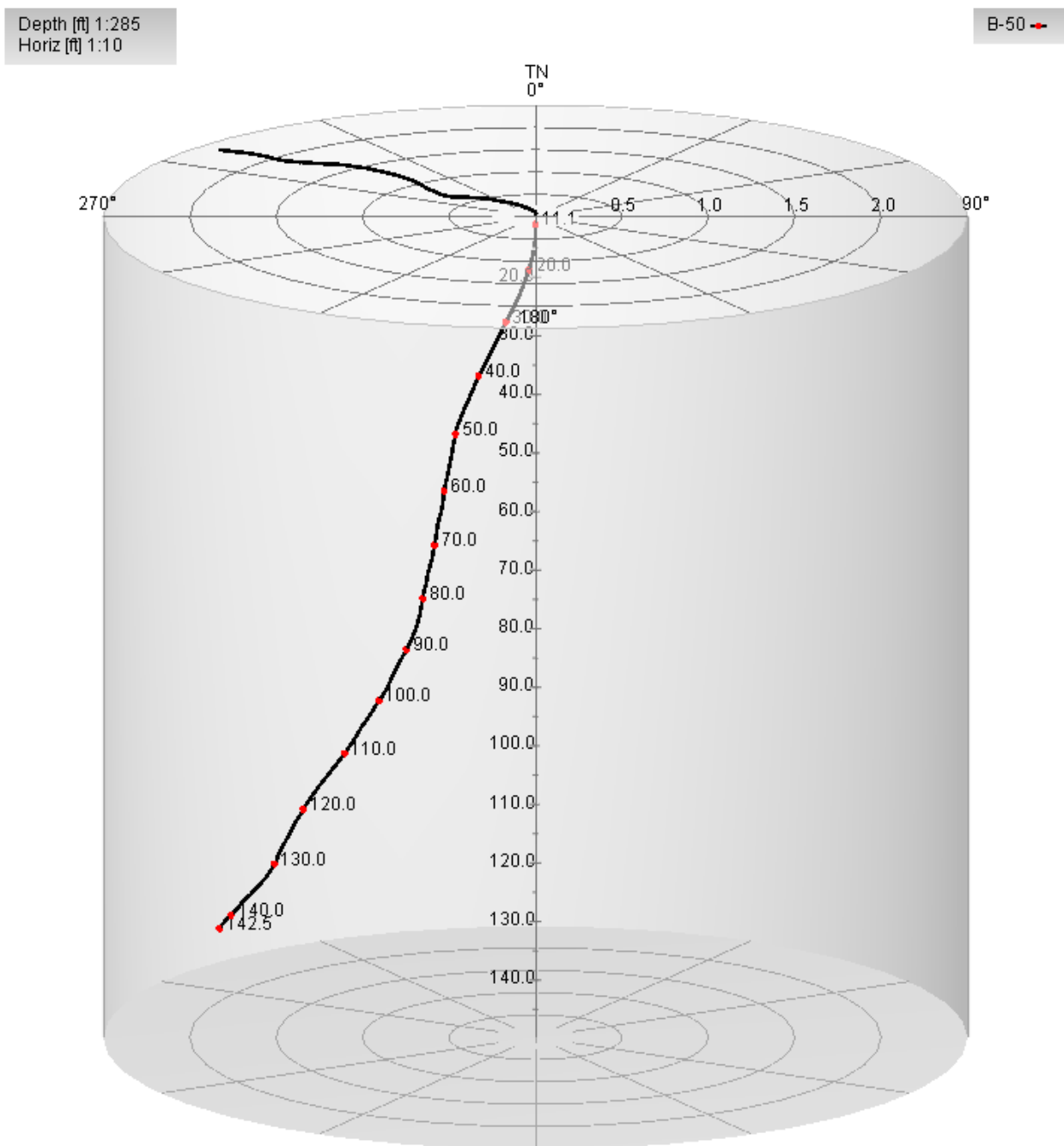


Figure 41. Borehole RC-20-019 (B-50), Acoustic Deviation Cylindrical Projection

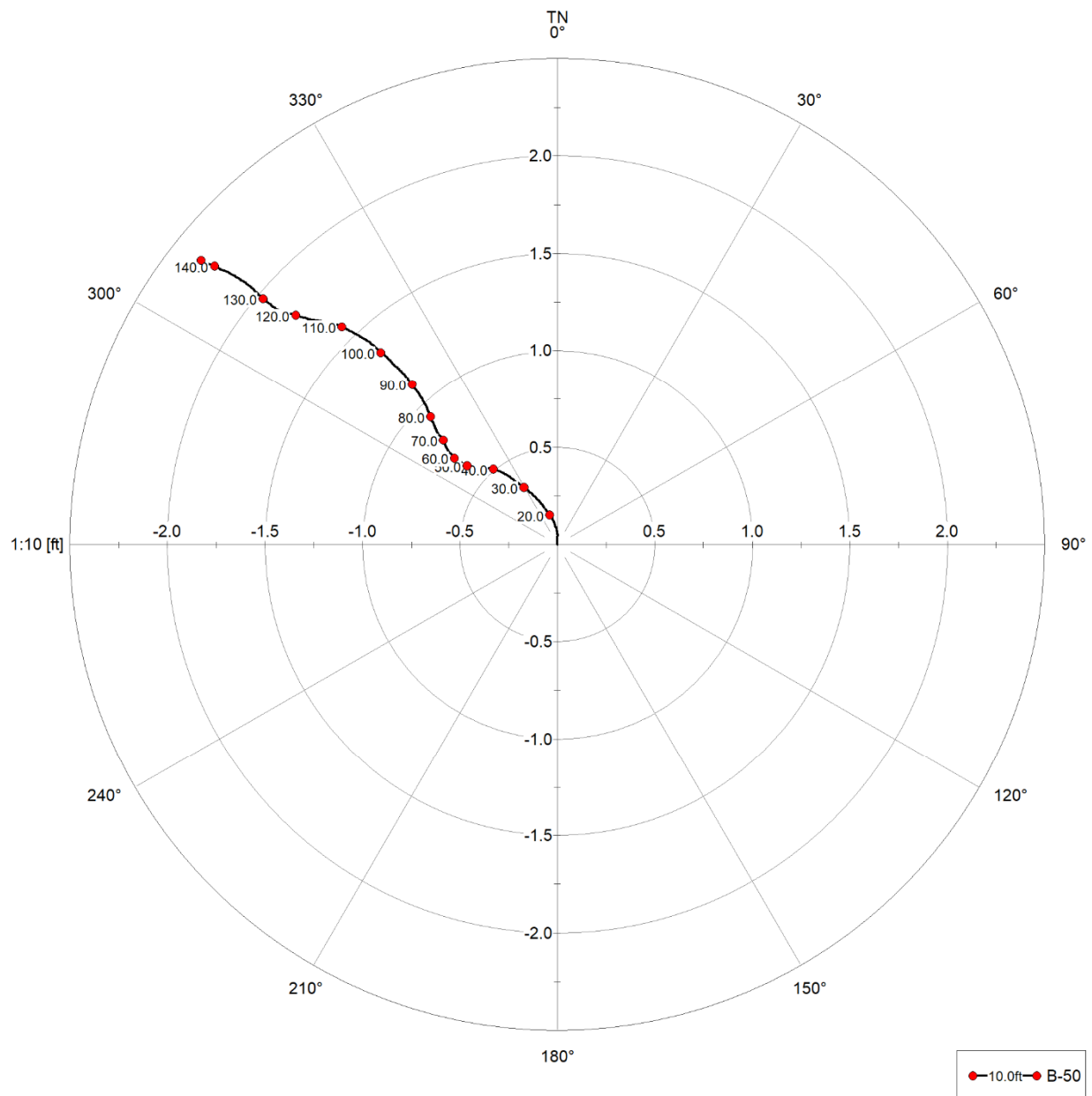



Figure 42. Borehole RC-20-019 (B-50), Acoustic Deviation Bullseye Projection

	LOG TYPE	PROJECT	Last Chance Grade
		WELL	B-50
CLIENT Kleinfelder	CAL NG DUIN	LOCATION	Last Chance Grade, HWY 101
		LOGGER	ATM
		DATE	17 Dec 2020

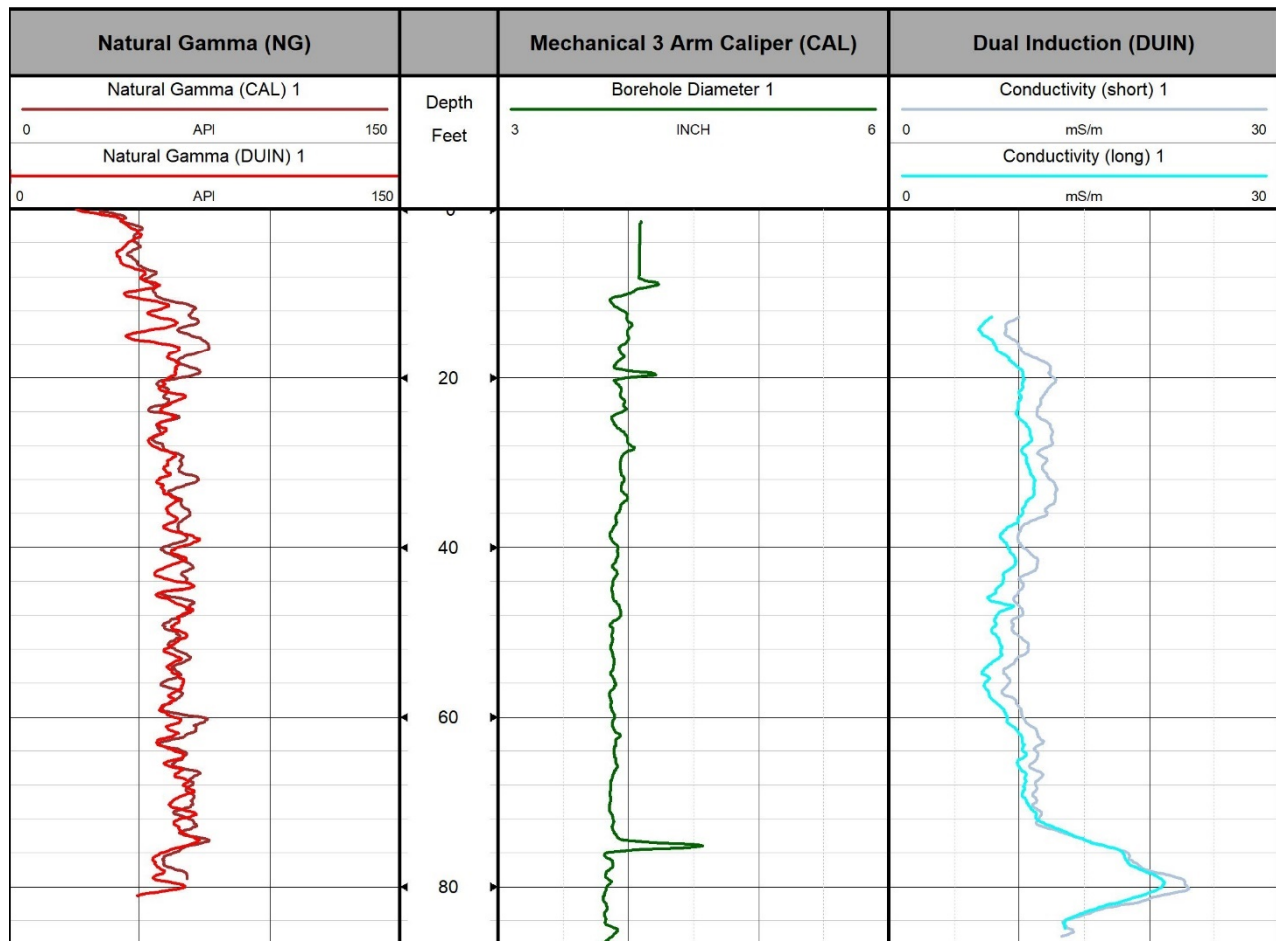


Figure 43. Borehole RC-20-019 (B-50), Induction, Caliper, and Natural Gamma Log

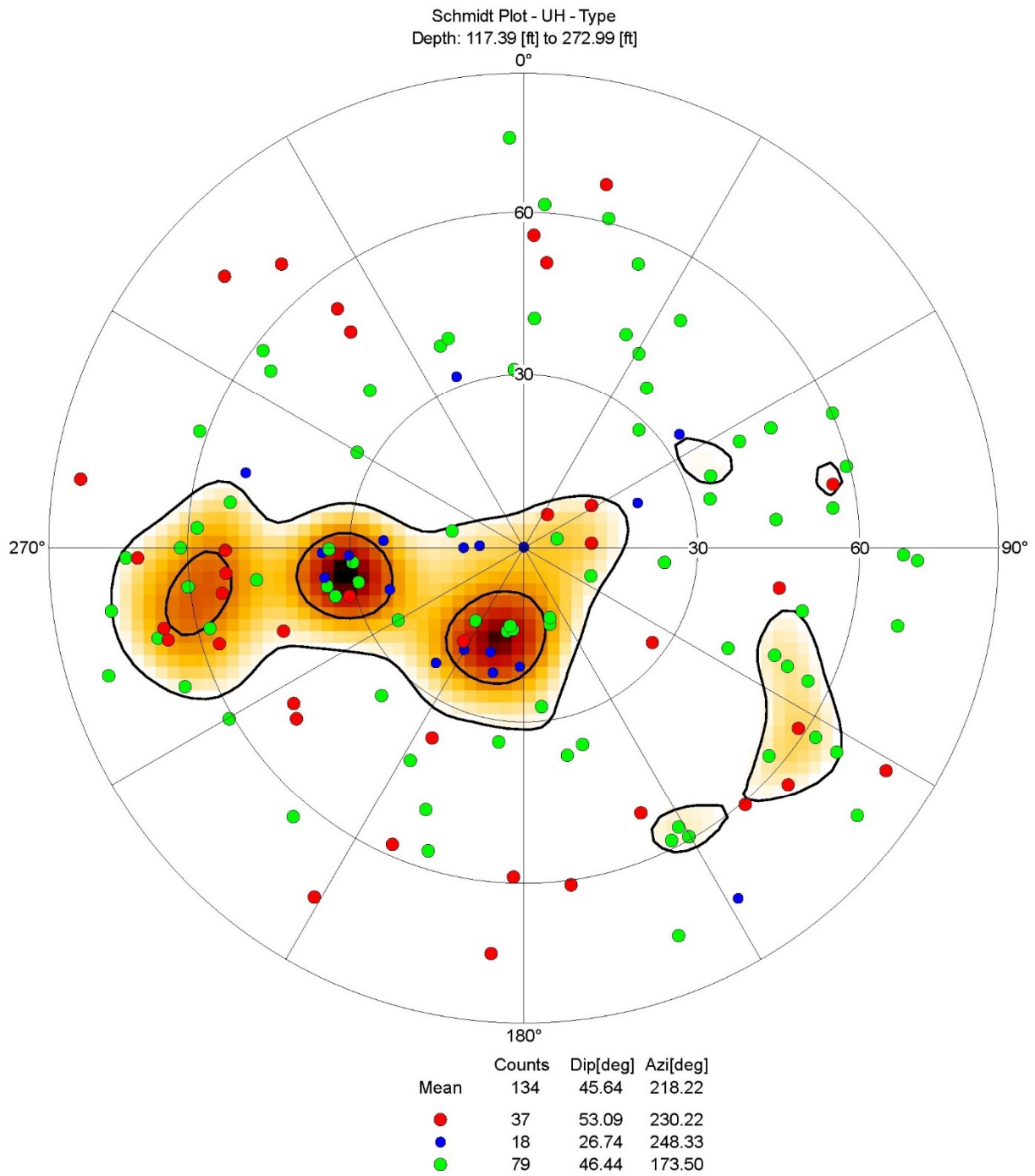


Figure 44. Borehole RC-20-016 (WP-3), Optical Stereonet Diagram

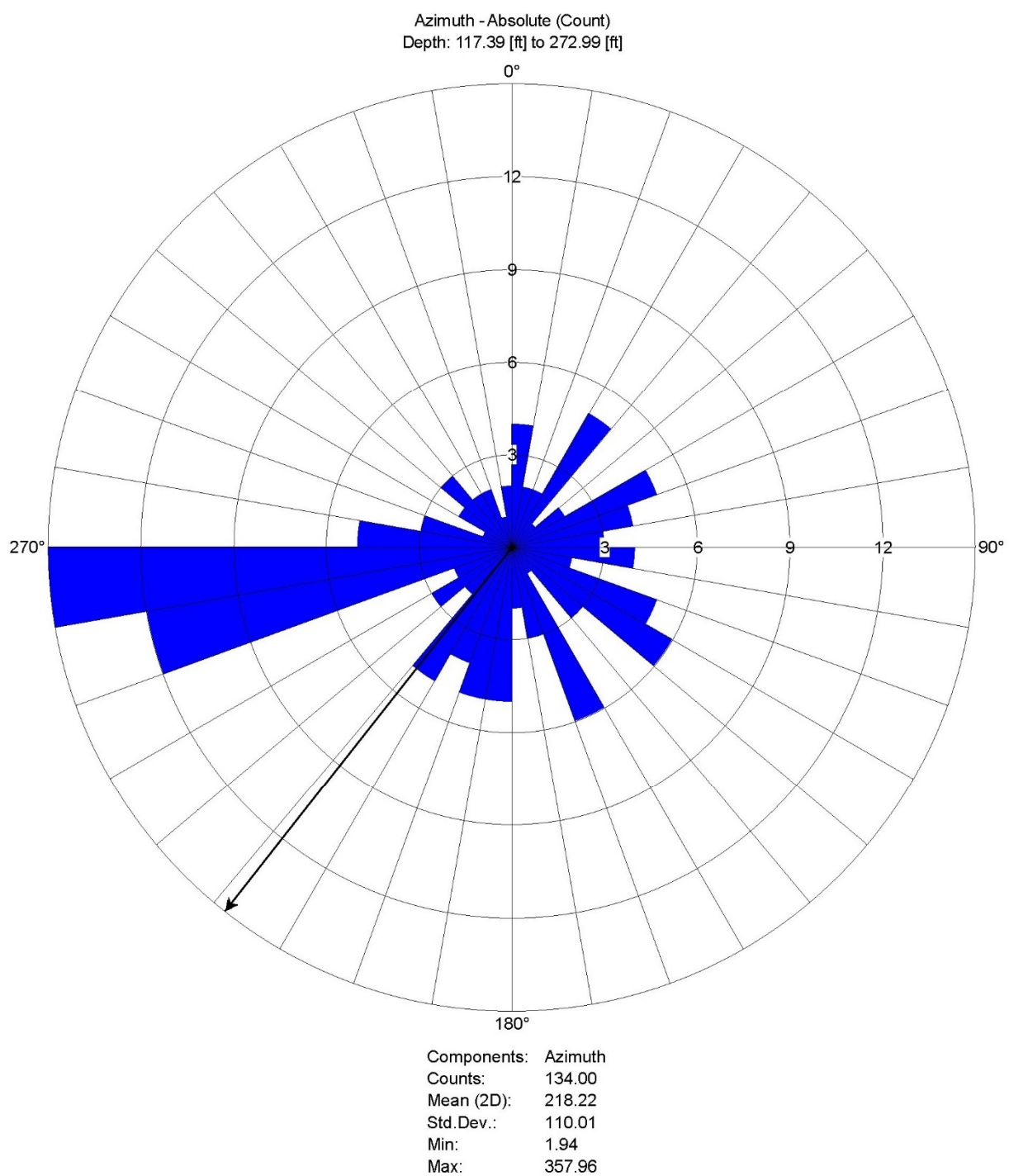


Figure 45. Borehole RC-20-016 (WP-3), Optical Rose Diagram

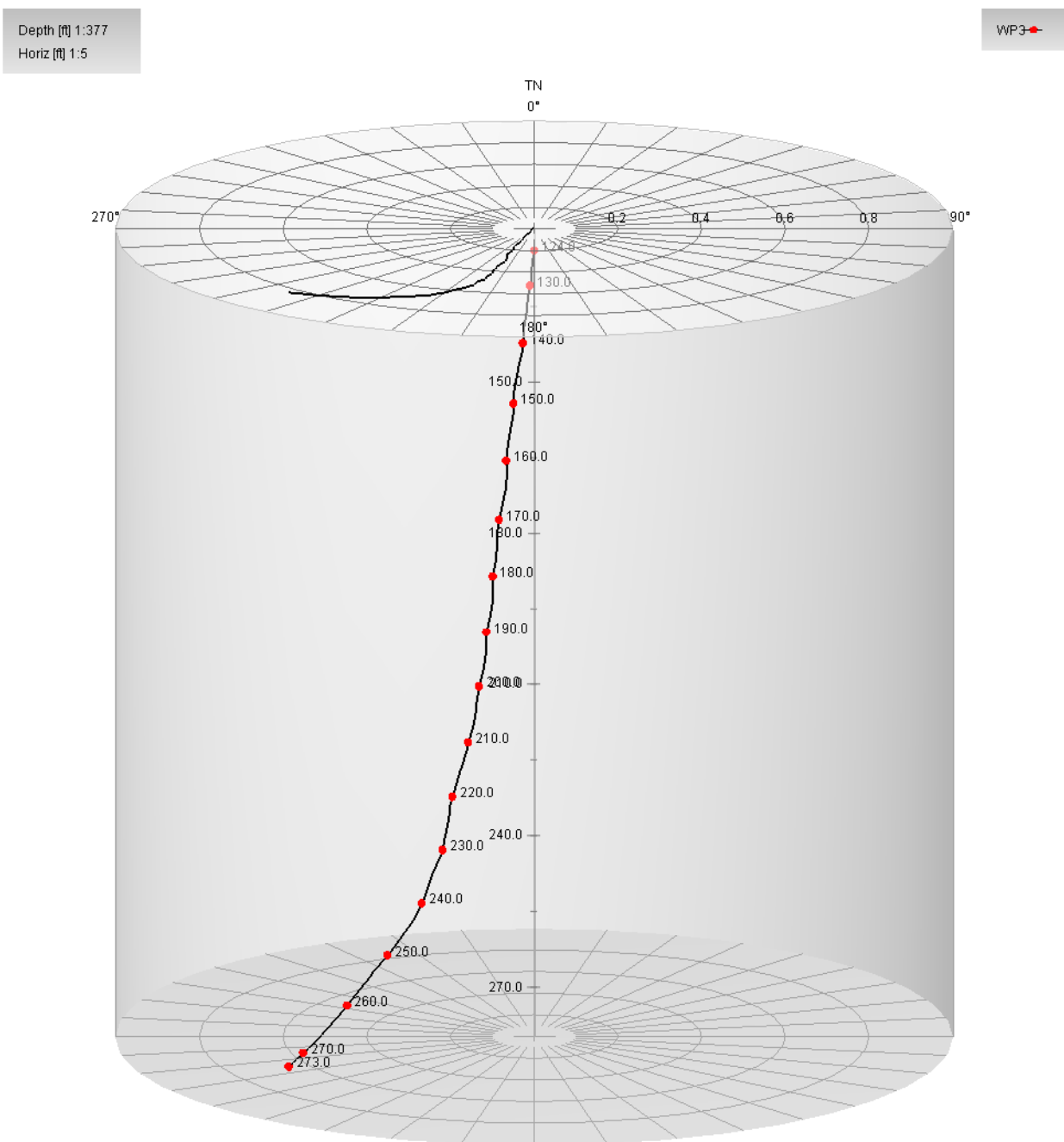


Figure 46. Borehole RC-20-016 (WP-3), Optical Deviation Cylindrical Projection

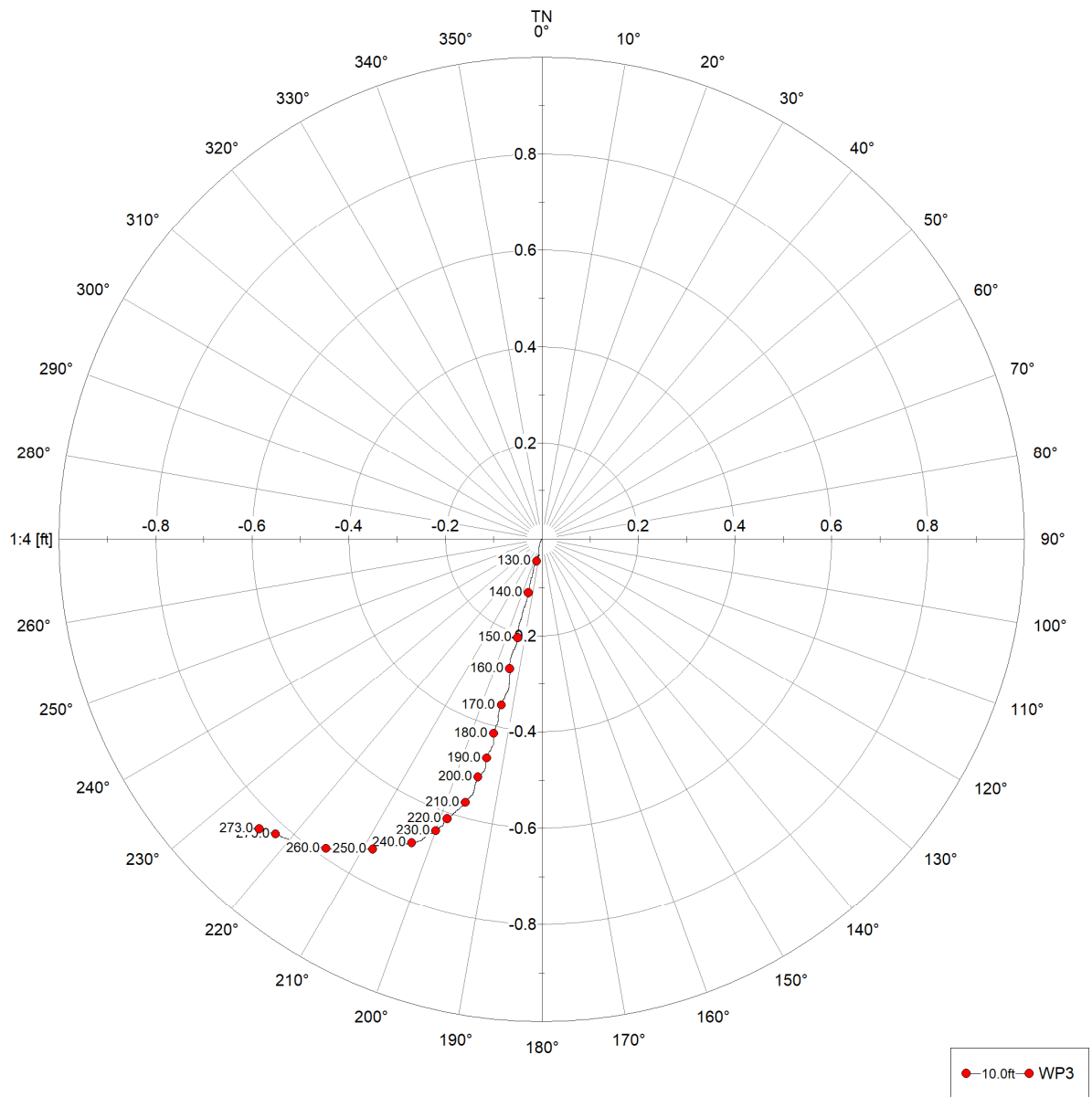


Figure 47. Borehole RC-20-016 (WP-3), Optical Deviation Bullseye Projection

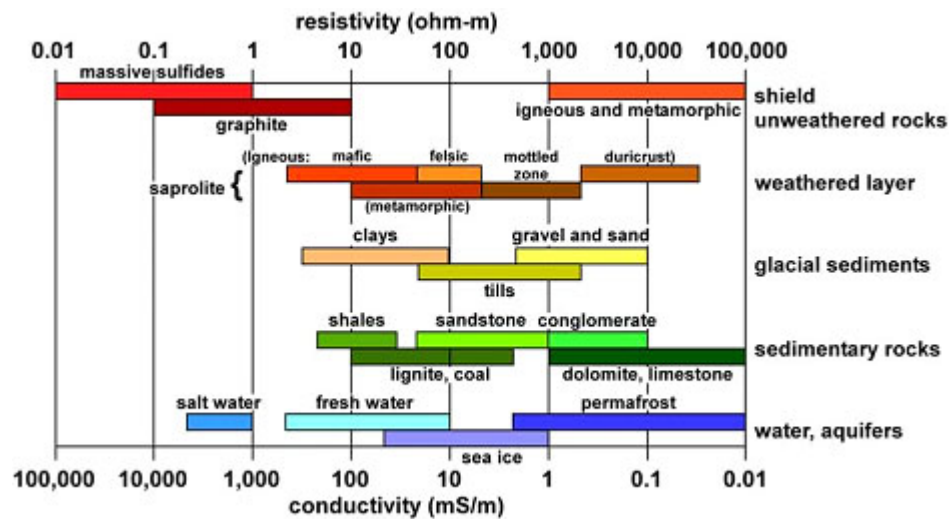


Figure 48. Interpreting Conductivity and Resistivity